



## Clonal hematopoiesis with JAK2V617F promotes pulmonary hypertension with ALK1 upregulation in lung neutrophils

メタデータ	言語: English 出版者: 公開日: 2022-05-24 キーワード (Ja): キーワード (En): 作成者: 君島, 勇輔 メールアドレス: 所属:
URL	<a href="https://fmu.repo.nii.ac.jp/records/2000387">https://fmu.repo.nii.ac.jp/records/2000387</a>

1  
2  
3  
4  
5  
6  
7  
8  
9  
10  
11  
12  
13  
14  
15  
16  
17  
18  
19  
20  
21  
22  
23  
24  
25  
26  
27  
28  
29  
30

# 学 位 論 文

## 学位論文名

Clonal hematopoiesis with JAK2V617F promotes pulmonary hypertension with ALK1 upregulation in lung neutrophils

(JAK2V617F 変異クローン性造血は肺好中球 ALK1 を介して肺高血圧症を増悪させる)

福島県立医科大学大学院医学研究科  
循環病態学 循環器内科学講座  
君島 勇輔

31  
32  
33  
34  
35  
36  
37  
38  
39  
40  
41  
42  
43  
44  
45  
46  
47  
48  
49  
50  
51  
52  
53  
54

**Clonal hematopoiesis with JAK2V617F promotes pulmonary hypertension with ALK1 upregulation in lung neutrophils**

Yusuke Kimishima, MD

Department of Cardiovascular Medicine, Fukushima Medical University

55 **Abstract**

56 Pulmonary hypertension (PH) is a progressive cardiopulmonary disease characterized by  
57 pulmonary arterial remodeling. Clonal somatic mutations including *JAK2V617F*, the  
58 most frequent driver mutation among myeloproliferative neoplasms, have recently been  
59 identified in healthy individuals without hematological disorders. Here, we reveal that  
60 clonal hematopoiesis with *JAK2V617F* exacerbates PH and pulmonary arterial  
61 remodeling in mice. *JAK2V617F*-expressing neutrophils specifically accumulate in  
62 pulmonary arterial regions, accompanied by increases in neutrophil-derived elastase  
63 activity and chemokines in chronic hypoxia-exposed *JAK2V617F* transgenic (*JAK2<sup>V617F</sup>*)  
64 mice, as well as recipient mice transplanted with *JAK2<sup>V617F</sup>* bone marrow cells.  
65 *JAK2V617F* progressively upregulates *Acvr11* (encoding ALK1) during the  
66 differentiation from bone marrow stem/progenitor cells peripherally into mature  
67 neutrophils of pulmonary arterial regions. *JAK2V617F*-mediated STAT3  
68 phosphorylation upregulates ALK1-Smad1/5/8 signaling. ALK1/2 inhibition completely  
69 prevents the development of PH in *JAK2<sup>V617F</sup>* mice. Finally, our prospective clinical study  
70 identified *JAK2V617F*-positive clonal hematopoiesis is more common in PH patients  
71 than in healthy subjects. These findings indicate that clonal hematopoiesis with  
72 *JAK2V617F* causally leads to PH development associated with ALK1 upregulation.

## 73 **Introduction**

74 Pulmonary hypertension (PH) is a complex cardiopulmonary disease characterized by  
75 increases in pulmonary vascular resistance and pulmonary arterial pressure. Despite  
76 recent advances in diagnosis and treatment, PH remains a serious condition, eventually  
77 leading to right heart failure with high mortality<sup>1</sup>. A pathological feature of PH is  
78 structural remodeling of the small pulmonary arteries, which is associated with intimal  
79 thickening, muscularization and the formation of plexiform lesions<sup>2</sup>. Bone marrow (BM)-  
80 derived progenitor cells, as well as perivascular inflammatory infiltrates, contribute to the  
81 process of pulmonary arterial remodeling<sup>3</sup>. It has been also reported that several  
82 hematological disorders, including myeloproliferative neoplasms (MPNs), are often  
83 complicated with PH<sup>4</sup>. The incidence of PH has been reported to be higher in MPN  
84 patients than in the general population, and high mortality due to cardiovascular diseases  
85 has been observed in MPN patients with PH<sup>5, 6</sup>. PH is categorized into five etiological  
86 groups according to the WHO clinical classification<sup>7</sup>. Based on the above observations,  
87 MPN-associated PH is classified into WHO Group V, which is an important heterogenous  
88 group that encompasses unclear multifactorial mechanisms<sup>7</sup>.

89 MPNs including polycythemia vera (PV), essential thrombocythemia (ET), and  
90 primary myelofibrosis (MF) are characterized by chronic proliferation of mature myeloid  
91 cells,<sup>8</sup> and the myeloproliferative phenotype is driven by somatic mutations in *JAK2*,  
92 *CALR*, and *MPL*. Among MPNs, *JAK2V617F*, an activating somatic mutation in *JAK2*,  
93 is the most frequently observed driver mutation; it has been observed in over 95% of PV  
94 patients as well as 50–60% of ET and primary MF patients<sup>9, 10, 11</sup>. *JAK2V617F* causes  
95 cytokine-independent activation of the JAK–STAT pathway, resulting in proliferation of  
96 mature myeloid cells<sup>11</sup>.

97       Recent advances in genetic analyses have led to the discovery of clonal hematopoiesis,  
98 whose hematopoietic stem/progenitor cells harbor somatic mutations in genes often  
99 mutated in myeloid cancers, including MPNs, in healthy individuals without any  
100 hematologic disorders<sup>12, 13</sup>. Among clonal hematopoiesis, age-related clonal  
101 hematopoiesis implies the presence of any detectable clonal events in hematopoietic cells,  
102 and its incidence increases with age. Clonal hematopoiesis of indeterminate potential  
103 (CHIP) is defined by somatic mutations with a variant allele frequency (VAF) of at least  
104 2%. Clonal hematopoiesis is quite common, and more than 15% of individuals are  
105 affected at age  $\geq 70$  years<sup>14</sup>. Whereas the rate of patients who progress from CHIP to  
106 myeloid malignancies is estimated to be only 0.5–1%, patients with CHIP exhibit  
107 markedly increased cardiovascular diseases such as atherosclerosis<sup>12, 15</sup>. Most frequently  
108 mutated genes in clonal hematopoiesis are epigenetic modifiers; *DNMT3A*, *TET2*, and  
109 *ASXL1*. *JAK2* is the next most often mutated gene, and the vast majority of these mutants  
110 are *JAK2V617F* in clonal hematopoiesis. Murine studies have suggested that CHIP with  
111 somatic mutations in epigenetic modifiers, as well as *JAK2V617F*, played causal roles in  
112 acceleration of atherosclerosis<sup>16, 17</sup>. MPN patients often show venous and arterial vascular  
113 complications<sup>18</sup>. In particular, MPN patients with *JAK2V617F* showed higher incidence  
114 of vascular complications compared to those with other driver mutations<sup>18</sup>. However,  
115 mechanistic relevance of clonal hematopoiesis with *JAK2V617F* in PH has yet to be  
116 elucidated.

117       Herein, we provide the evidence that clonal hematopoiesis with *JAK2V617F* plays  
118 causal roles in the development of PH with ALK1 upregulation in lung neutrophils.

119

120 **Results**

121 **JAK2<sup>V617F</sup> expression accelerates pulmonary hypertension in response to chronic**  
122 **hypoxia exposure in mice.**

123 To know the involvement of the JAK-STAT pathway in PH development, adult wild-type  
124 (WT) C57BL/6J mice were exposed to chronic hypoxia (10% O<sub>2</sub>), which is a well-  
125 established method to induce PH in mice<sup>19, 20</sup>. STAT3 phosphorylation levels on whole  
126 lung homogenates, not fractionated cells, were significantly increased after exposure to  
127 chronic hypoxia for 3 weeks (Supplementary Fig. 1), suggesting that JAK-STAT  
128 activation may play a pathophysiological role in chronic hypoxia-induced PH. To clarify  
129 the effects of JAK2<sup>V617F</sup> expression on the pathogenesis of PH, we used JAK2<sup>V617F</sup>  
130 female mice with transgenic expression of *Jak2*<sup>V617F</sup><sup>21</sup> after exposure to normoxia or  
131 chronic hypoxia. Starting from 2 weeks after chronic hypoxia exposure, we observed  
132 noticeable signs of cardio-respiratory distress such as reduced activity, diminished  
133 appetite, and piloerection in JAK2<sup>V617F</sup> mice, but not in WT mice. We determined to  
134 analyze the mice at the 2-week point to minimize the secondary alternation for  
135 investigation of the molecular mechanisms that cause PH (Fig. 1a). After normoxia  
136 exposure, JAK2<sup>V617F</sup> mice had significantly higher white blood cell and platelet counts,  
137 in comparison to WT littermates, indicating an MF-like phenotype in JAK2<sup>V617F</sup> mice  
138 (Fig. 1b), which is consistent with the results of our previous studies<sup>21, 22</sup>. Right  
139 ventricular systolic pressure (RVSP) and the ratio of right ventricle weight to left ventricle  
140 weight plus septum weight (RV/LV+S) did not differ between WT and JAK2<sup>V617F</sup> mice  
141 after normoxia exposure (Fig. 1c). Although chronic hypoxia significantly elevated  
142 hemoglobin values in both WT and JAK2<sup>V617F</sup> mice, there was no significant difference  
143 between them. Notably, we found that RVSP was significantly elevated in JAK2<sup>V617F</sup>

144 mice compared to WT mice in response to continuous hypoxia (Fig. 1c) in line with the  
145 echocardiographic evaluation of pulmonary hemodynamics (Supplementary Fig. 2).  
146 Additionally, RV/LV+S in JAK2<sup>V617F</sup> mice was significantly greater than that in WT mice,  
147 indicating more severe RV hypertrophy due to PH in chronic hypoxia-exposed JAK2<sup>V617F</sup>  
148 mice (Fig. 1c). LV fractional shortening or LV+S values were not different among the  
149 groups, suggesting that chronic hypoxia was not associated with LV systolic dysfunction  
150 or LV hypertrophy in JAK2<sup>V617F</sup> mice (Supplementary Fig. 2, 3). Of note, we found that  
151 even male JAK2<sup>V617F</sup> mice showed significant increases in RVSP and RV/LV+S  
152 compared to male WT mice 2 weeks after chronic hypoxia (Supplementary Fig. 4).  
153 Considering the clinical relevance of PH patients that women are more likely to be  
154 affected than men<sup>23</sup>, we thereafter used female mice in a whole series of the present study  
155 unless otherwise indicated.

156

157 **JAK2<sup>V617F</sup> mice exhibit pulmonary vascular remodeling accompanied by the**  
158 **increased perivascular neutrophil infiltration in the lungs after chronic hypoxia.**

159 Histological analyses revealed significant increases in medial wall thickness and  
160 muscularization of pulmonary vessels in JAK2<sup>V617F</sup> mice compared to WT mice after  
161 exposure to chronic hypoxia (Fig. 1d, e). The numbers of proliferating smooth muscle  
162 cells in the pulmonary arteries were significantly increased in JAK2<sup>V617F</sup> mice compared  
163 to WT mice after chronic hypoxia (Supplementary Fig. 5a). These data suggest that the  
164 JAK2<sup>V617F</sup> expression promoted PH with pulmonary arterial structural remodeling in  
165 response to chronic hypoxia, rather than spontaneous development of PH under  
166 normoxia. We observed increased cellular infiltration surrounding the pulmonary arteries  
167 in both normoxia- and chronic hypoxia-exposed JAK2<sup>V617F</sup> mice in H&E staining



168 (Supplementary Fig. 5b). Next, we characterized the infiltrating cells by  
169 immunohistochemical staining. There were significant increases in Ly6G<sup>+</sup> neutrophils  
170 specifically in pulmonary arterial regions of JAK2<sup>V617F</sup> lungs compared to WT lungs (Fig.  
171 1f, g), and more Ly6G-expressing cells within CD45<sup>+</sup> cells than F4/80<sup>+</sup> macrophages or  
172 CD45R<sup>+</sup> B cells (Supplementary Fig. 6). Of note, the numbers of Ly6G<sup>+</sup> cells in the  
173 perivascular and non-perivascular regions of JAK2<sup>V617F</sup> lungs were further increased after  
174 chronic hypoxia exposure compared to those after normoxia exposure (Supplementary  
175 Fig. 7). CD41<sup>+</sup> megakaryocytes and TER-119<sup>+</sup> erythroblasts were rarely observed in both  
176 WT and JAK2<sup>V617F</sup> lungs (Supplementary Fig. 5b). The activity of elastase, which mainly  
177 originates from neutrophils<sup>24</sup>, and mRNA expression levels of neutrophil-related  
178 chemokines and chemokine receptors, including *Ccl2*, *Cxcl1*, *Ccr1*, *Cxcr2*, as well as  
179 cytokines such as *Pdgfrb* and *Tgfb1*, were significantly increased in the lungs of  
180 JAK2<sup>V617F</sup> mice after chronic hypoxia (Fig. 1h, i, Supplementary Fig. 5c). Thus, the  
181 infiltrated neutrophils in perivascular regions accompanied by their increased functional  
182 activities might play important roles in pulmonary arterial structural remodeling in  
183 JAK2<sup>V617F</sup> mice. We confirmed that in the Sugen-hypoxia model, which is another PH  
184 model<sup>25</sup>, RVSP and RV/LV+S were significantly elevated in JAK2<sup>V617F</sup> mice compared  
185 to WT mice (Supplementary Fig. 8). There was no statistical significance regarding RVSP  
186 and RV/LV+S between aged WT and JAK2<sup>V617F</sup> mice (8–9 months old) without hypoxia  
187 stimulus, but some of the aged JAK2<sup>V617F</sup> mice displayed comparatively high RVSP and  
188 RV/LV+S (Supplementary Fig. 9).

189

190 **Hematopoietic cell clone with JAK2V617F exacerbates the development of**  
191 **pulmonary hypertension in response to chronic hypoxia in mice.**

192 We next investigated whether a hematopoietic cell clone, rather than lung tissue with  
193 JAK2V617F expression, contributes to the development of PH, by means of BM  
194 transplantation (BMT)<sup>22</sup>. Donor BM cells from JAK2<sup>V617F</sup> mice or control WT mice were  
195 injected into lethally irradiated recipient WT mice, so that the recipient mice had WT  
196 lungs (Fig. 2a). The BMT mice were exposed to chronic hypoxia for 3 weeks. The  
197 *Jak2V617F* VAF in blood leukocytes in the recipient mice transplanted with JAK2<sup>V617F</sup>  
198 BM cells (JAK2<sup>V617F</sup>-BMT) gradually elevated from 4 to 8 weeks after BMT; from 25.5  
199  $\pm$  1.1% to 34.9  $\pm$  6.7% in normoxia-exposed mice, and from 24.5  $\pm$  0.8% to 51.1  $\pm$  5.4%  
200 in chronic hypoxia-exposed mice (Fig. 2b), suggesting the nearly complete engraftment  
201 of hematopoietic cells with heterozygous *Jak2V617F*. However, blood cell counts in  
202 JAK2<sup>V617F</sup>-BMT mice did not exhibit significant increases compared to those in the  
203 recipient mice transplanted with WT BM cells (WT-BMT) after normoxia exposure (Fig.  
204 2c), differently from those in individual JAK2<sup>V617F</sup> mice (Fig. 1b). This finding was  
205 consistent with the previously established evidence that recipient mice transplanted with  
206 hematopoietic stem/progenitor cells carrying JAK2V617F often fail to show MPN-like  
207 phenotypes<sup>26</sup>. Although RVSP and RV/LV+S did not differ between WT-BMT and  
208 JAK2<sup>V617F</sup>-BMT mice after normoxia exposure, JAK2<sup>V617F</sup>-BMT mice showed  
209 significant increases in both RVSP and RV/LV+S compared to WT-BMT mice in response  
210 to exposure to chronic hypoxia for 3 weeks (Fig. 2d), which is consistent with the  
211 echocardiography used to assess pulmonary hemodynamics (Supplementary Fig. 10).  
212 LV+S values did not differ among the groups (Supplementary Fig. 11). Medial wall  
213 thickness, percentage of muscularized vessels and numbers of proliferating smooth  
214 muscle cells of pulmonary arteries were significantly increased in JAK2<sup>V617F</sup>-BMT mice  
215 compared to WT-BMT mice after hypoxia exposure (Fig. 2e, f, Supplementary Fig. 12a).

216 These findings strongly indicate that a hematopoietic cell clone with JAK2V617F could  
217 accelerate PH with pulmonary arterial remodeling in WT lung tissues in response to  
218 chronic hypoxia, even without phenotypic MPNs, mimicking PH due to clonal  
219 hematopoiesis, such as CHIP. The numbers of Ly6G<sup>+</sup> neutrophils in pulmonary arterial  
220 regions were significantly increased in JAK2<sup>V617F</sup>-BMT mice compared to WT-BMT  
221 mice either after normoxia or chronic hypoxia exposure, and the numbers of Ly6G<sup>+</sup> cells  
222 in both perivascular and non-perivascular regions in chronic hypoxia-exposed JAK2<sup>V617F</sup>-  
223 BMT mice were further increased compared to those in normoxia-exposed JAK2<sup>V617F</sup>-  
224 BMT mice (Fig. 2g, h, Supplementary Fig. 13, 14). Ly6G<sup>+</sup> cells significantly contributed  
225 to CD45<sup>+</sup> cells rather than F4/80<sup>+</sup> or CD45R<sup>+</sup> cells in hypoxia-exposed JAK2<sup>V617F</sup>-BMT  
226 lungs (Supplementary Fig. 13). The numbers of CD41<sup>+</sup> or TER-119<sup>+</sup> cells were not  
227 different between WT and JAK2<sup>V617F</sup>-BMT mice (Supplementary Fig. 12b). Notably,  
228 elastase activity, neutrophil-related chemokines and chemokine receptors, and cytokines  
229 were significantly elevated in the lungs of JAK2<sup>V617F</sup>-BMT mice in response to chronic  
230 hypoxia compared to the other groups (Fig. 2i, j, Supplementary Fig. 12c). Taken  
231 together, these data suggest that the neutrophils specifically infiltrating in pulmonary  
232 arterial regions induced by clonal hematopoiesis with JAK2V617F are involved in the  
233 development of PH.

234

235 **Characterization of bone marrow-derived hematopoietic cells with JAK2V617F in**  
236 **the lungs by using GFP-transgene.**

237 To visualize and further characterize BM-derived hematopoietic cells carrying  
238 JAK2V617F in pulmonary arterial remodeling, we generated double transgenic mice  
239 (JAK2<sup>V617F</sup>/CAG-EGFP mice) by crossing JAK2<sup>V617F</sup> mice with CAG-EGFP mice<sup>27</sup>. We

240 transplanted BM cells from JAK2<sup>V617F</sup>/CAG-EGFP mice or control WT/CAG-EGFP  
241 littermates into lethally irradiated WT mice. After BMT followed by exposure to chronic  
242 hypoxia for 3 weeks, immunostaining showed that the GFP<sup>+</sup> cells were substantially  
243 accumulated in pulmonary arterial regions in BMT recipients transplanted with BM cells  
244 from JAK2<sup>V617F</sup>/CAG-EGFP mice (JAK2<sup>V617F</sup>-GFP-BMT), whereas recipients  
245 transplanted with BM cells from WT/CAG-EGFP mice (WT-GFP-BMT) showed fewer  
246 GFP<sup>+</sup> cells in the lungs (Fig. 3a, b). There was no co-localization between GFP and  $\alpha$ -  
247 smooth muscle actin ( $\alpha$ SMA) in the lungs of either WT-GFP-BMT or JAK2<sup>V617F</sup>-GFP-  
248 BMT mice. In JAK2<sup>V617F</sup>-GFP-BMT mice, nearly half of the GFP<sup>+</sup> cells expressed Ly6G  
249 in pulmonary arterial regions, and Ly6G<sup>+</sup> cells predominantly contributed to BM-derived  
250 cells rather than F4/80<sup>+</sup> or CD45R<sup>+</sup> cells (Fig. 3c, d, Supplementary Fig. 15). The  
251 percentage of these Ly6G-expressing GFP<sup>+</sup> cells was significantly higher than that in WT-  
252 GFP-BMT mice, while all Ly6G<sup>+</sup> cells expressed GFP in both WT-GFP-BMT and  
253 JAK2<sup>V617F</sup>-GFP-BMT mice (Fig. 3e). These data indicate that the accumulated Ly6G<sup>+</sup>  
254 neutrophils carrying JAK2<sup>V617F</sup> are originated from BM to pulmonary arterial regions.

255

### 256 **Small clones with JAK2<sup>V617F</sup> lead to PH development.**

257 We next performed a competitive transplantation using different ratios of a mixture of  
258 WT-GFP or JAK2<sup>V617F</sup>-GFP BM cells and WT without GFP BM cells (Fig. 4a,  
259 Supplementary Fig. 16a). In the control non-competitive group, flow cytometry showed  
260 that chimerism assessed by GFP<sup>+</sup> cells within CD45<sup>+</sup> cells in the blood was significantly  
261 elevated at 8 weeks compared to that at 4 weeks in 100% WT-GFP-BMT and 100%  
262 JAK2<sup>V617F</sup>-GFP-BMT mice (Supplementary Fig. 16b). To determine the minimum  
263 threshold of PH aggravation in JAK2<sup>V617F</sup>-GFP-BMT mice, we categorized the recipient

264 mice according to the chimerism level 8-weeks after BMT. Interestingly, when we  
265 analyzed the recipients limited to the chimerism of 1–19% as well as 20–49% and 50–  
266 100%, the JAK2<sup>V617F</sup>-GFP-BMT mice showed significant increases in RVSP and  
267 RV/LV+S compared to the WT-GFP-BMT mice (Fig. 4b, Supplementary Fig. 16c–e).  
268 Moreover, the JAK2<sup>V617F</sup>-GFP-BMT mice with lower chimerism of <1% tended to  
269 display increases in RVSP and RV/LV+S compared to the WT-GFP-BMT mice  
270 (Supplementary Fig. 16f). These data suggest that even small clones with *Jak2*<sup>V617F</sup> are  
271 associated with PH development.

272

273 **JAK2V617F is associated with selective migration of neutrophils into the lungs and**  
274 **maturation for the myeloid lineage from hematopoietic precursors in the lungs.**

275 We isolated cell fraction from the lungs and the blood in WT-GFP-BMT and JAK2<sup>V617F</sup>-  
276 GFP-BMT mice with 1–19% chimerism at 8 weeks after BMT. The percentages of GFP<sup>+</sup>  
277 cells within Ly6G<sup>+</sup> neutrophils in JAK2<sup>V617F</sup>-GFP-BMT mice were significantly higher  
278 in the lungs than in the blood, while those in WT-GFP-BMT mice were not different  
279 between the lungs and the blood (Fig. 4c, d). These findings suggest that JAK2<sup>V617F</sup>  
280 neutrophils have an intrinsic capability of increased migration into the lungs, and this  
281 migration is enhanced in response to hypoxia. Accordingly, *ex vivo* analysis using  
282 chemotaxis assay revealed that JAK2<sup>V617F</sup>-Ly6G<sup>+</sup> cells in the blood displayed a higher  
283 capability of neutrophil migration than WT-Ly6G<sup>+</sup> cells (Fig. 4e). To investigate the  
284 involvement of hematopoietic progenitors in JAK2<sup>V617F</sup> lungs, CD117 (c-kit)<sup>+</sup> cells were  
285 sorted from the lungs and subjected to a colony-forming assay. There were substantial  
286 increases in the colony-forming ability of JAK2V617F-expressing progenitor cells,  
287 especially toward the myeloid lineage (Fig. 4f, Supplementary Fig. 17). These data

288 indicate that the accumulated Ly6G<sup>+</sup> neutrophils carrying JAK2V617F are migrated from  
289 BM to pulmonary arterial regions, and potentially proliferated and matured from the  
290 precursors in the lungs.

291

### 292 **Alternation of gene profiling during neutrophil differentiation with JAK2V617F.**

293 To elucidate the underlying mechanisms of how BM-derived neutrophils carrying  
294 JAK2V617F were causally related to PH development, we performed gene expression  
295 profiling of the neutrophils at several stages of differentiation by RNA sequencing in  
296 sorted Ly6G<sup>+</sup> cells from BM, peripheral blood (PB) and lungs of JAK2<sup>V617F</sup> mice in  
297 comparison to WT mice. The purity of the lung Ly6G<sup>+</sup> cell enrichment was confirmed by  
298 immunofluorescence (Supplementary Fig. 18). To compare these data with the cells at the  
299 hematopoietic stem/progenitor cell level, we used the available RNA sequencing results  
300 of lineage<sup>-</sup>Sca1<sup>+</sup>Kit<sup>+</sup> (LSK) cells in BM from our previous study<sup>22</sup>. We found that 451,  
301 849, 1142, and 1022 genes were upregulated, and 580, 841, 1123, and 1006 genes were  
302 downregulated in LSK cells and Ly6G<sup>+</sup> cells of the BM, PB and lungs, respectively, in  
303 JAK2<sup>V617F</sup> mice compared to WT mice (Fig. 5a, Supplementary Data 1). Differentially  
304 expressed genes in JAK2<sup>V617F</sup> mice were more frequently overlapped among the BM, PB  
305 and lung Ly6G<sup>+</sup> cells than between the LSK cells and BM Ly6G<sup>+</sup> cells. Next, we subjected  
306 these RNA sequencing results to the pathway analysis (Fig. 5b). Hierarchical clustering  
307 analysis showed that the gene profiling was branched from the LSK cells, and diverged  
308 into BM myeloid cells and neutrophils in the lungs and PB, suggesting that the neutrophils  
309 were spread peripherally. Some of the canonical pathways were commonly up- and down-  
310 regulated at each stage. There were also pathways that were enhanced in accordance with  
311 differentiation and that were specifically enhanced in the final stage before peripherally.

312 Thus, the gene expression profiles were differently altered from the LSK cells to lung  
313 neutrophils in JAK2<sup>V617F</sup> mice.

314

315 **Ly6G<sup>+</sup> cells carrying JAK2V617F progressively increased *Acvr11* gene expression**  
316 **during the process of differentiation into peripheral pulmonary arterial regions of**  
317 **the lungs.**

318 A gene set enrichment analysis revealed that the canonical IL6-JAK-STAT3 pathway was  
319 upregulated at each stage of neutrophil differentiation in JAK2<sup>V617F</sup> mice compared to  
320 WT mice (Fig. 5c), with some alterations of differentially expressed individual genes  
321 (Fig. 5d). Interestingly, *Activin A receptor like type 1 (Acvr11)*, which encodes ALK1 and  
322 is known as a type I transmembrane serine/threonine kinase receptor, is associated with  
323 the pathogenesis of PH<sup>7, 28</sup> and has been found to be the most upregulated gene in the  
324 canonical IL6-JAK-STAT3-pathway in Ly6G<sup>+</sup> neutrophils of the lungs and PB of  
325 JAK2<sup>V617F</sup> mice (Fig. 5d). *Acvr11* was slightly upregulated in the BM Ly6G<sup>+</sup> myeloid cells  
326 and LSK cells of JAK2<sup>V617F</sup> mice (Fig. 5d). Furthermore, the genes associated with  
327 neutrophil functions such as protein secretion, degranulation, and granulation were  
328 exclusively enriched in the periphery, especially in the lung Ly6G<sup>+</sup> neutrophils with  
329 JAK2V617F (Fig. 5e–g).

330

331 ***Acvr11* mRNA expressions and phosphorylation of Smad1/5/8 and Stat3 in the lungs**  
332 **of JAK2<sup>V617F</sup> mice in response to chronic hypoxia.**

333 *Acvr11* mRNA expression levels in the lung homogenates of JAK2<sup>V617F</sup> mice were higher  
334 than those of WT mice after exposure to normoxia (Fig. 6a). In response to chronic  
335 hypoxia, *Acvr11* levels were increased in both WT and JAK2<sup>V617F</sup> lungs, but the levels in

336 JAK2<sup>V617F</sup> lungs were greater than those in WT lungs. *Acvr1l* mRNA levels in sorted  
337 Ly6G<sup>+</sup> neutrophils were significantly elevated in JAK2<sup>V617F</sup> lungs compared to WT lungs  
338 after both normoxia and hypoxia, but not in CD31<sup>+</sup> endothelial cells, suggesting that the  
339 changes in *Acvr1l* in the lungs resulted from different expression levels of *Acvr1l* in  
340 Ly6G<sup>+</sup> neutrophils, although *Acvr1l* expression levels were higher in CD31<sup>+</sup> cells than in  
341 Ly6G<sup>+</sup> cells (Fig. 6a, Supplementary Fig. 19a). Similarly, phosphorylation levels of  
342 Smad1/5/8, which is down-stream of ALK1, were significantly elevated in JAK2<sup>V617F</sup>  
343 lungs compared to WT lungs after chronic hypoxia (Fig. 6b). There was a significant  
344 difference between the 10-fold increase in *Acvr1l* mRNA levels versus the 2-fold increase  
345 in phosphorylated Smad1/5/8 levels in chronic hypoxia-exposed JAK2<sup>V617F</sup> lungs,  
346 indicating that the relationship of *Acvr1l* mRNA expression and the phosphorylation of  
347 Smad1/5/8 was not completely linear, and Smad1/5/8 phosphorylation may be regulated  
348 by multiple pathways. *Acvr1* mRNA encoding the ALK2 in the lung homogenates was  
349 significantly increased after chronic hypoxia in both WT and JAK2<sup>V617F</sup> mice, but there  
350 were no differences between the groups after normoxia or hypoxia. However, *Acvr1*  
351 mRNA in Ly6G<sup>+</sup> cells was decreased in both WT and JAK2<sup>V617F</sup> mice after hypoxia, and  
352 the changes in *Acvr1* levels were observed in the opposite direction to those seen in *Acvr1l*  
353 (Supplementary Fig. 19b). There were no differences in *Bmpr2* mRNA between WT and  
354 JAK2<sup>V617F</sup> mice in the lung homogenates, Ly6G<sup>+</sup>, or CD31<sup>+</sup> cells (Supplementary Fig.  
355 19c). STAT3 phosphorylation levels were significantly increased in JAK2<sup>V617F</sup> lungs  
356 compared to WT lungs after normoxia exposure; however, after exposure to chronic  
357 hypoxia, these levels in JAK2<sup>V617F</sup> lungs were even more upregulated compared to the  
358 other groups (Fig. 6c). HIF1 $\alpha$  expression levels in the lungs were increased in both WT  
359 and JAK2<sup>V617F</sup> mice after chronic hypoxia, but there was no difference between the



360 groups (Supplementary Fig. 20). Immunoprecipitation analysis showed that STAT3  
361 protein weakly interacted with HIF1 $\alpha$  in JAK2<sup>V617F</sup> lungs at normoxia, and chronic  
362 hypoxia increased the bindings (Supplementary Fig. 21). The conditioned medium from  
363 hypoxia-exposed JAK2<sup>V617F</sup> neutrophils pretreated with a HIF1 $\alpha$  inhibitor partly  
364 attenuated the increases in the proliferation of pulmonary arterial smooth muscle cells  
365 (Supplementary Fig. 22). Thus, JAK-STAT3 signaling in the lungs was constitutively  
366 activated in JAK2<sup>V617F</sup> mice at baseline, whereas both the JAK-STAT3 and ALK1-  
367 Smad1/5/8 pathways were further upregulated in JAK2<sup>V617F</sup> lungs in response to chronic  
368 hypoxia, which may be associated with HIF1 $\alpha$ . These data suggest that ALK1-Smad1/5/8  
369 in the lungs is associated with PH development due to clonal hematopoiesis with  
370 JAK2V617F.

371

372 ***JAK2V617F* transcriptionally upregulates *ACVRL1* by STAT3-binding.**

373 To investigate the regulatory mechanisms of *ACVRL1* by *JAK2V617F*, heterozygous  
374 *JAK2V617F* knock-in (*JAK2*<sup>V617F/+</sup>) HCT116 cell lines were analyzed. Smad1/5/8 was  
375 phosphorylated by stimulation of BMP9, a high affinity in ALK1 ligand, in HCT116 cells  
376 (Supplementary Fig. 23). Phosphorylation levels of STAT3 in *JAK2*<sup>V617F/+</sup> cells were  
377 significantly elevated compared to those in *JAK2*<sup>+/+</sup> cells (Fig. 7a). *JAK2*<sup>V617F/+</sup> cells  
378 exhibited significant increases in the expression levels of *ACVRL1* mRNA as well as  
379 ALK1 protein and phosphorylation levels of Smad1/5/8 compared to *JAK2*<sup>+/+</sup> cells (Fig.  
380 7b, c, Supplementary Fig. 24), but not in *ACVRI* (ALK2) expressions (Supplementary  
381 Fig. 25). To assess the effects of *JAK2V617F* on the transcriptional activity of *ACVRL1*,  
382 an *in silico* analysis was performed, which identified putative STAT3 binding sites in the  
383 *ACVRL1* promoter region in both humans and mice (Fig. 7d). The chromatin

384 immunoprecipitation (ChIP) coupled with qPCR showed that the bindings of STAT3 and  
385 the putative *ACVRL1* promoter regions were significantly increased in *JAK2*<sup>V617F/+</sup>  
386 HCT116 cells compared to *JAK2*<sup>+/+</sup> HCT116 cells (Fig. 7e). Next, we performed the  
387 luciferase reporter assay using the luciferase construct containing the human *ACVRL1*  
388 putative promoter sequence from -1035 bp to +210 bp of the transcriptional start site<sup>29</sup>.  
389 The promoter activity of *ACVRL1* in *JAK2*<sup>V617F/+</sup> cells was significantly increased  
390 compared to those of *JAK2*<sup>+/+</sup> cells (Fig. 7f). Ruxolitinib, a specific JAK1/2 inhibitor,  
391 decreased the *ACVRL1* promoter activity in a dose-dependent manner in *JAK2*<sup>V617F/+</sup>  
392 HCT116 cells (Fig. 7g). In addition, the administration of stattic, an inhibitor of STAT3,  
393 attenuated the *ACVRL1* promoter activity (Fig. 7h). Taken together, *JAK2*<sup>V617F</sup>  
394 increased *ACVRL1* transcriptional activity via STAT3-binding, resulting in  
395 phosphorylation of Smad1/5/8 in HCT116 cells.

396

### 397 **Inhibition of ALK1/2 prevents chronic hypoxia-induced pulmonary hypertension in** 398 ***JAK2*<sup>V617F</sup> mice.**

399 We investigated whether the inhibition of ALK1 could ameliorate chronic hypoxia-  
400 induced PH in *JAK2*<sup>V617F</sup> mice (Fig. 8a). K02288, a chemical inhibitor of ALK1/2<sup>30,31</sup>  
401 clearly decreased the phosphorylation levels of Smad1/5/8 in chronic hypoxia-exposed  
402 *JAK2*<sup>V617F</sup> lungs as well as *JAK2*<sup>V617F/+</sup> HCT116 cells (Supplementary Fig. 26).  
403 Administration of K02288 did not affect blood cell counts in *JAK2*<sup>V617F</sup> mice (Fig. 8b).  
404 Remarkably, K02288 treatment significantly decreased RVSP and RV/LV+S in  
405 *JAK2*<sup>V617F</sup> mice compared to DMSO-treated *JAK2*<sup>V617F</sup> mice after exposure to chronic  
406 hypoxia (Fig. 8c, Supplementary Fig. 27). In contrast, K02288 administration did not  
407 significantly change the levels of RVSP or RV hypertrophy in chronic hypoxia-exposed

408 WT mice. There were significant decreases in medial wall thickness and muscularization,  
409 as well as in the numbers of proliferating smooth muscle cells in pulmonary arteries of  
410 K02288-treated  $JAK2^{V617F}$  mice compared to DMSO-treated  $JAK2^{V617F}$  mice (Fig. 8d, e,  
411 Supplementary Fig. 28). The numbers of Ly6G<sup>+</sup> neutrophils in perivascular regions were  
412 decreased in K02288-treated  $JAK2^{V617F}$  lungs compared to DMSO-treated  $JAK2^{V617F}$   
413 lungs (Fig. 8f, g). In addition, K02288 treatment significantly decreased elastase activity  
414 in  $JAK2^{V617F}$  lungs (Fig. 8h). Of note, we found that the treatment of LDN-212854,  
415 another ALK1/2 inhibitor,<sup>31</sup> significantly decreased RVSP and RV/LV+S in chronic  
416 hypoxia-exposed  $JAK2^{V617F}$  mice, similar to K02288 (Supplementary Fig. 29, 30).  
417 K02288 or LDN-212854 did not affect the levels of RVSP and RV/LV+S in WT or  
418  $JAK2^{V617F}$  mice after normoxia (Supplementary Fig. 31). A higher dose of K02288 did  
419 not attenuate the PH levels of hypoxia-exposed WT mice (Supplementary Fig. 32).  
420 Collectively, these results suggest that the ALK1/2 pathway is involved in chronic  
421 hypoxia-induced PH in  $JAK2^{V617F}$  mice.

422

#### 423 **Prevalence of $JAK2V617F$ -clonal hematopoiesis in PH patients.**

424 To clarify the clinical relevance of clonal hematopoiesis with  $JAK2V617F$  in PH, we  
425 prospectively recruited PH patients, and examined the prevalence of clonal hematopoiesis  
426 with  $JAK2V617F$  in 70 PH patients by allele specific quantitative PCR analysis<sup>32</sup>.  
427 Strikingly, we found that 7.1% of the PH patients (n = 5) showed  $JAK2V617F$  somatic  
428 mutation in peripheral leukocytes, which was significantly higher than that of the age-  
429 and sex-matched control subjects (Fig. 9a, Supplementary Table 1). Among these five PH  
430 patients with  $JAK2V617F$ , three patients, who were categorized into WHO Group IV  
431 (chronic thromboembolic pulmonary hypertension), were regarded as CHIP with a

432 *JAK2V617F* VAF of  $\geq 2\%$  (Fig. 9b, Supplementary Table 2). The *JAK2V617F* VAF was  
433  $< 2\%$  in the remaining two patients, who were classified into WHO Group I (pulmonary  
434 arterial hypertension). These two patients were in their 50s and 30s; younger than the  
435 average age of patients with age-related clonal hematopoiesis. Of note, none of the  
436 *JAK2V617F*-positive PH patients met the criteria of hematological disorders including  
437 MPNs<sup>33</sup>. There were no significant differences in clinical characteristics, laboratory data  
438 including blood cell counts, echocardiographic parameters, or hemodynamics between  
439 the PH patients with and without the *JAK2V617F* mutation (Fig. 9c, d, Supplementary  
440 Table 3). These data indicate that clonal hematopoiesis with *JAK2V617F* is related to the  
441 onset and development of PH in the carriers of this mutant, regardless of blood cell counts  
442 or PH severity.

443 **Discussion**

444 The present study demonstrates that clonal hematopoiesis with JAK2V617F accelerated  
445 PH in both the absence and presence of phenotypic MPNs in mice. Neutrophils-derived  
446 vascular remodeling was involved in JAK2V617F-mediated PH development.  
447 JAK2V617F progressively upregulated *Acvr11* expression from BM stem/progenitor cells  
448 into neutrophils in pulmonary arterial regions in the lungs. JAK2V617F further increased  
449 ALK1-Smad1/5/8 signaling accompanied with increases in neutrophil-derived elastase  
450 activity and multiple chemokines, resulting in pulmonary arterial remodeling after  
451 chronic hypoxia. Correspondingly, *JAK2V617F*-positive clonal hematopoiesis was more  
452 common in the PH patients than in the healthy subjects, despite no signs of hematological  
453 disorders.

454 In the current study, we employed two experimental mouse models mimicking  
455 hematological clinical scenarios. Namely, in one model, *JAK2<sup>V617F</sup>* mice which displayed  
456 an MPN-like phenotype were used, and in the other, recipient mice transplanted with  
457 *JAK2<sup>V617F</sup>* BM cells were used to model clonal hematopoiesis without hematologic  
458 phenotypes. Both *JAK2<sup>V617F</sup>* mice and *JAK2<sup>V617F</sup>*-BMT mice similarly showed that the  
459 number of neutrophils was prominently increased specifically in pulmonary arterial  
460 regions, accompanied by vascular remodeling after chronic hypoxia, suggesting that  
461 JAK2 activation in neutrophils play a central role in PH. It is likely that the *JAK2<sup>V617F</sup>*  
462 neutrophils largely migrated into pulmonary arterial regions from BM. *JAK2V617F* may  
463 increase the adhesion and rolling of neutrophils partly due to increases in formyl peptide  
464 receptor (FPR)<sup>17</sup>, as our RNA sequencing data demonstrated that both *Fpr1* and *Fpr2*  
465 were higher in the Ly6G<sup>+</sup> lung neutrophils of *JAK2<sup>V617F</sup>* mice (3.1- and 3.8-fold,  
466 respectively) than in those of WT mice. Moreover, it is possible that the *JAK2<sup>V617F</sup>*

467 hematopoietic precursor cells in the lungs can display the capacity to lodge and complete  
468 maturation there. PH patients with or without MPNs have increased circulating CD34<sup>+</sup>  
469 hematopoietic stem/progenitor cells<sup>34</sup>. Engraftment of hematopoietic progenitors from  
470 PH patients who did not display any hematological disorder into xenografts showed  
471 increases in the growth of myeloid colonies and the expression of myeloid transcription  
472 factors, resulting in pulmonary vascular remodeling and right heart hypertrophy<sup>35</sup>,  
473 suggesting that the intrinsic capability of hematopoietic progenitors is associated with  
474 PH. In line with our JAK2<sup>V617F</sup>-BMT model that did not show elevation of white blood  
475 cells or platelets, the activation of JAK-STAT in myeloid cells may lead to PH phenotypes  
476 even without elevation of leukocyte or platelet counts. The rheological effects of  
477 leukocytes and thrombocytes on PH need to be clarified. JAK2<sup>V617F</sup> mice developed a PH  
478 pathology in response to chronic hypoxia, but did not develop PH in normoxia, indicating  
479 that JAK2V617F alone is not sufficient to induce PH, and that a trigger such as chronic  
480 hypoxia is required for PH phenotypes in JAK2<sup>V617F</sup> mice. In contrast, patients with  
481 MPNs can develop PH in the setting of normoxia. However, not all MPN patients develop  
482 PH. As MPNs occurs later in life<sup>36</sup>, an additional genetic and/or environmental hit in  
483 addition to JAK2V617F may be needed for the onset and development of PH in  
484 predisposed subjects.

485       Enhanced neutrophil-derived elastase activity is involved in the response of pulmonary  
486 arterial smooth muscle cells, resulting in excessive muscularity of the vessels<sup>3, 24, 37</sup>.  
487 Neutrophils produce a wide range of substances that could contribute to exaggerated  
488 contractility and proliferation of vascular cells, leading to vascular remodeling in the  
489 lungs<sup>38</sup>. While the infiltration of neutrophils was increased by hematopoietic JAK2V617F  
490 expression even after normoxia exposure, the increased JAK2<sup>V617F</sup> neutrophils did not

491 induce pulmonary vascular remodeling or elevate RVSP. RNA sequencing indicated that  
492 the differentiated JAK2<sup>V617F</sup> neutrophils in the lungs and PB, but not in BM myeloid cells  
493 or LSK cells, were activated in terms of protein secretion, degranulation and granulation  
494 after normoxia exposure. However, elastase activity or neutrophil-derived chemokines  
495 were not elevated in JAK2<sup>V617F</sup> lungs after normoxia exposure. These findings raise the  
496 possibility that biological mechanisms such as elastase activity by neutrophils, leading to  
497 pulmonary vascular remodeling, might be compensated, unless there is an additional  
498 factor, such as chronic hypoxia. Increased physical interactions of HIF1 $\alpha$  and STAT3<sup>39</sup> in  
499 response to hypoxia might trigger PH phenotypes in JAK2<sup>V617F</sup> mice, but further  
500 mechanisms and investigation by other PH models such as the monocrotaline-pyrrole  
501 need to be clarified.

502 The binding of STAT3 to *ACVRL1* promoter regions induced by *JAK2V617F*  
503 upregulated *ACVRL1* gene expression at the transcriptional level, in addition to the  
504 previously reported finding of transcriptional regulation of *ACVRL1*<sup>29</sup>. It is known that  
505 *ACVRL1* is one of the genes affected by germline mutations identified in patients with  
506 pulmonary arterial hypertension<sup>28</sup>. Germline mutations of *ACVRL1* also cause hereditary  
507 hemorrhagic telangiectasia, a dominant autosomal vascular dysplasia, and PH is  
508 recognized as a severe complication of this disease<sup>40, 41</sup>. It has been reported that *ACVRL1*  
509 mutations in hereditary hemorrhagic telangiectasia led to a loss of function<sup>42,43</sup>. Most of  
510 *ACVRL1* mutations found in pulmonary arterial hypertension are the same mutations  
511 described in HHT which result in a loss of function. The loss-of-function mutations in  
512 *ACVRL1* are important causes of heritable pulmonary arterial hypertension.<sup>44</sup>  
513 Consistently, heterozygous ALK1 knockout mice developed PH in adulthood<sup>45</sup>. In  
514 contrast, the inhibition of BMP9 partly protected chronic hypoxia-induced PH in the adult

515 mice and systemic administration of ALK1 inhibitor, a ligand trap targeting ALK1,  
516 prevented the monocrotaline and Sugen hypoxia-induced PH in the adult rats<sup>46</sup>,  
517 suggesting that systemic blockade of the BMP9/ALK1 pathways is beneficial for PH in  
518 the adult rodents. In the present study, we showed that ALK1/2 inhibitor administration  
519 prevented the progression of chronic hypoxia-induced PH in *JAK2*<sup>V617F</sup> mice, indicating  
520 that *JAK2*V617F-related ALK1 upregulation in myeloid cells had detrimental effects in  
521 PH. Although the molecular roles of ALK1 have been investigated particularly in  
522 endothelial cells, ALK1 expressions in myeloid cells may have a different impact on PH  
523 from the lung endothelial cells. As the functional relevance of ALK1 in PH is not fully  
524 understood, a conditional knockout model of hematopoietic cells is needed to clarify the  
525 role of ALK1 on PH in the hematopoietic system.

526 It has recently been reported that clonal hematopoiesis was especially associated with  
527 atherosclerotic cardiovascular diseases<sup>12,15</sup>. Among the somatic mutations related to  
528 clonal hematopoiesis, individuals with *JAK2*V617F showed a higher risk of coronary  
529 heart disease compared to those without CHIP and those with mutations other than  
530 *JAK2*V617F<sup>15</sup>. We showed here the association between clonal hematopoiesis and PH.  
531 Importantly, five out of the 70 PH patients (7.1%) were carriers of *JAK2*V617F-positive  
532 clonal hematopoiesis, three of whom fulfilled the criteria of CHIP, with a *JAK2*V617F  
533 VAF exceeding 2%. The remaining two patients were in their 30s and 50s, younger than  
534 the average age of patients with age-related clonal hematopoiesis. Our murine study  
535 demonstrated that even small clones with *JAK2*V617F led to PH development. Given that  
536 *JAK2*V617F VAF as low as 0.1–2% was associated with the elevation of blood cell  
537 counts, manifestations of MPNs, thrombotic events, and survival in both *JAK2*V617F-  
538 positive general populations without MPNs and patients with MPNs,<sup>47,48,49,50</sup> the presence



539 of *JAK2V617F*, even with low VAF, may have a clinically biological impact. Further  
540 study into the relationship between *JAK2V617F* VAF levels and PH prevalence is  
541 required.

542 Currently, no treatment has yet been established to prevent or directly modify clonal  
543 hematopoiesis-associated cardiovascular diseases. The JAK1/2 inhibitor ruxolitinib is  
544 now routinely used in patients with MF and PV for improvements of splenomegaly and  
545 disease-related symptoms<sup>51, 52</sup>. For MPN patients with PH complications, ruxolitinib has  
546 been shown efficacy to ameliorate PH only in a small number of patients<sup>53,54</sup> or has  
547 actually exacerbated PH in some cases<sup>55</sup>. There are concerns, such as hematologic  
548 toxicities, dysfunction of lymphocytes, and reactivation of viral infections, regarding the  
549 use of ruxolitinib for patients with clonal hematopoiesis without any hematologic  
550 disorders. The only possible treatment to eliminate clones with somatic mutations,  
551 including *JAK2V617F*, is hematopoietic stem cell transplantation, which is however often  
552 associated with serious comorbidity and treatment-related mortality. Moreover, it has  
553 recently been reported that PH is associated with poor outcome of hematopoietic stem  
554 cell transplantation in patients with MPNs<sup>56</sup>. Therefore, transplantation may not be a  
555 suitable strategy for PH patients with MPNs or clonal hematopoiesis, unless the patient  
556 is in a severe hematologic condition, such as acute leukemia.

557 Although medical therapies for PH, such as prostanoids and endothelin receptor  
558 antagonists, have been greatly improved, PH remains a progressive and fatal disease<sup>1</sup>.  
559 Precision medicine may be a novel approach that identifies *JAK2V617F*-positive PH  
560 patients regardless of the etiologies of PH. In the present study, we did not find any  
561 significant differences in clinical characteristics, including blood cell counts or  
562 hemodynamics, between the *JAK2V617F*-positive and -negative PH patients. In turn,

563 these findings suggest that examination of *JAK2V617F* may be a potential strategy, which  
564 may help in the diagnosis and treatment of *JAK2V617F*-positive PH patients.  
565 Furthermore, three patients with *JAK2V617F* were categorized into Group IV, implying  
566 that *JAK2V617F* promotes venous thrombosis resulting in pulmonary embolisms<sup>57</sup>;  
567 however, our murine data showed that pulmonary arterial structural remodeling was  
568 accelerated in the presence of hematopoietic *JAK2V617F* with no distinct features of  
569 venous thrombosis in the lungs. Notably, ALK1/2 inhibitors completely prevented  
570 chronic hypoxia-induced PH in *JAK2V617F*-mediated clonal hematopoiesis, without  
571 causing hematologic toxicity. Inhibition of ALK1/2 may be effective especially in the  
572 *JAK2V617F* lung neutrophils. Although we cannot exclude the potential effects of ALK2  
573 on PH, ALK1 is a promising therapeutic target for PH patients with clonal hematopoiesis  
574 induced by *JAK2V617F*.

575 A limitation of this study was that overexpression levels of the transgenic mice  
576 expressing murine *JAK2V617F* might non-specifically affect the varieties of individual  
577 phenotypes; therefore, we also used BMT models. In human studies, inherited genetic  
578 backgrounds or other CHIP-related mutations could not be determined in the PH patients  
579 in a small sample size. Future work is needed to validate our findings in larger cohorts.

580 In conclusion, we unveiled that a hematopoietic cell clone with *JAK2V617F* was  
581 involved in the development of PH with neutrophil-derived vascular remodeling with  
582 ALK1 upregulation. Our study provides an approach for precision medicine that  
583 identifies *JAK2V617F* in PH patients, and suggests ALK1 as a possible candidate of  
584 therapeutic target.

585

586 **Methods**

587 **Animals**

588 JAK2<sup>V617F</sup> mice of transgenic-*Jak2*<sup>V617F</sup> with a C57BL/6J background were obtained  
589 as described previously<sup>21,22</sup>. Female JAK2<sup>V617F</sup> mice aged between 8 and 10 weeks (body  
590 weight range, 18–24 g) were used in the present study. WT littermates were used as  
591 controls. CAG-EGFP reporter mice with a C57BL/6J background were purchased from  
592 Japan SLC. JAK2<sup>V617F</sup> mice were crossed with CAG-EGFP mice to generate  
593 JAK2<sup>V617F</sup>/CAG-EGFP double transgenic mice (JAK2<sup>V617F</sup>-GFP)<sup>27</sup>, and WT littermates  
594 were used as controls (WT-GFP). We used female mice unless otherwise indicated. Mice  
595 were housed with food and water ad libitum during 12-hour light/12-hour dark cycles  
596 (light, 7:00–19:00; dark, 19:00–7:00), and ambient temperature (21.5 °C) and humidity  
597 (55 ± 10%) were monitored.

598

599 **Peripheral blood analysis**

600 Blood was collected from the tail vein and blood cell counts were determined using  
601 Sysmex pochH-100i (Sysmex).

602

603 **Exposure to chronic hypoxia**

604 The mice were exposed to normoxia (21% O<sub>2</sub>) or hypoxia (10% O<sub>2</sub>) for 2 or 3 weeks in  
605 a ventilated chamber<sup>20</sup>. The hypoxic environment was kept in a mixture of air and  
606 nitrogen (Teijin Ltd.). The chamber was kept closed, and was only opened to supply food  
607 and water as well as for cleaning twice a week. In a Sugden-hypoxia model, the mice  
608 received a single weekly injection of a VEGF inhibitor, SU-5416 (HY-10374, Med Chem  
609 Express), at 20 mg/kg followed by 2 weeks of hypoxia (10% O<sub>2</sub>).

610

### 611 **Echocardiography**

612 Transthoracic echocardiography was performed using Vevo 2100 High-Resolution In  
613 Vivo Imaging System (Visual Sonics Inc.) with a 40-MHz imaging transducer. Mice were  
614 lightly anesthetized by titrating isoflurane (0.5–1.5%) to achieve a heart rate of around  
615 400/min. RV fractional area change, RV diastolic dimension, PA acceleration time, PA  
616 ejection time, RV anterior wall diameter, tricuspid annular plane systolic excursion,  
617 cardiac output, and LV fractional shortening were determined<sup>58</sup>.

618

### 619 **Hemodynamics and assessment for right ventricular hypertrophy**

620 After chronic exposure to normoxia or hypoxia, the mice were anesthetized by  
621 intraperitoneal injection of 2,2,2-tribromo-ethanol (0.25 mg/g per body weight)<sup>20</sup>. A 1.2F  
622 micromanometer catheter (Transonic Scisense Inc.) was inserted from the right jugular  
623 vein, and RVSP was continuously measured. The RVSP was blindly analyzed by  
624 LabScribe3 software (IWORX) and averaged over 10 sequential beats. To evaluate RV  
625 hypertrophy, the RV was dissected from the LV, including the septum, and RV/LV+S  
626 was calculated.

627

### 628 **Histological analysis**

629 Lung samples were fixed in 4% paraformaldehyde solution for paraffin embedding.  
630 Frozen lung tissues were embedded in the O.C.T. compound (Tissue-Tek). The paraffin-  
631 embedded sections were stained with H&E or Elastica-Masson (EM), or they were used  
632 for immunostaining. In the EM-stained sections, the wall area between the internal and  
633 external lamina of the pulmonary arteries with a diameter between 50 and 100  $\mu\text{m}$  was

634 measured and expressed as the percentage of medial wall thickness divided by the vessel  
635 area using ImageJ software (National Institutes of Health)<sup>58</sup>. In the sections stained with  
636  $\alpha$ SMA (M0851, Dako), the pulmonary vessels with a diameter of less than 50  $\mu$ m were  
637 classified into three groups; the vessels with  $\alpha$ SMA-positives throughout the entire  
638 circumference of the vessel cross-section was defined as “fully” muscularized, the vessels  
639 with  $\alpha$ SMA-positives with 5–99% around the vessel was defined as “partially”  
640 muscularized, and the vessels with  $\alpha$ SMA-positives with < 5% around the vessel was  
641 classified as “non” muscularized.<sup>58</sup> Based on the anatomical characteristics, pulmonary  
642 arteries, distributed along the bronchi and displayed an eccentric morphology with thick  
643 and elastic walls, are distinguishable from pulmonary veins. The percentage of  
644 muscularized pulmonary vessels was determined by dividing the sum of the partially and  
645 fully muscular vessels by the total number of vessels<sup>58</sup>. For immunofluorescence staining,  
646 the paraffin-embedded tissue sections were incubated with primary antibodies against  
647 Ly6G (1:100, ab25377, Abcam), CD45 (1:100, 70257, Cell Signaling Technology; sc-  
648 53665, Santa Cruz Biotechnology Inc.), F4/80 (1:100, 70076, Cell Signaling  
649 Technology), CD45R (1:100, 103201, Biolegend), Ki67 (1:100, ab15580, Abcam),  
650  $\alpha$ SMA (1:100, M0851, Dako; 19245, Cell Signaling Technology), or GFP (1:100, NBP2-  
651 22111, Novus Biologicals). This was followed by incubation with the appropriate  
652 secondary antibodies, including Alexa Fluor 488 (1:1000, ab150105, Abcam), Alexa  
653 Fluor 594 (1:1000, R37119, A-21211; Thermo Fisher Scientific), and Alexa Fluor 647  
654 (1:1000, ab150159, Abcam), then mounted with DAPI-containing mounting media  
655 (Fluoro Gel II, Electron Microscopy Sciences). Immunohistochemical staining of the  
656 paraffin-embedded or O.C.T.-embedded sections was performed with the following  
657 primary antibodies; CD41 (1:100, ab63983, Abcam) or TER-119 (1:100, 116201,

658 BioLegend) followed by anti-rabbit or anti-rat IgG antibody labeled with peroxidase  
659 (14341F, 414311F, Nichirei Bioscience) with DAB peroxidase substrate system (Dojin  
660 Co., Ltd.) and counterstaining with hematoxylin. For quantification of perivascular  
661 cellular infiltration, more than 100 cells were counted around the distal pulmonary  
662 arteries, with a diameter of 50–100  $\mu\text{m}$  in each mouse<sup>59</sup>. All images were acquired by a  
663 microscope (BZ-X700, Keyence Co.) using Keyence BZ II Viewer software (Keyence  
664 Co.).

665

#### 666 **Western blot analysis**

667 Snap frozen mouse lung samples or cultured cells were initially homogenized in lysis  
668 buffer (Cell Lysis Buffer, Cell Signaling Technology) containing protease inhibitor  
669 cocktail (BD Biosciences)<sup>60</sup>. Protein concentration was determined using a Pierce BCA  
670 Protein Assay Kit (Thermo Fisher Scientific). Aliquots of proteins were subjected to  
671 SDS-polyacrylamide gel electrophoresis, transferred onto polyvinylidene difluoride  
672 membranes (Merck Millipore), and probed with the following primary antibodies; HIF1 $\alpha$   
673 (1:1000, 36169, Cell Signaling Technology), Phospho-STAT3 (1:1000, 9145, Cell  
674 Signaling Technology), STAT3 (1:1000, 4904, Cell Signaling Technology), Phospho-  
675 Smad1/Smad5/Smad8 (1:1000, AB3848-I, Merck Millipore), Smad1 (1:1000, 9743, Cell  
676 Signaling Technology), ALK1 (1:1000, 14745-1-AP, Proteintech), ALK2 (1:1000,  
677 MAB637, R&D Systems) and GAPDH (1:1000, 60004-1-Ig, Proteintech) followed by  
678 appropriate goat anti-rabbit or mouse horseradish peroxidase-conjugated secondary  
679 antibodies (1:10000, sc-2357, sc-516102, Santa Cruz Biotechnology Inc.).  
680 Immunoreactive bands were visualized by an Amersham ECL system (Amersham  
681 Pharmacia Biotech UK Ltd.), and signals were detected with an ImageQuant LAS-4000

682 digital imaging system (GE Healthcare). Or fluorescent immunoreactive bands were  
683 detected by an Odyssey CLX imaging system (LI-COR Biosciences) when the  
684 appropriate IRDye 680 or IRDye 800 secondary antibodies (1:20000, 925-68070, 925-  
685 68071, 925-32210, 925-32210, LI-COR Biosciences) were used. Optical densities of  
686 individual bands were analyzed using ImageJ software or Image Studio software (LI-  
687 COR Biosciences).

688

### 689 **Reverse transcription quantitative polymerase chain reaction (RT-qPCR)**

690 Total RNA was extracted from mouse lungs, sorted cells or cultured cells using Trizol  
691 reagent according to the manufacture's protocol (Thermo Fisher Scientific). The RNA  
692 from the lung samples was further purified using RNeasy Fibrous Tissue Mini Kit  
693 (Qiagen Inc.). cDNA was synthesized using ReverTra Ace qPCR RT Master Mix  
694 (Toyobo Co., Ltd.). Quantitative PCR was performed to determine the mRNA expression  
695 of *Ccl2*, *Cxcl1*, *Ccr1*, *Cxcr2*, *Pdgfrb*, *Tgfb1*, *Acvr11*, *Acvr1*, and *Bmpr2* using  
696 THUNDERBIRD SYBR qPCR Mix (Toyobo Co., Ltd.) in a CFX Connect real-time PCR  
697 System (Bio-Rad) with Bio-Rad CFX Manager 3.1 software (Bio-Rad). A standard curve  
698 method on serially diluted templates was applied for the lung samples, and a delta CT  
699 method was used for the cell samples. All data were normalized to *18s rRNA* and  
700 expressed as a fold increase of the control group. Primer sequences are described in  
701 Supplementary Table 4.

702

### 703 **Elastase assay**

704 Elastase activity in the lung tissue was evaluated using the EnzChek Elastase Assay Kit  
705 (Molecular Probes)<sup>24, 61</sup>. Briefly, the frozen lung samples (20 mg) were homogenized and

706 mixed with the extraction buffer containing NaAc and Na azide, and then rotated  
707 overnight at 4°C. After centrifuge, the pellet was reextracted by adding (NH<sub>4</sub>)<sub>2</sub>SO<sub>4</sub> buffer.  
708 After overnight precipitation, the centrifuged pellet was resuspended in 50 mM TrisHCl  
709 assay buffer (pH 8.0) to reactivate the elastase. Elastase activity was then measured by  
710 adding bovine DQ-Elastin as a fluorogenic substrate in duplicate wells.

711

### 712 **Bone marrow transplantation (BMT)**

713 Recipient female C57BL/6J mice aged between 8 and 10 weeks (Charles River Japan,  
714 Inc.) were lethally irradiated with a total dose of 9.0 Gy 24 h before BMT<sup>22</sup>. Whole BM  
715 cells were harvested from donor femurs and tibiae. The cells were washed with PBS and  
716  $5.0 \times 10^6$  of BM cells were injected in the recipient mice via the tail vein. Peripheral blood  
717 parameters and chimerism were analyzed at 4 weeks after transplantation and at the  
718 termination of the experiments. DNA was isolated using the QuickGene DNA whole  
719 blood kit (KURABO) and quantitative PCR was performed using THUNDERBIRD  
720 SYBR qPCR Mix with the following primers; forward primer for donor and recipients,  
721 5'-CTTTCTTCGAAGCAGCAAGCATGA-3', reverse primer for recipients; 5'-  
722 CTGGCTTTACTTACTCTCCTCTCCACAGAC-3' reverse primer for donors; 5'-  
723 AACCAGAATGTTCTCCTCTCCACAGAA-3'. Delta Ct ( $Ct_{\text{donor}} - Ct_{\text{total}}$ ) was calculated  
724 to estimate *Jak2*<sup>V617F</sup> VAF in JAK2<sup>V617F</sup>-BMT mice.

725

### 726 **Magnetic-activated cell sorting (MACS)**

727 Myeloid cells and neutrophils from the BM, PB and lungs were isolated by using MACS  
728 MS columns (Miltenyi Biotec GmbH) with Ly6G MicroBeads according to the  
729 manufacturer's protocols. To form a cell suspension from the lungs, the tissues were



730 minced and digested in 2 mg/mL collagenase type II (Worthington Biochemical) for 30  
731 min. Then the tissues were passed through an 18-gauge needle and a 70 µm cell strainer.  
732 The purity of the neutrophils was > 98% as determined by May-Giemsa staining, and the  
733 specificity was confirmed with positive immunostaining by anti-Ly6G (ab25377, Abcam)  
734 and anti-Myeloperoxidase (ab9535, Abcam) antibodies and with negative  
735 immunostaining by an anti-CD31 antibody (102401, BioLegend). The hematopoietic  
736 stem progenitor cells from the lungs were isolated using CD117 MicroBeads. The  
737 endothelial cells from the lungs were isolated by CD31 MicroBeads. All MicroBeads  
738 were purchased from Miltenyi Biotec GmbH.

739

#### 740 **Flow cytometry**

741 Leukocytes were isolated from the peripheral blood and the lungs. The single cell  
742 suspensions from the lung tissues were prepared by the same methods described in  
743 MACS. After lysing red blood cells using an ammonium chloride-containing buffer, cells  
744 were stained with the relevant antibodies (CD45.2, 109814, BioLegend; Ly6G, 560599,  
745 BD Biosciences), assessed by flow cytometry using a FACSCanto II (BD Biosciences)  
746 and analyzed by FlowJo (version 10.2, Tree Star Inc.).<sup>22</sup> HCT116 cells were collected  
747 and incubated with an anti-ALK1 antibody (14745-1-AP, Proteintech) followed by R-  
748 PE-conjugated donkey anti-rabbit secondary antibody (711-116-152, Jackson  
749 ImmunoResearch). The gating strategies are provided in Supplementary Fig. 33.

750

#### 751 **Transwell chemotaxis assays**

752 Chemotaxis in neutrophils from mouse blood was assessed using CytoSelect 96-well (3  
753 µm, Fluorometric Format) according to the manufacturer's protocol.

754

755 **Colony assay**

756 The MACS-isolated lung CD117<sup>+</sup> cells were cultured in 1 mL of MethoCult M3434  
757 (Stemcell Technologies) on a 35-mm plate. After 7 days, types of colonies and colony  
758 numbers were determined based on manufacturer's instructions. Images were captured  
759 by BZ-X700 microscope.

760

761 **RNA sequencing**

762 RNA from MACS-isolated Ly6G<sup>+</sup> cells from the BM, PB and lungs was purified using  
763 an RNeasy Plus Micro Kit (Qiagen) according to the manufacturer's protocol. RNA  
764 concentrations and integrities were evaluated using the TapeStation (Agilent). Total RNA  
765 was subjected to reverse transcription and amplification with the SMARTer Ultra Low  
766 Input RNA Kit for Sequencing (Clontech). After sonication using ultrasonicator  
767 (Covaris), the libraries for RNA sequencing were generated from fragmented DNA with  
768 10 cycles of amplification using a NEB Next Ultra DNA Library Prep Kit (New England  
769 BioLabs). After the libraries were quantified using the TapeStation (Agilent), the samples  
770 were subjected to sequencing with Hiseq2500 (Illumina) and 61 cycles of the sequencing  
771 reactions were performed. TopHat2 (version 2.0.13; with default parameters) and  
772 Bowtie2 (version 2.1.0) were used for alignment to the reference mouse genome (mm10  
773 from the University of California, Santa Cruz Genome Browser;  
774 <http://genome.ucsc.edu/>). Levels of gene expression were quantified using Cuffdiff  
775 (Cufflinks version 2.2.1; with default parameters). We also used the data from our  
776 previous study's RNA sequencing of flow cytometry-sorted LSK cells.<sup>22</sup>

777

778 **Analyses of pathways and gene set enrichment**

779 Affected pathways or gene set enrichment were compared among Ly6G<sup>+</sup> cells from the  
780 lungs, PB, and BM, and LSK cells from our previous study<sup>22</sup> using the comparison  
781 analysis in IPA™ (Ingenuity Pathways Analysis, Qiagen) or Gene Set Enrichment  
782 Analysis (GSEA, Broad Institute), respectively, according to the RPKM+1 value for each  
783 gene determined by RNA sequencing.

784

785 **Immunoprecipitation**

786 Samples of JAK2<sup>V617F</sup> mouse lung tissue were lysed with lysis buffer (75 mmol/L NaCl,  
787 50 mmol/L Tris-HCl, 0.5% Nonidet P-40, pH 8.0) with a protease inhibitor cocktail.  
788 Protein was subjected to immunoprecipitation using protein A-coupled magnetic beads  
789 (Thermo Fisher Scientific) and an anti-HIF1 $\alpha$  antibody (36169, Cell Signaling  
790 Technology) for 1 h at room temperature. Rabbit IgG was used as control.

791

792 **Preparation of primary pulmonary arterial smooth muscle cells (PASMCs) and**  
793 **assessment of proliferation using neutrophil-derived conditioned medium**

794 Mouse PASMCs were isolated from WT mice with a C57BL/6J background by  
795 enzymatic dissociation of the minced lung with collagenase type II (Worthington)<sup>58</sup> and  
796 cultured in DMEM (Wako) containing 20% fetal bovine serum. The PASMCs were  
797 seeded in 96-well plates or on coverslips in 24-well plates. Conditioned medium from  
798 neutrophils in hypoxia incubator chamber (10% O<sub>2</sub>, ASTEC) 3 h after incubation was  
799 collected. The neutrophils were pretreated with Echinomycin (Sigma) prior to hypoxia  
800 for 1 h. Then, the PASMCs were incubated with the conditioned medium for 48 h and  
801 then subjected to CellTiter 96 AQueous One Solution Cell Proliferation Assay (Promega)

802 and immunofluorescent analysis with anti-Ki67 (NB600-1252, Novus Biologicals) and  
803  $\alpha$ SMA (19245, Cell Signaling Technology) antibodies.

804

#### 805 **Cell culture**

806 *JAK2*<sup>V617F/+</sup> knock-in HCT116 cells as well as wild-type *JAK2*<sup>+/+</sup> HCT116 cells were  
807 purchased from Horizon Discovery Ltd. The cells were cultured in RPMI 1640 (Sigma)  
808 containing 2 mM L-glutamine and 25 mM sodium bicarbonate supplemented with 10%  
809 FBS, 100 mg/mL of streptomycin and 100 IU/mL of penicillin at 37 °C in the presence  
810 of 5% CO<sub>2</sub>. Recombinant human BMP9 was purchased from Biolegend, Inc. Cells were  
811 transfected with scrambled negative control siRNA (1022076, Qiagen) or *ACVRL1*-  
812 specific siRNA (VHS41063, 129001, Thermo Fisher Scientific) using Lipofectamine  
813 RNAiMAX (Thermo Fisher Scientific) according to manufacturer's instructions.

814

#### 815 **Prediction of STAT binding sites on *ACVRL1* promotor**

816 To search for putative STAT binding sites on *ACVRL1* promotor, the *in silico* analysis  
817 was performed using the online databases JASPAR and TFBIND/TRANSFAC<sup>62</sup>.

818

#### 819 **ChIP-qPCR**

820 ChIP assays were performed using SimpleChIP enzymatic chromatin IP kit with magnetic  
821 beads (9003, Cell Signaling Technology). The crosslinked chromatin was digested with  
822 micrococcal nuclease followed by sonication to break into 150–900 bp fragments.  
823 Immunoprecipitation was performed using anti-STAT3 (4904, Cell Signaling  
824 Technology) or Rabbit IgG. The enriched fragments were purified and analyzed by qPCR.  
825 The signal relative to input was evaluated using the formula as follows; percent input =

826  $2\% \times 2^{(CT\ 2\% \text{ input sample} - CT\ \text{IP sample})}$ , where CT indicates threshold cycle of qPCR reaction;  
827 IP, immunoprecipitation. The qPCR primers used are listed in Supplementary Table 5.

828

### 829 **Construction of DNA plasmid and dual luciferase assay**

830 The putative human *ACVRL1* promoter sequence (GeneBank: NC\_000012.12, position  
831 51906383 to 51907627) was amplified by the forward primer; 5'-  
832 GGGGGTACCATAACCAGGAGGCTAGG-3' and the reverse primer; 5'-  
833 TTTAAGCTTCGCGGCCGCAGTTG-3'. The obtained fragment was then subcloned  
834 into pGL3-basic vector (Promega) at the KpnI and HindIII sites<sup>29</sup>. The construct was  
835 verified by restriction digestion and DNA sequencing. The pGL3-basic vector containing  
836 the putative *ACVRL1* promoter region and pNL1.1.TK [Nluc/TK] as a control vector were  
837 co-transfected by using ScreenFect A Plus (Wako) according to the manufacturer's  
838 protocol. The promoter activity of *ACVRL1* was determined by using Dual-Glo  
839 Luciferase Assay System (Promega). The cells were incubated with ruxolitinib (Novartis  
840 Pharmaceuticals) or stattic (Cayman Chemical) for 24 h prior to the luciferase assay. Each  
841 experiment was performed in duplicate.

842

### 843 **Administration of ALK1/2 inhibitors**

844 The ALK1/2 inhibitor, K02288 (12 or 24 mg/kg body weight, Selleck Chemicals) or  
845 LDN-212854 (9 mg/kg body weight, Selleck Chemicals), dissolved in DMSO was  
846 administered to mice via an intraperitoneal injection a week for 2 weeks. DMSO was used  
847 as a control.

848

### 849 **Human blood samples and clinical data**

850 We prospectively analyzed the blood samples taken from patients with PH (n = 70) and  
851 control subjects (n = 83) between April 2018 and April 2020 at Fukushima Medical  
852 University Hospital. PH was diagnosed according to the 2015 European Respiratory  
853 Society guidelines<sup>1</sup> by independent cardiologists. For the control group, we recruited  
854 healthy volunteers or patients with no history of PH or no history of cardiopulmonary  
855 diseases. The blood samples were collected in a polypropylene tube containing EDTA-  
856 2Na (TERUMO). Genomic DNA was extracted from 200  $\mu$ L whole blood by using a  
857 QuickGene DNA whole blood kit. The *JAK2V617F* VAF was determined by an allelic  
858 discrimination PCR assay using THUNDERBIRD Probe qPCR Mix (TOYOBO) in a  
859 QuantStudio 3 real-time PCR system (Thermo Fisher Scientific). We used the primers,  
860 probe and protocols described in Assay 5 in previous literature (Supplementary Table  
861 6)<sup>32</sup>. The *JAK2V617F* VAF was calculated by Delta Ct ( $Ct_{JAK2V617F} - Ct_{wild-type}$ ) and  
862 expressed as the percentage of *JAK2V617F* divided by total *JAK2* ( $JAK2V617F /$   
863  $JAK2V617F + JAK2_{wild-type}$ )<sup>63</sup>. Clinical information, including hospital laboratory  
864 data, echocardiographic analysis and hemodynamic assessment by right heart  
865 catheterization, was collected with our standard clinical practice<sup>64, 65</sup>.

866

### 867 **Ethical statement**

868 All animal studies were reviewed and approved by the Fukushima Medical University  
869 Animal Research Committee (approval number; 2019084). The protocols were compliant  
870 with relevant ethical regulations, and all experiments were performed in accordance with  
871 the guidelines provided in the Guide for the Use and Care of Laboratory Animals from  
872 the Institute for Laboratory Animal Research. All efforts were made to minimize the  
873 suffering of the animals. The protocols for human participants were approved by the

874 institutional ethics committee of Fukushima Medical University Hospital (approval  
875 number; 29348). Written informed consent was given by all subjects. This study complied  
876 with all relevant regulations regarding the use of human study participants and was  
877 conducted in accordance to the criteria set by the 1975 Declaration of Helsinki.

878

### 879 **Statistical analysis**

880 Comparisons of values between two groups were performed by the unpaired or paired  
881 Student's t-test, or Mann-Whitney U-test. When more than two groups were evaluated,  
882 one-way ANOVA or two-way ANOVA was performed followed by multiple comparisons  
883 with the Tukey test. Categorical variables were compared using Fisher's exact test or Chi-  
884 square test. Statistical analyses were performed using the Statistical Package for Social  
885 Sciences version 26 (SPSS Inc) or GraphPadPrism version 8.1.2 (GraphPad Software). A  
886 value of  $P < 0.05$  was considered statistically significant.

887

### 888 **Data availability**

889 The RNA sequencing data generated in this study have been deposited in the DNA Data  
890 Bank of Japan database under accession code DDBJ PRJDB9389  
891 [<https://ddbj.nig.ac.jp/DRAsearch/study?acc=DRP007018>]. The putative STAT binding  
892 sites were assessed using JASPAR [<http://jaspar.genereg.net/>] and TFBIND/TRANSFAC  
893 [<https://tfbind.hgc.jp/>] databases. Source data are provided with this paper. Any remaining  
894 raw data will be available from the corresponding author upon reasonable request.

895

896

897 **References**

898

899 1. Galie N, *et al.* 2015 ESC/ERS Guidelines for the diagnosis and treatment of  
900 pulmonary hypertension: The Joint Task Force for the Diagnosis and Treatment  
901 of Pulmonary Hypertension of the European Society of Cardiology (ESC) and the  
902 European Respiratory Society (ERS): Endorsed by: Association for European  
903 Paediatric and Congenital Cardiology (AEPC), International Society for Heart  
904 and Lung Transplantation (ISHLT). *Eur Heart J* **37**, 67-119 (2016).

905

906 2. Tudor RM, Marecki JC, Richter A, Fijalkowska I, Flores S. Pathology of  
907 pulmonary hypertension. *Clin Chest Med* **28**, 23-42, vii (2007).

908

909 3. Rabinovitch M, Guignabert C, Humbert M, Nicolls MR. Inflammation and  
910 immunity in the pathogenesis of pulmonary arterial hypertension. *Circ Res* **115**,  
911 165-175 (2014).

912

913 4. Machado RF, Farber HW. Pulmonary hypertension associated with chronic  
914 hemolytic anemia and other blood disorders. *Clin Chest Med* **34**, 739-752 (2013).

915

916 5. Dingli D, Utz JP, Krowka MJ, Oberg AL, Tefferi A. Unexplained pulmonary  
917 hypertension in chronic myeloproliferative disorders. *Chest* **120**, 801-808 (2001).

918

919 6. Venton G, *et al.* Pulmonary hypertension in patients with myeloproliferative  
920 neoplasms: A large cohort of 183 patients. *Eur J Intern Med* **68**, 71-75 (2019).



921

922 7. Simonneau G, *et al.* Updated clinical classification of pulmonary hypertension. *J*  
923 *Am Coll Cardiol* **62**, D34-41 (2013).

924

925 8. Levine RL, Gilliland DG. Myeloproliferative disorders. *Blood* **112**, 2190-2198  
926 (2008).

927

928 9. Vainchenker W, Kralovics R. Genetic basis and molecular pathophysiology of  
929 classical myeloproliferative neoplasms. *Blood* **129**, 667-679 (2017).

930

931 10. Campbell PJ, Green AR. The myeloproliferative disorders. *N Engl J Med* **355**,  
932 2452-2466 (2006).

933

934 11. James C, *et al.* A unique clonal JAK2 mutation leading to constitutive signalling  
935 causes polycythaemia vera. *Nature* **434**, 1144-1148 (2005).

936

937 12. Jaiswal S, *et al.* Age-related clonal hematopoiesis associated with adverse  
938 outcomes. *N Engl J Med* **371**, 2488-2498 (2014).

939

940 13. Genovese G, *et al.* Clonal hematopoiesis and blood-cancer risk inferred from  
941 blood DNA sequence. *N Engl J Med* **371**, 2477-2487 (2014).

942

943 14. Bejar R. CHIP, ICUS, CCUS and other four-letter words. *Leukemia* **31**, 1869-  
944 1871 (2017).

945

946 15. Jaiswal S, *et al.* Clonal Hematopoiesis and Risk of Atherosclerotic Cardiovascular  
947 Disease. *N Engl J Med* **377**, 111-121 (2017).

948

949 16. Fuster JJ, *et al.* Clonal hematopoiesis associated with TET2 deficiency accelerates  
950 atherosclerosis development in mice. *Science* **355**, 842-847 (2017).

951

952 17. Wang W, *et al.* Macrophage Inflammation, Erythrophagocytosis, and Accelerated  
953 Atherosclerosis in Jak2 (V617F) Mice. *Circ Res* **123**, e35-e47 (2018).

954

955 18. Barbui T, *et al.* Development and validation of an International Prognostic Score  
956 of thrombosis in World Health Organization-essential thrombocythemia (IPSET-  
957 thrombosis). *Blood* **120**, 5128-5133; quiz 5252 (2012).

958

959 19. Gomez-Arroyo J, *et al.* A brief overview of mouse models of pulmonary arterial  
960 hypertension: problems and prospects. *Am J Physiol Lung Cell Mol Physiol* **302**,  
961 L977-991 (2012).

962

963 20. Sugimoto K, Yokokawa T, Misaka T, Nakazato K, Ishida T, Takeishi Y.  
964 Senescence Marker Protein 30 Deficiency Exacerbates Pulmonary Hypertension  
965 in Hypoxia-Exposed Mice. *Int Heart J* **60**, 1430-1434 (2019).

966

967 21. Shide K, *et al.* Development of ET, primary myelofibrosis and PV in mice  
968 expressing JAK2 V617F. *Leukemia* **22**, 87-95 (2008).

969

970 22. Ueda K, *et al.* Hmga2 collaborates with JAK2V617F in the development of  
971 myeloproliferative neoplasms. *Blood Adv* **1**, 1001-1015 (2017).

972

973 23. Farber HW, *et al.* Five-Year outcomes of patients enrolled in the REVEAL  
974 Registry. *Chest* **148**, 1043-1054 (2015).

975

976 24. Cowan KN, Heilbut A, Humpl T, Lam C, Ito S, Rabinovitch M. Complete reversal  
977 of fatal pulmonary hypertension in rats by a serine elastase inhibitor. *Nat Med* **6**,  
978 698-702 (2000).

979

980 25. Ciucan L, *et al.* A novel murine model of severe pulmonary arterial hypertension.  
981 *Am J Respir Crit Care Med* **184**, 1171-1182 (2011).

982

983 26. Lundberg P, *et al.* Myeloproliferative neoplasms can be initiated from a single  
984 hematopoietic stem cell expressing JAK2-V617F. *J Exp Med* **211**, 2213-2230  
985 (2014).

986

987 27. Okabe M, Ikawa M, Kominami K, Nakanishi T, Nishimune Y. 'Green mice' as a  
988 source of ubiquitous green cells. *FEBS Lett* **407**, 313-319 (1997).

989

990 28. Soubrier F, *et al.* Genetics and genomics of pulmonary arterial hypertension. *J Am*  
991 *Coll Cardiol* **62**, D13-21 (2013).

992

- 993 29. Garrido-Martin EM, *et al.* Characterization of the human Activin-A receptor type  
994 II-like kinase 1 (ACVRL1) promoter and its regulation by Sp1. *BMC Mol Biol* **11**,  
995 51 (2010).
- 996
- 997 30. Sanvitale CE, *et al.* A new class of small molecule inhibitor of BMP signaling.  
998 *PLoS One* **8**, e62721 (2013).
- 999
- 1000 31. Mohedas AH, Xing X, Armstrong KA, Bullock AN, Cuny GD, Yu PB.  
1001 Development of an ALK2-biased BMP type I receptor kinase inhibitor. *ACS Chem*  
1002 *Biol* **8**, 1291-1302 (2013).
- 1003
- 1004 32. Jovanovic JV, *et al.* Establishing optimal quantitative-polymerase chain reaction  
1005 assays for routine diagnosis and tracking of minimal residual disease in JAK2-  
1006 V617F-associated myeloproliferative neoplasms: a joint European  
1007 LeukemiaNet/MPN&MPNr-EuroNet (COST action BM0902) study. *Leukemia*  
1008 **27**, 2032-2039 (2013).
- 1009
- 1010 33. Arber DA, *et al.* The 2016 revision to the World Health Organization classification  
1011 of myeloid neoplasms and acute leukemia. *Blood* **127**, 2391-2405 (2016).
- 1012
- 1013 34. Farha S, *et al.* Hypoxia-inducible factors in human pulmonary arterial  
1014 hypertension: a link to the intrinsic myeloid abnormalities. *Blood* **117**, 3485-3493  
1015 (2011).
- 1016

- 1017 35. Asosingh K, *et al.* Pulmonary vascular disease in mice xenografted with human  
1018 BM progenitors from patients with pulmonary arterial hypertension. *Blood* **120**,  
1019 1218-1227 (2012).  
1020
- 1021 36. Srour SA, *et al.* Incidence and patient survival of myeloproliferative neoplasms  
1022 and myelodysplastic/myeloproliferative neoplasms in the United States, 2001-12.  
1023 *Br J Haematol* **174**, 382-396 (2016).  
1024
- 1025 37. Zaidi SH, You XM, Ciura S, Husain M, Rabinovitch M. Overexpression of the  
1026 serine elastase inhibitor elafin protects transgenic mice from hypoxic pulmonary  
1027 hypertension. *Circulation* **105**, 516-521 (2002).  
1028
- 1029 38. Taylor S, Dirir O, Zamanian RT, Rabinovitch M, Thompson AAR. The Role of  
1030 Neutrophils and Neutrophil Elastase in Pulmonary Arterial Hypertension. *Front*  
1031 *Med (Lausanne)* **5**, 217 (2018).  
1032
- 1033 39. Pawlus MR, Wang L, Hu CJ. STAT3 and HIF1alpha cooperatively activate HIF1  
1034 target genes in MDA-MB-231 and RCC4 cells. *Oncogene* **33**, 1670-1679 (2014).  
1035
- 1036 40. McDonald J, Wooderchak-Donahue W, VanSant Webb C, Whitehead K,  
1037 Stevenson DA, Bayrak-Toydemir P. Hereditary hemorrhagic telangiectasia:  
1038 genetics and molecular diagnostics in a new era. *Front Genet* **6**, 1 (2015).  
1039
- 1040 41. Yokokawa T, *et al.* A Case of Pulmonary Hypertension and Hereditary

- 1041 Hemorrhagic Telangiectasia Related to an ACVRL1 Mutation. *Intern Med*,  
1042 (2019).  
1043
- 1044 42. Ricard N, *et al.* Functional analysis of the BMP9 response of ALK1 mutants from  
1045 HHT2 patients: a diagnostic tool for novel ACVRL1 mutations. *Blood* **116**, 1604-  
1046 1612 (2010).  
1047
- 1048 43. Alaa El Din F, *et al.* Functional and splicing defect analysis of 23 ACVRL1  
1049 mutations in a cohort of patients affected by Hereditary Hemorrhagic  
1050 Telangiectasia. *PLoS One* **10**, e0132111 (2015).  
1051
- 1052 44. Trembath RC, *et al.* Clinical and molecular genetic features of pulmonary  
1053 hypertension in patients with hereditary hemorrhagic telangiectasia. *N Engl J Med*  
1054 **345**, 325-334 (2001).  
1055
- 1056 45. Jerkic M, *et al.* Pulmonary hypertension in adult Alk1 heterozygous mice due to  
1057 oxidative stress. *Cardiovasc Res* **92**, 375-384 (2011).  
1058
- 1059 46. Tu L, *et al.* Selective BMP-9 Inhibition Partially Protects Against Experimental  
1060 Pulmonary Hypertension. *Circ Res* **124**, 846-855 (2019).  
1061
- 1062 47. Nielsen C, Bojesen SE, Nordestgaard BG, Kofoed KF, Birgens HS. JAK2V617F  
1063 somatic mutation in the general population: myeloproliferative neoplasm  
1064 development and progression rate. *Haematologica* **99**, 1448-1455 (2014).

1065

1066 48. Perricone M, *et al.* The relevance of a low JAK2V617F allele burden in clinical  
1067 practice: a monocentric study. *Oncotarget* **8**, 37239-37249 (2017).

1068

1069 49. Cordua S, Kjaer L, Skov V, Pallisgaard N, Hasselbalch HC, Ellervik C. Prevalence  
1070 and phenotypes of JAK2 V617F and calreticulin mutations in a Danish general  
1071 population. *Blood* **134**, 469-479 (2019).

1072

1073 50. Limvorapitak W, Parker J, Hughesman C, McNeil K, Foltz L, Karsan A. No  
1074 Differences in Outcomes Between JAK2 V617F-Positive Patients with Variant  
1075 Allele Fraction < 2% Versus 2-10%: A 6-Year Province-wide Retrospective  
1076 Analysis. *Clin Lymphoma Myeloma Leuk* **20**, e569-e578 (2020).

1077

1078 51. Harrison C, *et al.* JAK inhibition with ruxolitinib versus best available therapy for  
1079 myelofibrosis. *N Engl J Med* **366**, 787-798 (2012).

1080

1081 52. Vannucchi AM, *et al.* Ruxolitinib versus standard therapy for the treatment of  
1082 polycythemia vera. *N Engl J Med* **372**, 426-435 (2015).

1083

1084 53. Tabarroki A, *et al.* Ruxolitinib leads to improvement of pulmonary hypertension  
1085 in patients with myelofibrosis. *Leukemia* **28**, 1486-1493 (2014).

1086

1087 54. Miyawaki H, *et al.* Long-term Effects of the Janus Kinase 1/2 Inhibitor  
1088 Ruxolitinib on Pulmonary Hypertension and the Cardiac Function in a Patient

- 1089 with Myelofibrosis. *Intern Med* **59**, 229-233 (2020).
- 1090
- 1091 55. Low AT, Howard L, Harrison C, Tulloh RM. Pulmonary arterial hypertension  
1092 exacerbated by ruxolitinib. *Haematologica* **100**, e244-245 (2015).
- 1093
- 1094 56. Gupta R, *et al.* Pulmonary hypertension is associated with increased nonrelapse  
1095 mortality after allogeneic hematopoietic cell transplantation for myelofibrosis.  
1096 *Bone Marrow Transplant*, (2019).
- 1097
- 1098 57. Edelmann B, *et al.* JAK2-V617F promotes venous thrombosis through  
1099 beta1/beta2 integrin activation. *J Clin Invest* **128**, 4359-4371 (2018).
- 1100
- 1101 58. Kikuchi N, *et al.* Selenoprotein P Promotes the Development of Pulmonary  
1102 Arterial Hypertension. *Circulation* **138**, 600-623 (2018).
- 1103
- 1104 59. Chen G, *et al.* Inhibition of CRTH2-mediated Th2 activation attenuates  
1105 pulmonary hypertension in mice. *J Exp Med* **215**, 2175-2195 (2018).
- 1106
- 1107 60. Misaka T, *et al.* Deficiency of senescence marker protein 30 exacerbates  
1108 angiotensin II-induced cardiac remodelling. *Cardiovasc Res* **99**, 461-470 (2013).
- 1109
- 1110 61. Spiekerkoetter E, *et al.* Reactivation of gammaHV68 induces neointimal lesions  
1111 in pulmonary arteries of S100A4/Mts1-overexpressing mice in association with  
1112 degradation of elastin. *Am J Physiol Lung Cell Mol Physiol* **294**, L276-289 (2008).



1113

1114 62. Wasserman WW, Sandelin A. Applied bioinformatics for the identification of  
1115 regulatory elements. *Nat Rev Genet* **5**, 276-287 (2004).

1116

1117 63. Levine RL, *et al.* X-inactivation-based clonality analysis and quantitative  
1118 JAK2V617F assessment reveal a strong association between clonality and  
1119 JAK2V617F in PV but not ET/MMM, and identifies a subset of JAK2V617F-  
1120 negative ET and MMM patients with clonal hematopoiesis. *Blood* **107**, 4139-4141  
1121 (2006).

1122

1123 64. Takahashi T, *et al.* Associations between diabetes mellitus and pulmonary  
1124 hypertension in chronic respiratory disease patients. *PLoS One* **13**, e0205008  
1125 (2018).

1126

1127 65. Misaka T, *et al.* Plasma levels of melatonin in dilated cardiomyopathy. *J Pineal*  
1128 *Res* **66**, e12564 (2019).

1129

1130 **Acknowledgments**

1131 The authors thank Ms Tomiko Miura and Ms Shoko Sato in the Department of  
1132 Cardiovascular Medicine, Fukushima Medical University, and Ms Chisato Kubo in the  
1133 Office for Gender Equality Support, Fukushima Medical University, for their technical  
1134 assistance. This work was supported by JSPS KAKENHI grant JP19K17609 to YK and  
1135 JP19K08523 to YT, and research grant from the Uehara Memorial Foundation 201890006  
1136 to KI.

1137

1138 **Author contributions**

1139 YK and TM designed the research, performed the experiments, analyzed the results, and  
1140 wrote the manuscript. TY, KW, KU, K. Sugimoto, and KM performed the experiments  
1141 and analyzed the results. MO, SK and AI performed and analyzed the RNA sequencing,  
1142 supervised the research, and wrote the manuscript. KN and TI supervised the study. K.  
1143 Shide and K. Shimoda provided JAK2<sup>V617F</sup> mice and interpreted the results. KI designed  
1144 the research, analyzed the data, and wrote the manuscript. YT designed and supervised  
1145 the research and approved the final version of the manuscript.

1146

1147 **Competing interests**

1148 TM's department is supported by Fukuda Denshi Co., Ltd., Japan. TY and KS's  
1149 department is supported by Actelion Pharmaceuticals Japan, Ltd., Japan. Ruxolitinib was  
1150 provided by Novartis Pharmaceuticals to KI. These companies were not associated with  
1151 the contents of this study. All other authors declare no competing interests.

1152

1153

1154 **Figure legends**

1155 **Figure 1. *JAK2<sup>V617F</sup>* mice accelerate pulmonary hypertension accompanied by**  
1156 **perivascular neutrophil infiltration in response to chronic hypoxia.**

1157 **Figure 2. Clonal hematopoiesis with *JAK2V617F* exacerbates pulmonary**  
1158 **hypertension and infiltration of perivascular neutrophils in bone marrow**  
1159 **transplanted recipients with wild-type lungs in response to chronic hypoxia.**

1160 **Figure 3. Characterization of bone marrow-derived *JAK2V617F* hematopoietic cells**  
1161 **in the lungs by the use of GFP-transgene.**

1162 **Figure 4. Small clones with *JAK2V617F* lead to PH development, associated with**  
1163 **selective migration of neutrophils into the lungs and maturation from the lung**  
1164 **hematopoietic precursors for the myeloid lineage.**

1165 **Figure 5. Gene expression profiles of neutrophils with *JAK2V617F* at several**  
1166 **differential stages.**

1167 **Figure 6. *Acvr11* mRNA expressions and phosphorylation of Smad1/5/8 and STAT3**  
1168 **in the lungs of *JAK2<sup>V617F</sup>* mice in response to chronic hypoxia.**

1169 **Figure 7. *JAK2V617F* transcriptionally upregulates *ACVRL1* by STAT3-binding.**

1170 **Figure 8. Inhibition of ALK1/2 improves chronic hypoxia-induced pulmonary**  
1171 **hypertension in *JAK2<sup>V617F</sup>* mice.**

1172 **Figure 9. Prevalence of *JAK2V617F*-positive clonal hematopoiesis in PH patients.**

1173 **Supplementary Figure 1. Changes in phosphorylation levels of STAT3 on whole lung**  
1174 **homogenates during chronic hypoxia in the wild-type (WT) mice.**

1175 **Supplementary Figure 2. Echocardiographic analysis in *JAK2V617F* mice after**  
1176 **exposure to chronic hypoxia.**

1177 **Supplementary Figure 3. Left ventricular weight in JAK2V617F mice after exposure**  
1178 **to chronic hypoxia.**

1179 **Supplementary Figure 4. Male JAK2V617F mice also develop pulmonary**  
1180 **hypertension in response to exposure to chronic hypoxia.**

1181 **Supplementary Figure 5. Histological images and mRNA expression of the lung in**  
1182 **JAK2V617F mice after exposure to chronic hypoxia.**

1183 **Supplementary Figure 6. Characterization of the infiltrated leukocytes in the**  
1184 **pulmonary arterial regions in JAK2V617F mice after exposure to chronic hypoxia.**

1185 **Supplementary Figure 7. Chronic hypoxia increased Ly6G<sup>+</sup> neutrophils in**  
1186 **perivascular regions as well as non-perivascular regions of the lungs in JAK2V617F**  
1187 **mice.**

1188 **Supplementary Figure 8. Pulmonary hypertension is accelerated in JAK2V617F**  
1189 **mice in a Sugden-hypoxia model.**

1190 **Supplementary Figure 9. Characterization of aged JAK2V617F mice in the setting**  
1191 **of normoxia.**

1192 **Supplementary Figure 10. Echocardiographic analyses in JAK2V617F-BMT mice**  
1193 **after exposure to chronic hypoxia.**

1194 **Supplementary Figure 11. Left ventricular weight in JAK2V617F-BMT mice after**  
1195 **exposure to chronic hypoxia.**

1196 **Supplementary Figure 12. Histological images and mRNA expression of the lungs in**  
1197 **JAK2V617F-BMT mice after exposure to chronic hypoxia.**

1198 **Supplementary Figure 13. Characterization of the infiltrated leukocytes in the**  
1199 **pulmonary arterial regions in JAK2V617F-BMT mice after exposure to chronic**  
1200 **hypoxia.**

1201 **Supplementary Figure 14. Chronic hypoxia increased Ly6G<sup>+</sup> neutrophils in**  
1202 **perivascular regions as well as non-perivascular regions of the lungs in JAK2V617F-**  
1203 **BMT mice.**

1204 **Supplementary Figure 15. Characterization of bone marrow-derived JAK2V617F**  
1205 **hematopoietic cells in the lungs by the use of GFP-transgene.**

1206 **Supplementary Figure 16. A competitive transplantation model using JAK2V617F-**  
1207 **GFP bone marrow cells.**

1208 **Supplementary Figure 17. Colony-forming assay to estimate the presence of**  
1209 **hematopoietic progenitor cells in the JAK2V617F lungs for the myeloid lineage.**

1210 **Supplementary Figure 18. Immunofluorescence of sorted cells from the mouse lung.**

1211 **Supplementary Figure 19. Acvrl1, Acvr1, and Bmpr2 mRNA expressions in the lung**  
1212 **homogenates or sorted cells from the lungs after exposure to chronic hypoxia.**

1213 **Supplementary Figure 20. HIF1 $\alpha$  expression in the lungs of JAK2V617F mice in**  
1214 **response to exposure to chronic hypoxia.**

1215 **Supplementary Figure 21. Binding of HIF1 $\alpha$  and STAT3 in the lungs.**

1216 **Supplementary Figure 22. Inhibition of HIF1 $\alpha$  in JAK2V617F-expressing**  
1217 **neutrophils reduced the mouse pulmonary artery smooth muscle cell (PASMC)**  
1218 **proliferation.**

1219 **Supplementary Figure 23. Smad1/5/8 phosphorylation in response to BMP9**  
1220 **stimulation in HCT116 cells to express an active ALK1 receptor.**

1221 **Supplementary Figure 24. ALK1 expression in JAK2V617F/+ HCT116 cells by flow**  
1222 **cytometry.**

1223 **Supplementary Figure 25. ACVR1 (ALK2) expressions in JAK2V617F/+ HCT116**  
1224 **cells.**

1225 **Supplementary Figure 26. Effects of K02288, an ALK1/2 inhibitor, on the**  
1226 **phosphorylation of Smad1/5/8 in the mouse lung and HCT116 cells.**

1227 **Supplementary Figure 27. Left ventricular weight in K02288-treated JAK2V617F**  
1228 **mice after exposure to chronic hypoxia.**

1229 **Supplementary Figure 28. K02288, an ALK1/2 inhibitor, attenuates chronic**  
1230 **hypoxia-induced proliferation of pulmonary arterial smooth muscle cells in**  
1231 **JAK2V617F mice.**

1232 **Supplementary Figure 29. Effects of LDN-212854, an ALK1/2 inhibitor, on the**  
1233 **phosphorylation of Smad1/5/8 in the mouse lungs and HCT116 cells.**

1234 **Supplementary Figure 30. LDN-212854, an ALK1/2 inhibitor, improves chronic**  
1235 **hypoxia-induced pulmonary hypertension in JAK2V617F mice.**

1236 **Supplementary Figure 31. No effects of ALK1/2 inhibitors of K02288 or LDN-**  
1237 **212854 on pulmonary hypertension in WT mice and JAK2V617F mice under**  
1238 **normoxia.**

1239 **Supplementary Figure 32. Effects of a high dose of K02288, an ALK1/2 inhibitor, on**  
1240 **pulmonary hypertension in WT mice after chronic hypoxia.**

1241 **Supplementary Figure 33. Gating strategy used in the present study.**

1242

1243

1244

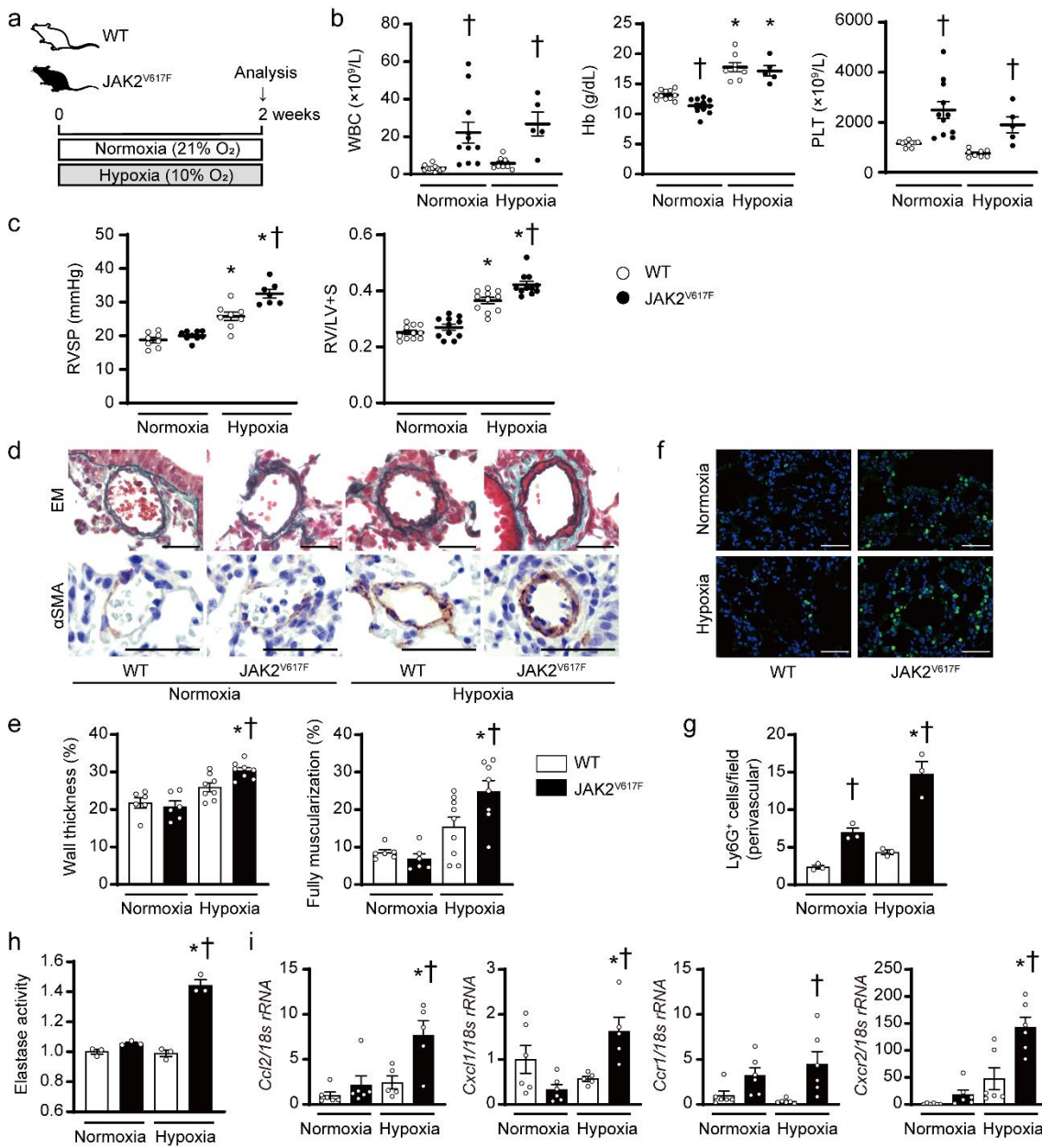
1245

1246

1247

1248

1249 **Figure 1.**



1250

1251 **a** Experimental design. Wild-type (WT) mice and mice with transgenic expression of

1252 *Jak2*<sup>V617F</sup> (*JAK2*<sup>V617F</sup>) exposed to normoxia (21% O<sub>2</sub>) or hypoxia (10% O<sub>2</sub>) for 2 weeks

1253 were analyzed. **b** Peripheral blood cell counts in WT mice or *JAK2*<sup>V617F</sup> mice under

1254 normoxia or hypoxia for 2 weeks (n = 11, 11, 8, 5, †P = 0.0036 [left], 0.0185 [right] for

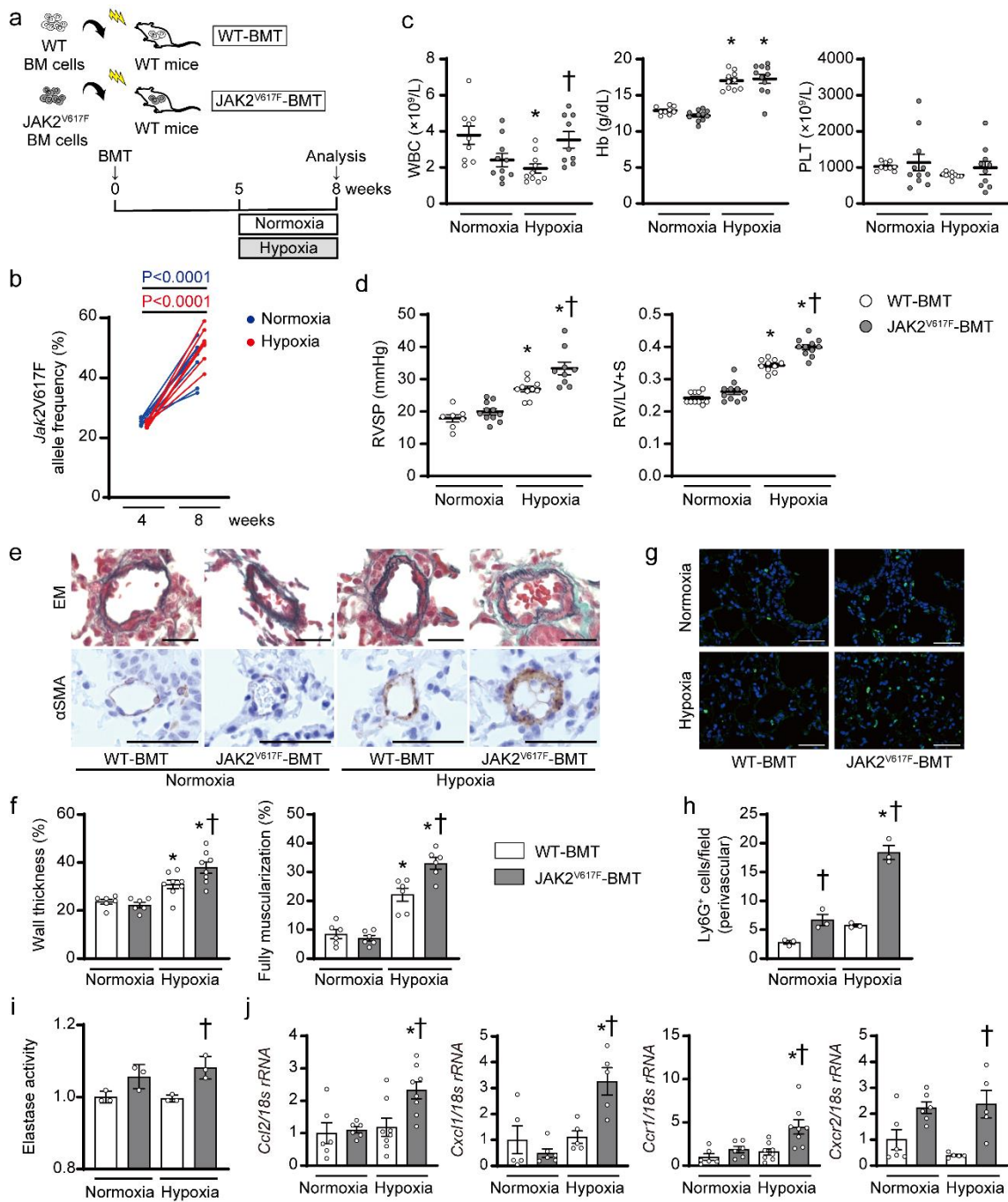
1255 WBC, n = 11, 11, 8, 5, \*P < 0.0001 [left], < 0.0001 [right], †P = 0.0335 for Hb, n = 10,

1256 11, 8, 5, †P = 0.0008 [left], 0.0396 [right] for PLT). **c** Right ventricular systolic pressure  
1257 (RVSP, n = 8, 9, 8, 7, \*P < 0.0001 [left], < 0.0001 [right], †P = 0.0002) and right ventricular  
1258 hypertrophy determined by the ratio of right ventricle (RV) weight to left ventricle weight  
1259 plus septum weight (RV/LV+S, n = 11 in each group, \*P < 0.0001 [left], < 0.0001 [right],  
1260 †P = 0.0027). **d** Representative images of Elastica-Masson (EM)-stained sections and  
1261 sections immunostained with anti- $\alpha$ -smooth muscle actin ( $\alpha$ SMA) antibody from WT  
1262 mice and JAK2<sup>V617F</sup> mice. Scale bars, 25  $\mu$ m. **e** Quantitative analysis of medial wall  
1263 thickness in EM-stained sections (left, n = 6, 6, 8, 8, \*P < 0.0001, †P = 0.0413) and the  
1264 percentage of muscularized distal pulmonary vessels in  $\alpha$ SMA-immunostained sections  
1265 (right, n = 6, 6, 9, 8, \*P = 0.0001, †P = 0.0263). **f** Representative immunofluorescence  
1266 images of lung sections stained with anti-Ly6G (green) antibody and DAPI (blue). Scale  
1267 bars, 50  $\mu$ m. **g** Quantitative analysis of Ly6G-positive cells in perivascular regions (n = 3  
1268 in each group, \*P = 0.0015, †P = 0.0318 [left], 0.0002 [right]). **h** Elastase activity in the  
1269 lungs from WT and JAK2<sup>V617F</sup> mice. The average value from normoxia-exposed WT mice  
1270 was set to 1 (n = 3 in each group, \*P < 0.0001, †P < 0.0001). **i** Relative mRNA expression  
1271 levels of *Ccl2*, *Cxcl1*, *Ccr1*, and *Cxcr2* in the lungs. The *18s rRNA* was used for  
1272 normalization. The average value from normoxia-exposed WT mice was set to 1 (n = 6,  
1273 6, 5, 5, \*P = 0.0049, †P = 0.0105 for *Ccl2*, n = 6, 6, 5, 5, \*P = 0.0044, †P = 0.0284 for  
1274 *Cxcl1*, n = 6, 6, 6, 6, †P = 0.0139 for *Ccr1*, n = 6, 6, 6, 6, \*P < 0.0001, †P = 0.0008 for  
1275 *Cxcr2*). All data are presented as mean  $\pm$  SEM. \*P < 0.05 versus the corresponding  
1276 normoxia-exposed group and †P < 0.05 versus the corresponding WT mice by the one-  
1277 way ANOVA with Tukey post-hoc analysis. WBC, white blood cell count; Hb,  
1278 hemoglobin concentration; PLT, platelet count.

1279



1280 **Figure 2.**



1281

1282 **a** Schematic diagram of the experimental design. Bone marrow (BM) cells from WT or  
 1283  $JAK2^{V617F}$  mice were injected into lethally irradiated recipient WT mice with the same  
 1284 C57BL/6J background. Five weeks after BM transplantation (BMT), the recipient mice  
 1285 transplanted with  $JAK2^{V617F}$  BM cells ( $JAK2^{V617F}$ -BMT) or WT BM cells (WT-BMT)

1286 were exposed to normoxia or hypoxia for 3 weeks. **b** *Jak2*<sup>V617F</sup> allele frequencies (%)  
1287 in peripheral blood of each *JAK2*<sup>V617F</sup>-BMT mouse at 4 and 8 weeks after BMT at  
1288 normoxia (blue circles, n = 8) or chronic hypoxia exposure (red circles, n = 8). Statistical  
1289 comparison was performed by the paired Student's t-test (two-sided). **c** Peripheral blood  
1290 cell counts in WT-BMT or *JAK2*<sup>V617F</sup>-BMT mice after exposure to normoxia or hypoxia  
1291 (n = 9, 10, 10, 9, \*P = 0.0121, †P = 0.0388 for WBC, n = 9, 11, 10, 11, \*P < 0.0001 [left],  
1292 < 0.0001 [right] for Hb, n = 9, 11, 10, 10 for PLT). **d** RVSP and RV hypertrophy  
1293 determined by RV/LV+S in WT-BMT or *JAK2*<sup>V617F</sup>-BMT mice after exposure to  
1294 normoxia or hypoxia (n = 7, 11, 10, 9, \*P = 0.0002 [left], < 0.0001 [right], †P = 0.0054 for  
1295 RVSP, n = 10, 11, 10, 11, \*P < 0.0001 [left], < 0.0001 [right], †P < 0.0001 for RV/LV+S).  
1296 **e** Representative images of EM-stained sections and sections immunostained with anti-  
1297  $\alpha$ SMA antibody from WT-BMT and *JAK2*<sup>V617F</sup>-BMT mice. Scale bars, 25  $\mu$ m. **f**  
1298 Quantitative analysis of medial wall thickness in EM-stained sections (left, n = 6, 6, 8, 8,  
1299 \*P = 0.0465 [left], < 0.0001 [right], †P = 0.0346) and the percentage of muscularized distal  
1300 pulmonary vessels in  $\alpha$ SMA-immunostained sections (right, n = 6 in each group, \*P =  
1301 0.0001 [left], < 0.0001 [right], †P = 0.0016). **g** Representative immunofluorescence  
1302 images of lung sections stained with anti-Ly6G (green) antibody and DAPI (blue). Scale  
1303 bars, 50  $\mu$ m. **h** Quantitative analysis of Ly6G-positive cells in the perivascular regions (n  
1304 = 3 in each group, \*P < 0.0001, †P = 0.0387 [left], < 0.0001 [right]). **i** Elastase activity in  
1305 the lungs from WT -BMT and *JAK2*<sup>V617F</sup>-BMT mice. The average value of normoxia-  
1306 exposed WT-BMT mice was set to 1 (n = 3 in each group, †P = 0.0128). **j** Relative mRNA  
1307 expression levels of *Ccl2*, *Cxcl1*, *Ccr1* and *Cxcr2* in the lungs. The *18s rRNA* was used  
1308 for normalization. The average value from the normoxia-exposed WT-BMT mice was set  
1309 to 1 (n = 6, 6, 8, 8, \*P = 0.0171, †P = 0.0159 for *Ccl2*, n = 5, 6, 5, 5 \*P = 0.0004, †P =

1310 0.0065 for *Cxcl1*, 6, 6, 8, 8, \*P = 0.0171, †P = 0.0040 for *Ccr1*, n = 6, 6, 5, 5, †P = 0.0056  
1311 for *Cxcr2*). The data are presented as mean ± SEM. \*P < 0.05 versus the corresponding  
1312 normoxia-group and †P < 0.05 versus the corresponding WT-BMT mice by the one-way  
1313 ANOVA with Tukey post-hoc analysis. WT-BMT, recipient WT mice transplanted with  
1314 BM cells of WT mice; JAK2<sup>V617F</sup>-BMT, recipient WT mice transplanted with BM cells  
1315 of JAK2<sup>V617F</sup> mice. WBC, white blood cell count; Hb, hemoglobin concentration; PLT,  
1316 platelet count.

1317

1318

1319

1320

1321

1322

1323

1324

1325

1326

1327

1328

1329

1330

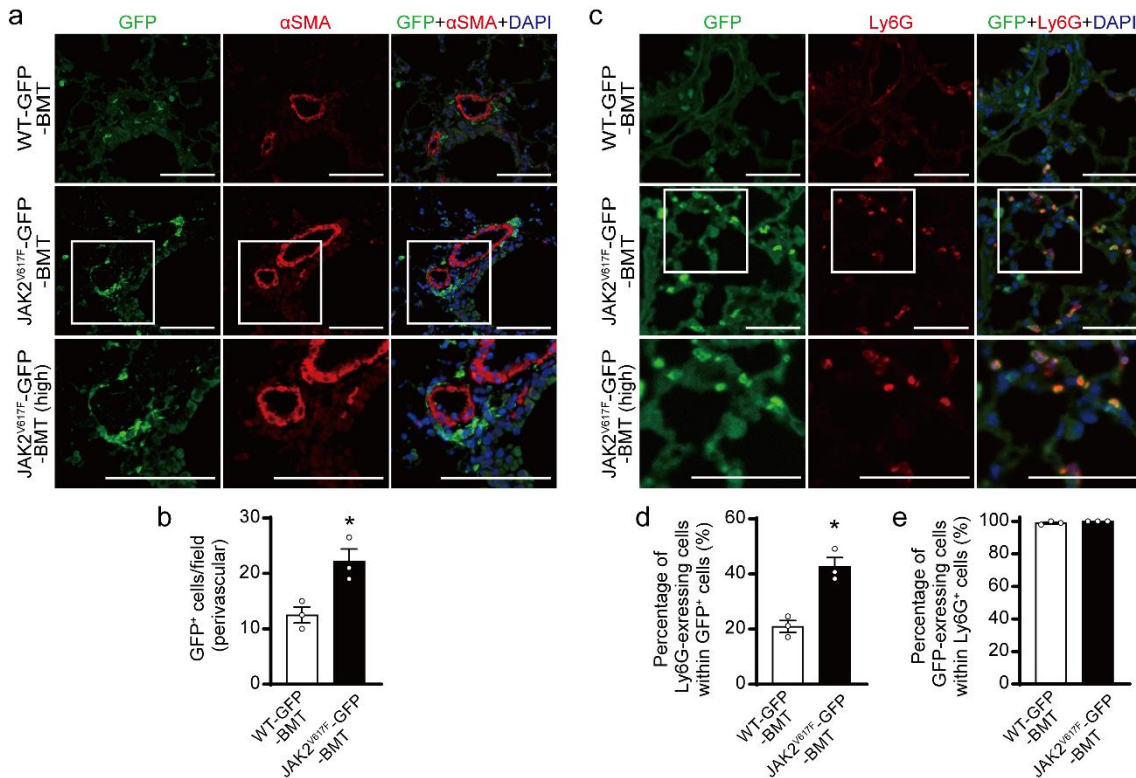
1331

1332

1333

1334

1335 **Figure 3.**



1336

1337 **a** Lethally irradiated WT mice were transplanted with bone marrow (BM) cells from  
 1338 control WT/CAG-EGFP (WT-GFP) or JAK2<sup>V617F</sup>/CAG-EGFP (JAK2<sup>V617F</sup>-GFP) double  
 1339 transgenic mice. Five weeks after BM transplantation (BMT), the recipient mice were  
 1340 subjected to chronic hypoxia for 3 weeks, and then the lungs were fixed and stained with  
 1341 the indicated antibodies. Representative immunofluorescence images of lung sections  
 1342 stained with anti-GFP (green) and anti- $\alpha$ SMA (red) antibodies and DAPI (blue) in WT-  
 1343 GFP-BMT or JAK2<sup>V617F</sup>-GFP-BMT mice. The boxed areas from JAK2<sup>V617F</sup>-GFP-BMT  
 1344 mice at higher magnifications (high) are shown in the bottom panels. Scale bars, 100  $\mu$ m.

1345 **b** Quantitative analysis of Ly6G<sup>+</sup> cells in the perivascular regions (n = 3 in each group,  
 1346 \*P = 0.0223). **c** Representative immunofluorescence images of lung sections stained with  
 1347 anti-GFP (green) and anti-Ly6G (red) antibodies, as well as DAPI (blue) in WT-GFP-  
 1348 BMT or JAK2<sup>V617F</sup>-GFP-BMT mice. The boxed areas from JAK2<sup>V617F</sup>-GFP-BMT mice

1349 at higher magnifications are shown in the bottom panels (high). Scale bars, 100  $\mu\text{m}$ . **d, e**  
1350 Quantitative analysis of Ly6G-expressing cells in GFP<sup>+</sup> cells (**d**, n = 3 in each group, \*P =  
1351 0.0052) and GFP-expressing cells in Ly6G<sup>+</sup> cells (**e**, n = 3 in each group). More than 100  
1352 GFP<sup>+</sup> cells and Ly6G<sup>+</sup> cells were counted in each section and expressed as the percentage  
1353 of the cells. All data are presented as mean  $\pm$  SEM. WT-GFP-BMT, recipient WT mice  
1354 transplanted with WT-GFP BM cells; JAK2<sup>V617F</sup>-GFP-BMT, recipient WT mice  
1355 transplanted with JAK2<sup>V617F</sup>-GFP BM cells. \*P < 0.05 versus WT-GFP recipients by the  
1356 unpaired t-test (two-sided).

1357

1358

1359

1360

1361

1362

1363

1364

1365

1366

1367

1368

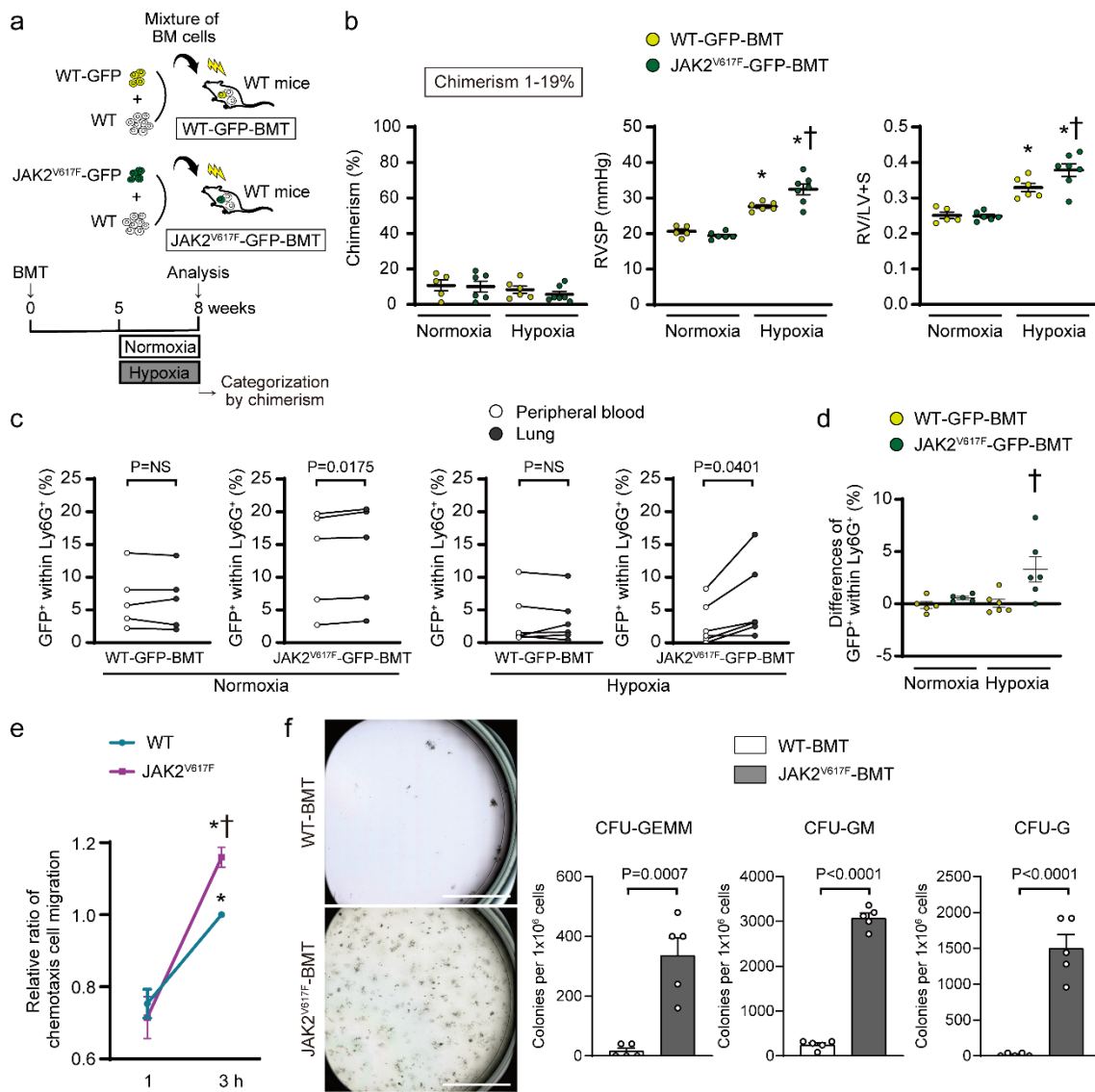
1369

1370

1371

1372

1373 **Figure 4.**



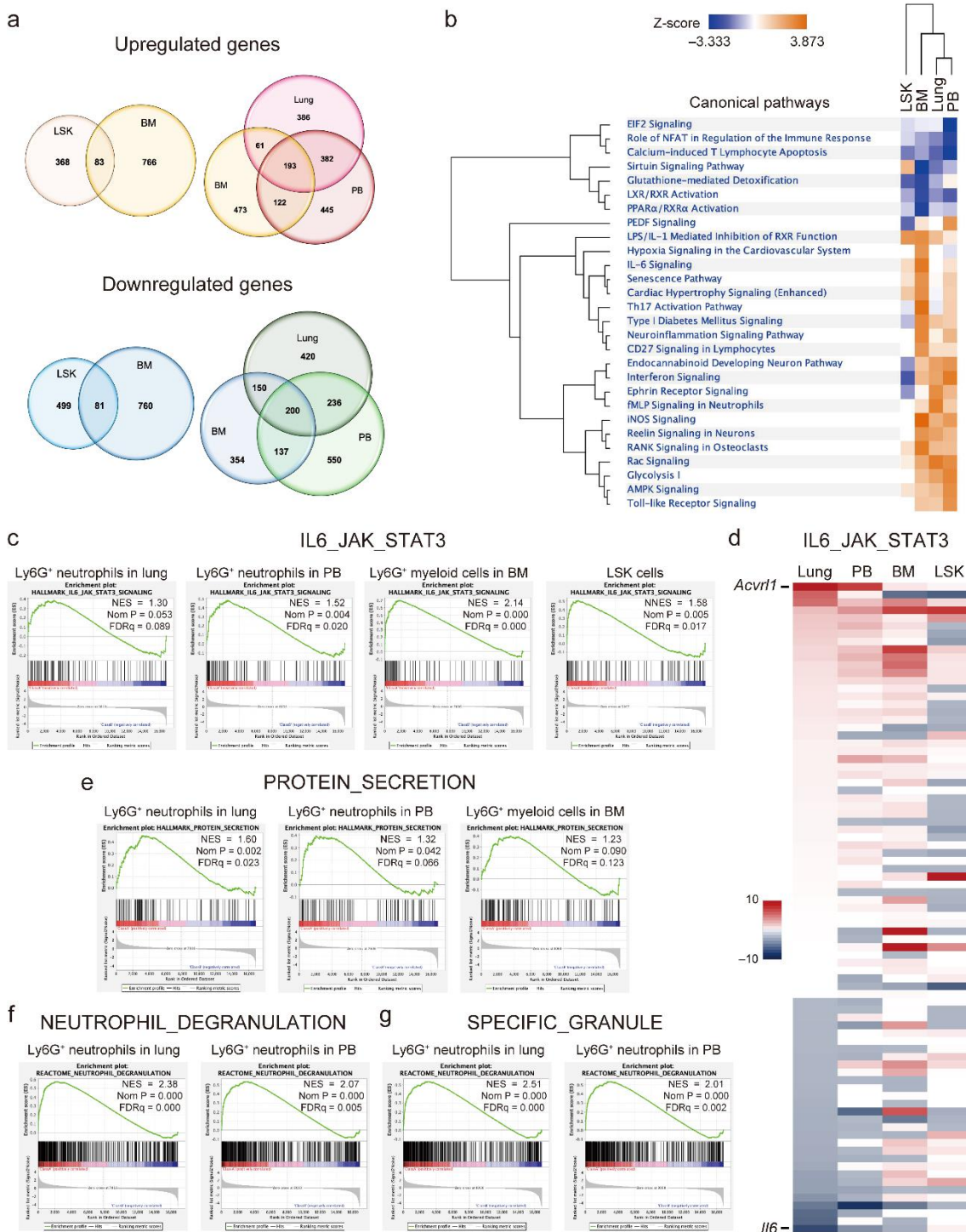
1374

1375 **a** Schematic depiction of the competitive transplantation. The different ratios of WT-GFP  
 1376 or JAK2<sup>V617F</sup>-GFP and WT without GFP competitor were transplanted into the lethally  
 1377 irradiated recipient WT mice. **b** The recipients with donor chimerism of 1–19% at 8 weeks  
 1378 after bone marrow transplantation (BMT), determined by the percentages of GFP<sup>+</sup> cells  
 1379 within CD45<sup>+</sup> cells by flow cytometry, were enrolled for statistical comparison (n = 5, 6,  
 1380 6, 7). The other categories of the donor chimerism are presented in Supplementary Figure  
 1381 16. RVSP and RV/LV+S are shown (n = 5, 6, 6, 7, \*P = 0.0008 [left], < 0.0001 [right], †P

1382 = 0.0113 for RVSP, n = 5, 6, 6, 7 \*P = 0.0029 [left], < 0.0001 [right], †P = 0.0049 for  
1383 RV/LV+S). \*P < 0.05 versus the corresponding normoxia-group and †P < 0.05 versus the  
1384 corresponding WT-GFP-BMT mice by the one-way ANOVA with Tukey post-hoc  
1385 analysis. **c, d** JAK2<sup>V617F</sup> neutrophils showed an intrinsic increased migration capability  
1386 into the lungs. The percentages of GFP<sup>+</sup> cells within CD45<sup>+</sup> cells in the peripheral blood  
1387 and the lungs were analyzed at 8 weeks in the BMT mice with 1–19% chimerism by flow  
1388 cytometry (**c**, n = 5, 5, 6, 6). The comparison was performed by the paired Student's t-test  
1389 (two-sided). NS, not significant. The differences of GFP<sup>+</sup> cells within CD45<sup>+</sup> cells  
1390 between the lungs and the peripheral blood are shown (**d**, n = 5, 5, 6, 6). †P = 0.0173  
1391 versus the corresponding WT-GFP-BMT mice by the one-way ANOVA with Tukey post-  
1392 hoc analysis. **e** Chemotaxis migration assay. The sorted Ly6G<sup>+</sup> neutrophils from the blood  
1393 in WT or JAK2<sup>V617F</sup> mice were placed on the top of Transwell in triplicate and were  
1394 allowed to migrate for 1 or 3 h. Data are expressed as a relative ratio to WT-3 h from six  
1395 independent experiments and presented as mean ± SEM. \*P < 0.01 versus corresponding  
1396 1 h (\*P = 0.0009 for WT, <0.0001 for JAK2<sup>V617F</sup>) and †P = 0.0342 versus WT-3 h by the  
1397 two-way ANOVA with Tukey post-hoc analysis. **f** Colony-forming assay of the  
1398 hematopoietic progenitors in the lungs. CD117 (c-kit)<sup>+</sup> cells sorted from the lungs of WT-  
1399 BMT and JAK2<sup>V617F</sup>-BMT mice were grown in the methylcellulose-based medium for 7  
1400 days. Representative images of the 35 mm plates are shown in the left panels. Scale bars,  
1401 10 mm. Right, quantification of numbers of the colonies derived from colony-forming  
1402 unit (CFU)-granulocyte, -erythroid, -macrophage, -megakaryocyte (CFU-GEMM), CFU-  
1403 granulocyte, -monocyte (CFU-GM), CFU-granulocyte (CFU-G). The comparison was  
1404 performed by the two-sided unpaired Student's t-test (n = 5 in each group). All data are  
1405 presented as mean ± SEM.



1406 **Figure 5.**



1407

1408 **a** Venn diagrams show the numbers of upregulated and downregulated genes (> 1.5-fold)

1409 in Ly6G<sup>+</sup> neutrophils in lungs and peripheral blood (PB), and Ly6G<sup>+</sup> myeloid cells in BM,

1410 and lineage Sca1<sup>+</sup>Kit<sup>+</sup> (LSK) cells isolated from JAK2<sup>V617F</sup> mice (n = 3) compared to



1411 those from WT mice (n = 5) by RNA sequencing. **b** Strongly affected pathways ( $|z| >$   
1412 2.58) at least one cell type according to the gene expression of Ly6G<sup>+</sup> neutrophils and  
1413 LSK cells from JAK2<sup>V617F</sup> mice relative to those from WT mice. Hierarchical clustering  
1414 of pathways and cell types are also shown. **c–g** A gene set enrichment analysis (GSEA)  
1415 of RNA sequencing. Among Hallmark analyses, the IL6-JAK-STAT3 pathway was  
1416 consistently enriched in JAK2<sup>V617F</sup> myeloid cells at each differential stage (**c**), but the  
1417 expression profiles of the individual genes were different between the stem/progenitor  
1418 and periphery levels (**d**). The expression level of *Acvr11* was the highest in the lung and  
1419 PB neutrophils, while slightly upregulated in the BM myeloid cells and LSK cells in this  
1420 pathway. **e–g** Gene sets of PROTEIN-SECRETION (**e**), NEUTROPHIL-  
1421 DEGRANULATION (**f**), and SPECIFIC-GRANULE (**g**) were enriched in mature Ly6G<sup>+</sup>  
1422 neutrophils.

1423

1424

1425

1426

1427

1428

1429

1430

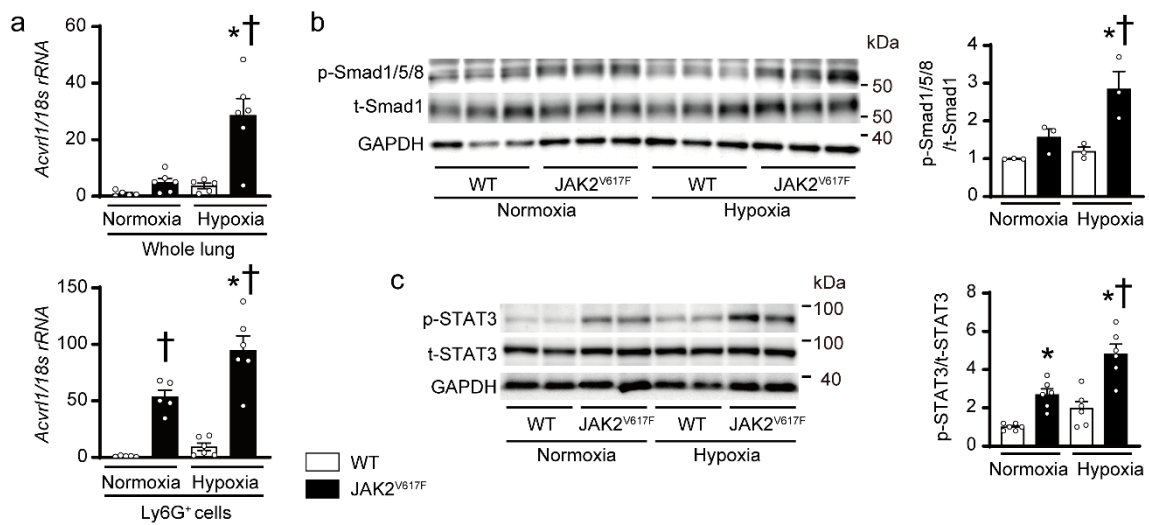
1431

1432

1433

1434

1435 **Figure 6.**



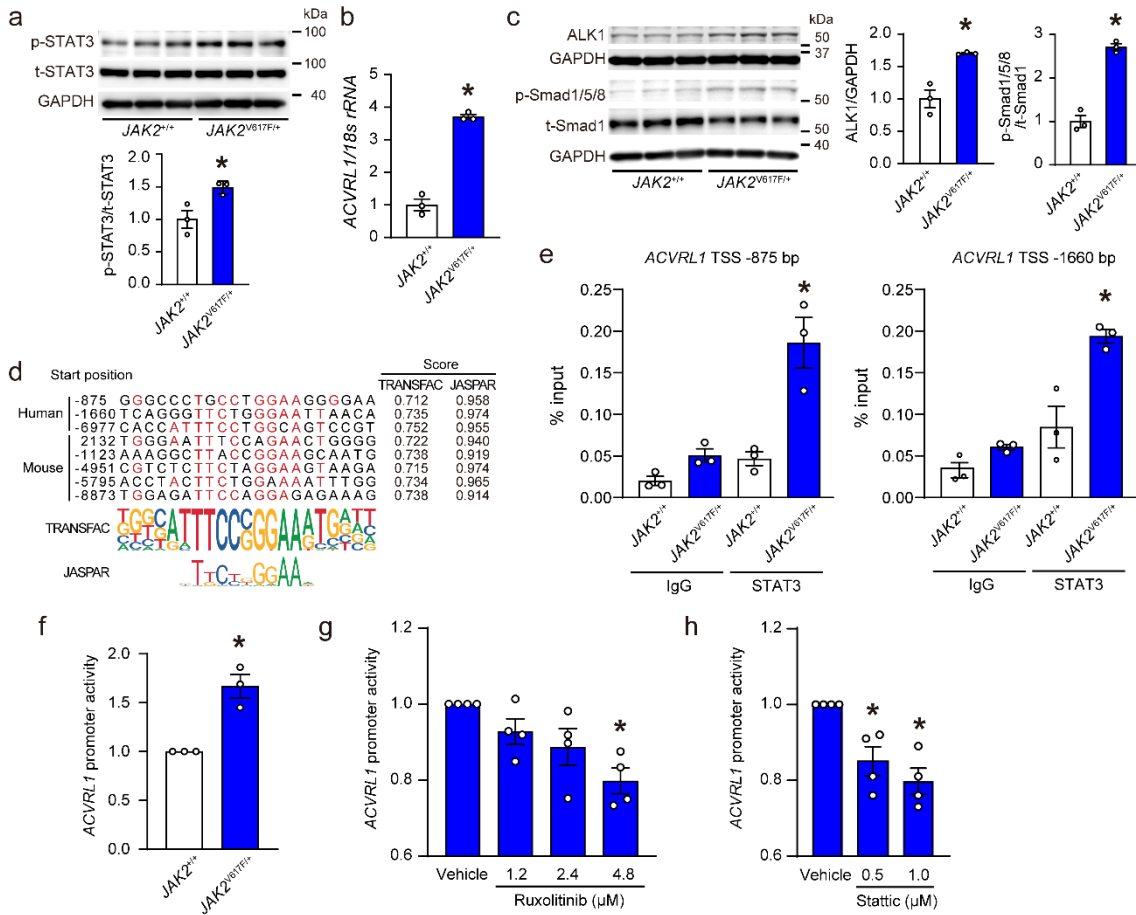
1436

1437 **a** mRNA expression of *Acvr11* in whole lung extracts (top) or the sorted Ly6G<sup>+</sup> cells from  
 1438 the lungs (bottom) of WT mice and JAK2<sup>V617F</sup> mice exposed to normoxia or hypoxia. The  
 1439 data were normalized to *18s rRNA* levels (n = 5, 6, 5, 6, \*P = 0.0004, †P = 0.0004 for  
 1440 whole lung extracts, n = 5, 5, 6, 6, \*P = 0.0069, †P = 0.0012 [left], < 0.0001 [right] for  
 1441 sorted Ly6G<sup>+</sup> cells). **b, c** Western blot analysis on the SMAD (**b**) and STAT (**c**) pathways  
 1442 in the lungs. Lung extracts from WT mice or JAK2<sup>V617F</sup> mice were immunoblotted with  
 1443 the indicated antibodies. The ratios of phosphorylated Smad1/5/8 (p-Smad1/5/8) to total  
 1444 Smad1 (t-Smad1) and phosphorylated-STAT3 (p-STAT3) to total STAT3 (t-STAT3) are  
 1445 shown in the bar graphs. The average value for normoxia-WT mice was set to 1 (**b**, n = 3  
 1446 in each group, \*P = 0.0382, †P = 0.0100; **c**, n = 6 in each group, \*P = 0.0125 [left], 0.0019  
 1447 [right], †P < 0.0001). GAPDH was used as the loading control. All data are presented as  
 1448 mean ± SEM. \*P < 0.05 versus the corresponding normoxia-group and †P < 0.05 versus  
 1449 the corresponding WT mice by the one-way ANOVA with Tukey post-hoc analysis.

1450

1451

1452 **Figure 7.**



1453

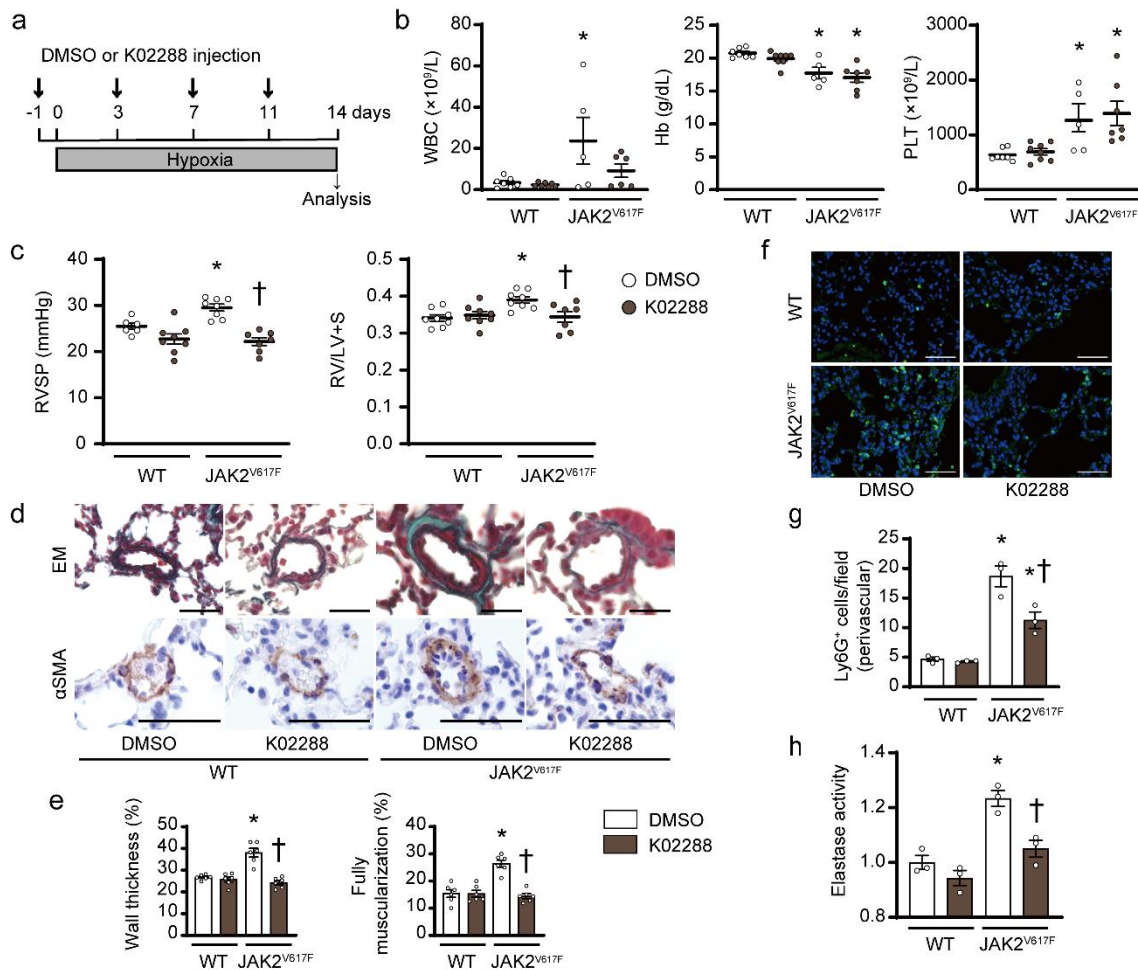
1454 **a** Western blot analysis of STAT3 in *JAK2*<sup>V617F/+</sup> knock-in HCT116 cells. p-STAT3 and t-  
 1455 STAT3 indicate phosphorylated and total STAT3, respectively. p-STAT3 to t-STAT3 ratios  
 1456 are shown in the bar graph (n = 3, \*P = 0.0296). The average value of *JAK2*<sup>+/+</sup> HCT116  
 1457 cells was set to 1. **b** mRNA expression in *ACVRL1* in *JAK2*<sup>V617F/+</sup> cells. The data were  
 1458 normalized to *18s rRNA* levels. The average value of *JAK2*<sup>+/+</sup> cells was set to 1 (n = 3, \*P  
 1459 = 0.0001). **c** Western blot analysis of the ALK1-SMAD pathway. The graphs show the  
 1460 densitometric analysis for ALK1, p-Smad1/5/8 and t-Smad1 (n = 3 in each, \*P = 0.0070,  
 1461 0.0004, respectively). p-Smad1/5/8 and t-Smad1 indicate phosphorylated Smad1/5/8 and  
 1462 total Smad1, respectively. GAPDH was used as the loading control. **d** Sequence  
 1463 alignments of putative STAT3 binding sites of *Acvr1l* in human (hg19) and mouse (m10).

1464 Numbers are given according to the genomic sequence from transcriptional start site  
1465 (TSS). The sequences of the STAT3 binding motifs are highlighted in red. Sequence logos  
1466 for the motifs analyzed by TRANSFAC and JASPAR databases are displayed. **e** ChIP-  
1467 qPCR analysis for STAT3 binding to the putative *ACVRL1* promoter. Chromatin was  
1468 extracted from *JAK2<sup>+/+</sup>* and *JAK2<sup>V617F/+</sup>* HCT116 cells, and then precipitated with an anti-  
1469 STAT3 antibody or IgG (negative control). The genomic DNA fragments of *ACVRL1*  
1470 promoter were evaluated for enrichment by qPCR using the specific primers to the *Acvrl1*  
1471 promoter given from TSS. Data are expressed as the respective DNA inputs (n = 3  
1472 independent experiments, \*P = 0.0015, 0.0026, respectively). **f** Dual luciferase reporter  
1473 assays for the *ACVRL1* gene promoter. The pGL3-basic vector containing the putative  
1474 *ACVRL1* promoter region (TSS -875 bp) and pNL1.1.TK [Nluc/TK] as a control vector  
1475 were co-transfected in *JAK2<sup>V617F/+</sup>* HCT116 cells. Twenty-four h after transfection, cell  
1476 lysates were collected, and relative luciferase activity was determined by the ratio of  
1477 firefly luciferase to Nano luciferase activity (n = 3 independent experiments, \*P =  
1478 0.0051). **g, h** Inhibition of JAK1/2 or STAT3 reduced the elevated *ACVRL1* promoter  
1479 activity in *JAK2<sup>V617F/+</sup>* cells. Twenty-four h after transfection, the *JAK2<sup>V617F/+</sup>* HCT116  
1480 cells were incubated with a specific JAK1/2 inhibitor, ruxolitinib or a specific STAT3  
1481 inhibitor, stattic, at the indicated concentration for a further 24 h, and then luciferase  
1482 activity was measured (n = 4 independent experiments, **g**, \*P = 0.0059; **h**, n =4, \*P =  
1483 0.0164 [left], 0.0027 [right]). All data are presented as mean ± SEM. \*P < 0.05 versus  
1484 *JAK2<sup>+/+</sup>* cells or vehicle by the unpaired Student's t-test (two-sided) or the one-way  
1485 ANOVA with Tukey post-hoc analysis.

1486

1487

1488 **Figure 8.**



1489

1490 **a** Schematic protocol. Vehicle (DMSO) or an ALK1/2 inhibitor, K02288 was  
 1491 administered via an intraperitoneal injection of 12 mg/kg body weight during 2-week  
 1492 chronic hypoxia-exposure, as indicated. **b** Peripheral blood cell counts in DMSO- or  
 1493 K02288-treated WT mice and JAK2<sup>V617F</sup> mice after exposure to chronic hypoxia for 2  
 1494 weeks (n = 7, 7, 5, 6, \*P = 0.0381 for WBC, n = 7, 8, 5, 7, \*P = 0.0074 [left], 0.0037 [right]  
 1495 for Hb, n = 7, 8, 5, 7, \*P = 0.0401 [left], 0.0120 [right] for PLT). **c** RVSP and RV  
 1496 hypertrophy determined by RV/LV+S in DMSO- or K02288-treated WT mice and  
 1497 JAK2<sup>V617F</sup> mice (n = 6, 8, 8, 7, \*P = 0.0238 for RVSP, n = 8, 8, 8, 7, \*P = 0.0112, †P =  
 1498 0.0240 for RV/LV+S). **d** Representative images of EM-stained sections and sections

1499 immunostained with anti- $\alpha$ SMA antibody from DMSO- or K02288-treated WT mice and  
1500 JAK2<sup>V617F</sup> mice. Scale bar, 25  $\mu$ m. **e** Quantitative analysis of medial wall thickness in  
1501 EM-stained sections (left, n = 6 in each group, \*P < 0.0001, †P < 0.0001) and the  
1502 percentage of muscularized distal pulmonary vessels in  $\alpha$ SMA-immunostained sections  
1503 (right, n = 6 in each group, \*P < 0.0001, †P < 0.0001). **f** Representative  
1504 immunofluorescence images of lung sections stained with anti-Ly6G (green) antibody  
1505 and DAPI (blue). Scale bars, 50  $\mu$ m. **g** Quantitative analysis of the numbers of Ly6G<sup>+</sup>  
1506 cells in the perivascular regions (n = 3 in each group, \*P = 0.0001 [left], 0.0103 [right],  
1507 †P = 0.0074). **h** Elastase activity in the lung extracts from DMSO- or K02288-treated WT  
1508 mice and JAK2<sup>V617F</sup> mice. The average value for DMSO-treated WT mice was set to 1 (n  
1509 = 3 in each group, \*P = 0.0017, †P = 0.0075). All data are presented as mean  $\pm$  SEM. \*P  
1510 < 0.05 versus the corresponding WT mice and †P < 0.05 versus DMSO-treated JAK2<sup>V617F</sup>  
1511 mice by the one-way ANOVA with Tukey post-hoc analysis. WBC; white blood cell  
1512 count, Hb; hemoglobin concentration; PLT, platelet count.

1513

1514

1515

1516

1517

1518

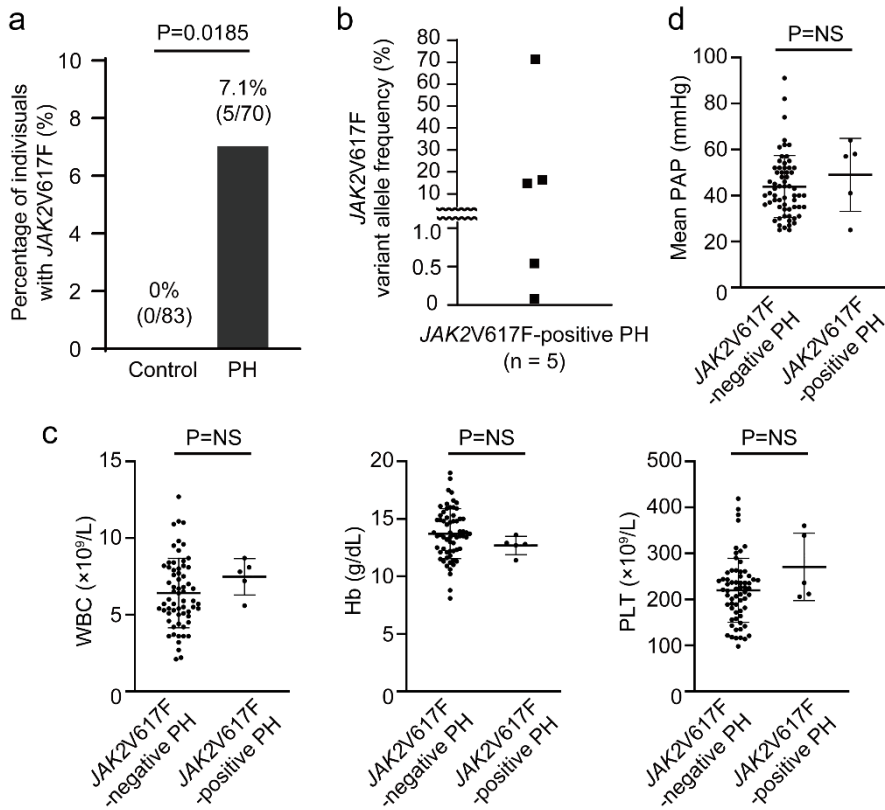
1519

1520

1521

1522

1523 **Figure 9.**



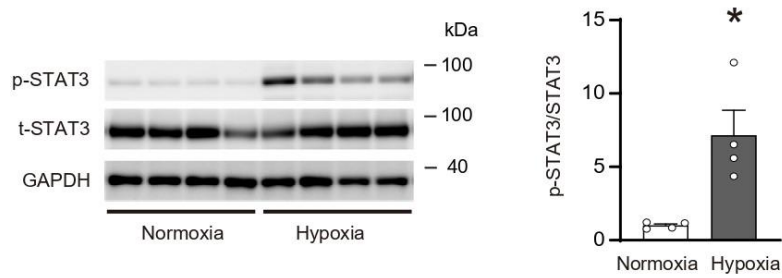
1524

1525 **a** *JAK2V617F*-positive clonal hematopoiesis was more common in PH patients. The  
 1526 comparison between PH patients (n = 70) and age- and sex-matched control subjects (n  
 1527 = 83) was made by Fisher's exact test (two-sided). **b** *JAK2V617F* variant allele frequency.  
 1528 **c, d**, Peripheral blood cell counts, and mean PAP (pulmonary arterial pressure) evaluated  
 1529 by right heart catheterization between *JAK2V617F*-negative and *JAK2V617F*-positive  
 1530 PH patients (n = 64, 5 for WBC, Hb, PLT and n = 63, 5 for mean PAP). **d**. Data are  
 1531 presented as mean  $\pm$  SD. Comparisons of values between the two groups were performed  
 1532 by the unpaired Student's t-test (two-sided). WBC, white blood cell count; Hb,  
 1533 hemoglobin concentration; PLT, platelet count; NS, not significant.

1534

1535

1536 **Supplementary Figure 1.**

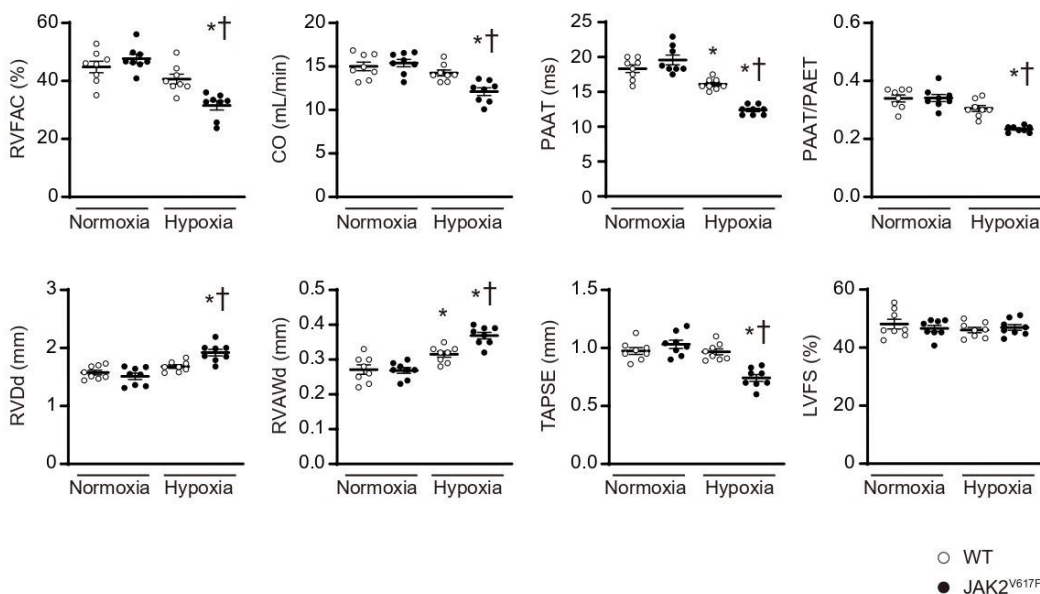


1537

1538 Lung homogenates obtained from the adult WT mice with a C57BL/6J background after  
 1539 normoxia (21% O<sub>2</sub>) or chronic hypoxia (10% O<sub>2</sub>) for 3 weeks were analyzed by  
 1540 immunoblotting with anti-phosphorylated-STAT3 and STAT3 antibodies. p-STAT3 and t-  
 1541 STAT3 indicate phosphorylated and total STAT3, respectively. p-STAT3 to t-STAT3 ratios  
 1542 are shown in the bar graph (n = 4 in each group). Data are presented as mean ± SEM. \*P  
 1543 = 0.0116 versus the normoxia group by the unpaired Student's t-test (two-sided).

1544

1545 **Supplementary Figure 2.**



1546

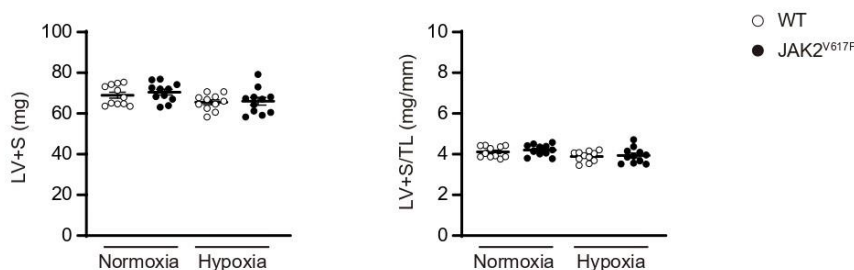
1547 Echocardiography was performed to evaluate pulmonary hemodynamics and cardiac  
 1548 function 2 weeks after normoxia or chronic hypoxia (n = 8 in each group). All data are



1549 presented as mean  $\pm$  SEM. \*P < 0.05 versus the corresponding normoxia-exposed group  
 1550 and †P < 0.05 versus the corresponding WT mice by one-way ANOVA with Tukey post-  
 1551 hoc analysis. \*P < 0.0001, †P = 0.0039 for RVFAC, \*P < 0.0001, †P = 0.0078 for CO, \*P  
 1552 = 0.0134 [left], < 0.0001 [right], †P < 0.0001 for PAAT, \*P < 0.0001, †P = 0.0002 for  
 1553 PAAT/PAET, \*P < 0.0001, †P = 0.0052 for RVDd, \*P = 0.0235 [left], < 0.0001 [right],  
 1554 †P = 0.0042 for RVAWd, \*P < 0.0001, †P < 0.0001 for TAPSE. RVFAC, right ventricular  
 1555 fractional area change; CO, cardiac output; PAAT, pulmonary artery acceleration time;  
 1556 PAET, pulmonary artery ejection time; RVDd, right ventricular diastolic diameter,  
 1557 RVAWd, right ventricular anterior wall diameter; TAPSE, tricuspid annular plane systolic  
 1558 excursion; LVFS, left ventricular fractional shortening; WT, wild-type mice;  
 1559 JAK2V617F, JAK2V617F-expressing transgenic mice.

1560

1561 **Supplementary Figure 3.**



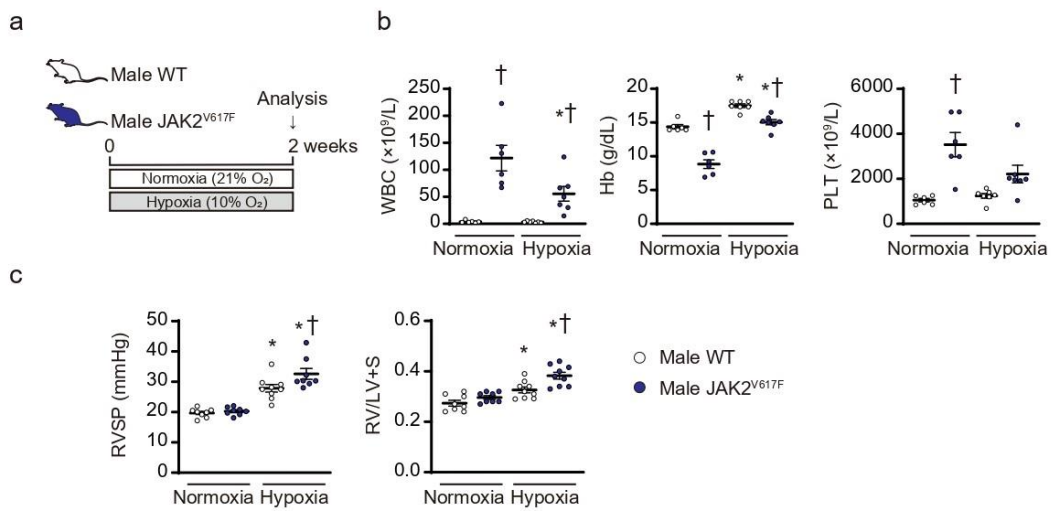
1562

1563 Left ventricular (LV) weight including septum (S) was measured after exposure to  
 1564 normoxia or chronic hypoxia for 2 weeks (n = 11 in each group). LV+S was normalized  
 1565 by tibia length (TL). All data are presented as mean  $\pm$  SEM. The statistical comparison  
 1566 was performed by the one-way ANOVA. WT, wild-type mice; JAK2V617F,  
 1567 JAK2V617F-expressing transgenic mice. Source data are provided as a Source Data file.

1568

1569

1570 **Supplementary Figure 4.**



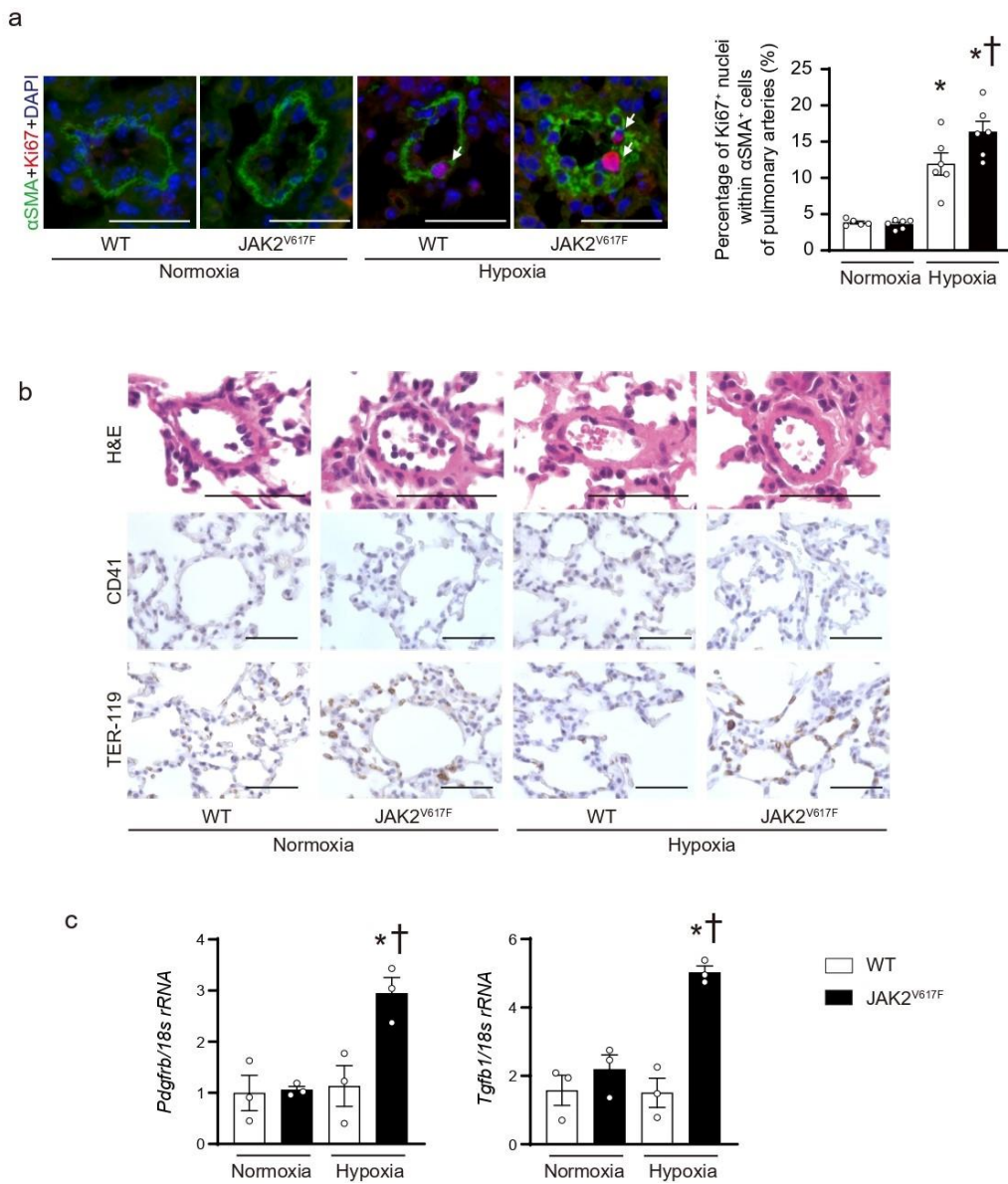
1571

1572 (a) Experimental design. Male wild-type (WT) mice and male JAK2V617F mice aged  
 1573 between 8 and 10 weeks were exposed to normoxia (21% O<sub>2</sub>) or hypoxia (10% O<sub>2</sub>) for  
 1574 2 weeks. (b) Peripheral blood cell counts in WT mice or JAK2V617F mice after normoxia  
 1575 or hypoxia for 2 weeks (n = 6, 6, 7, 7, \*P = 0.0088, †P < 0.0001 [left], 0.0360 [right] for  
 1576 WBC, n = 6, 6, 7, 7, \*P = 0.0002 [left], < 0.0001 [right], †P < 0.0001 [left], 0.0015 [right]  
 1577 for Hb, n = 6, 6, 7, 7, †P = 0.0003 for PLT). (c) Right ventricular systolic pressure (RVSP)  
 1578 and right ventricular hypertrophy determined by the ratio of right ventricle (RV) weight  
 1579 to left ventricle weight plus septum weight (RV/LV+S) (n = 8, 8, 9, 8, \*P < 0.0001 [left],  
 1580 < 0.0001 [right], †P = 0.0302 for RVSP, n = 8, 8, 9, 8, \*P = 0.0171 [left], < 0.0001 [right],  
 1581 †P = 0.00052 for RV/LV+S). All data are presented as mean  $\pm$  SEM. \*P < 0.05 versus the  
 1582 corresponding normoxia-exposed group and †P < 0.05 versus the corresponding WT mice  
 1583 by the one-way ANOVA with Tukey post-hoc analysis. WBC, white blood cell count; Hb,  
 1584 hemoglobin concentration; PLT, platelet count. WT, wild-type mice; JAK2V617F,  
 1585 JAK2V617F-expressing transgenic mice.

1586

1587

1588 **Supplementary Figure 5.**



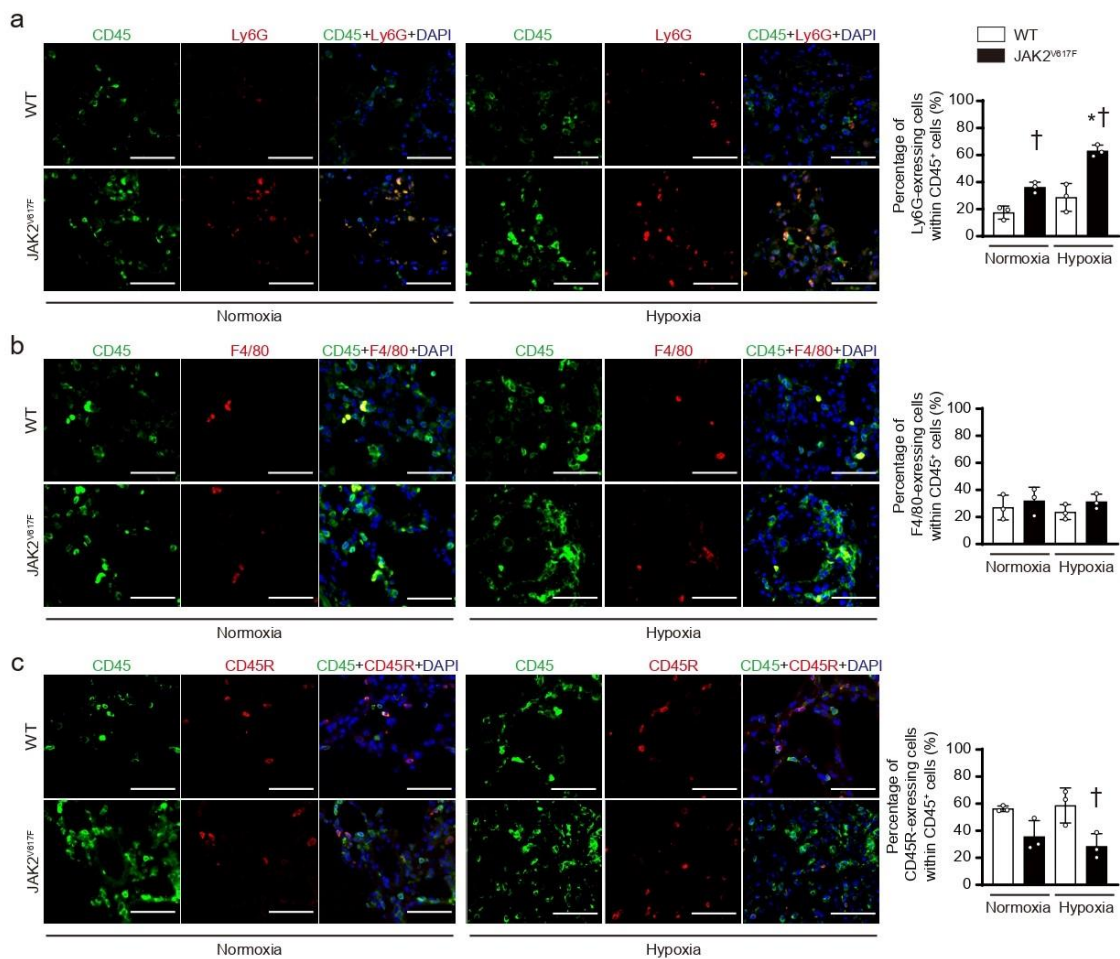
1589

1590 (a) Left, triple-labeled immunofluorescent staining ( $\alpha$ SMA, green; Ki67, red; DAPI, blue)  
 1591 of the lung sections. Right, quantitative analyses of the percentage of Ki67-positive nuclei  
 1592 within  $\alpha$ SMA+ cells of distal pulmonary arteries with a diameter of 50-100  $\mu$ m (n = 5, 6,  
 1593 6, 6, \*P = 0.0005 [left], < 0.0001 [right], †P = 0.0448). More than 80  $\alpha$ SMA+ cells were  
 1594 counted. White arrows indicate Ki67-positive nuclei within  $\alpha$ SMA+ cells. Scale bars, 50  
 1595  $\mu$ m. (b) Representative images of the lung sections of H&E staining and immunostaining

1596 for CD41 and TER-119 from WT mice and JAK2V617F mice after normoxia and chronic  
 1597 hypoxia. Scale bars, 50  $\mu$ m. (c) mRNA levels of *Pdgfrb* and *Tgfb1* in the lungs. The 18s  
 1598 rRNA was used for the normalization. Data are presented as mean  $\pm$  SEM. The average  
 1599 value for the normoxia-WT mice was set to 1 (n = 3 in each group, \*P = 0.0105, †P =  
 1600 0.0132 for *Pdgfrb*, \*P = 0.0036, †P = 0.0009 for *Tgfb1*). All data are presented as mean  
 1601  $\pm$  SEM. \*P < 0.05 versus the corresponding normoxia-exposed group and †P < 0.05  
 1602 versus the corresponding WT mice by the one-way ANOVA with Tukey post-hoc  
 1603 analysis. WT, wild-type mice; JAK2V617F, JAK2V617F-expressing transgenic mice.

1604

1605 **Supplementary Figure 6.**

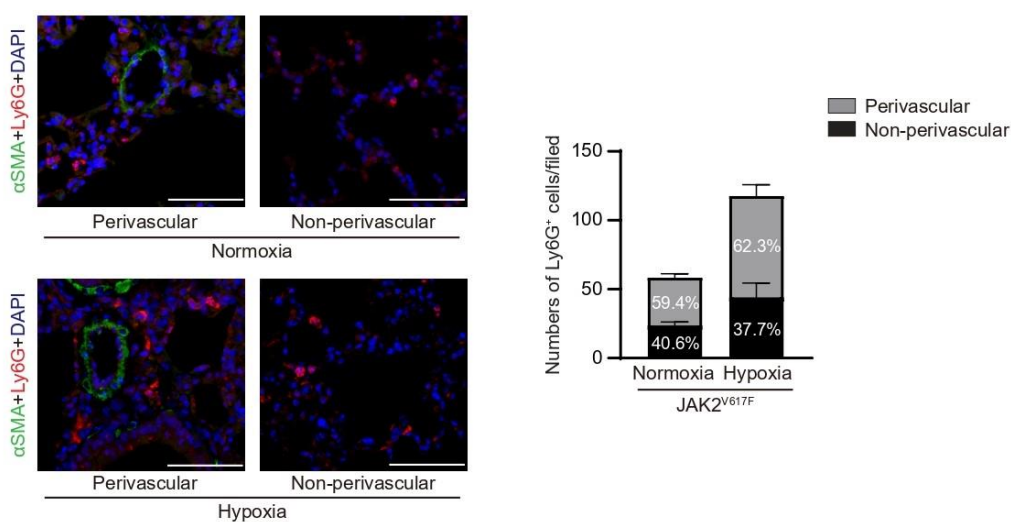


1606

1607 (a) Left, triple-labeled immunofluorescent staining (CD45, green; Ly6G, red; DAPI, blue)  
 1608 of the lung sections from WT mice and JAK2V617F mice after normoxia or chronic  
 1609 hypoxia. Right, quantitative analyses of the Ly6G-expressing cells within CD45+ cells (n  
 1610 = 3 in each group, \*P = 0.0038, †P = 0.0297 [left], 0.0008 [right]). (b) Left, triple-labeled  
 1611 immunofluorescent staining (CD45, green; F4/80, red; DAPI, blue). Right, quantitative  
 1612 analyses of the F4/80-expressing cells within CD45+ cells (n = 3 in each group). (c) Left,  
 1613 triple-labeled immunofluorescent staining (CD45, green; CD45R, red; DAPI, blue).  
 1614 Right, quantitative analyses of the CD45R-expressing cells within CD45+ cells (n = 3 in  
 1615 each group, †P = 0.0250). At least 100 CD45+ cells were counted in each. Data are  
 1616 presented as mean ± SEM. \*P < 0.05 versus the corresponding normoxia-exposed group  
 1617 and †P < 0.05 versus the corresponding WT mice by the one-way ANOVA with Tukey  
 1618 post-hoc analysis. Scale bars, 50 μm. WT, wild-type mice; JAK2V617F, JAK2V617F-  
 1619 expressing transgenic mice.

1620

1621 **Supplementary Figure 7.**

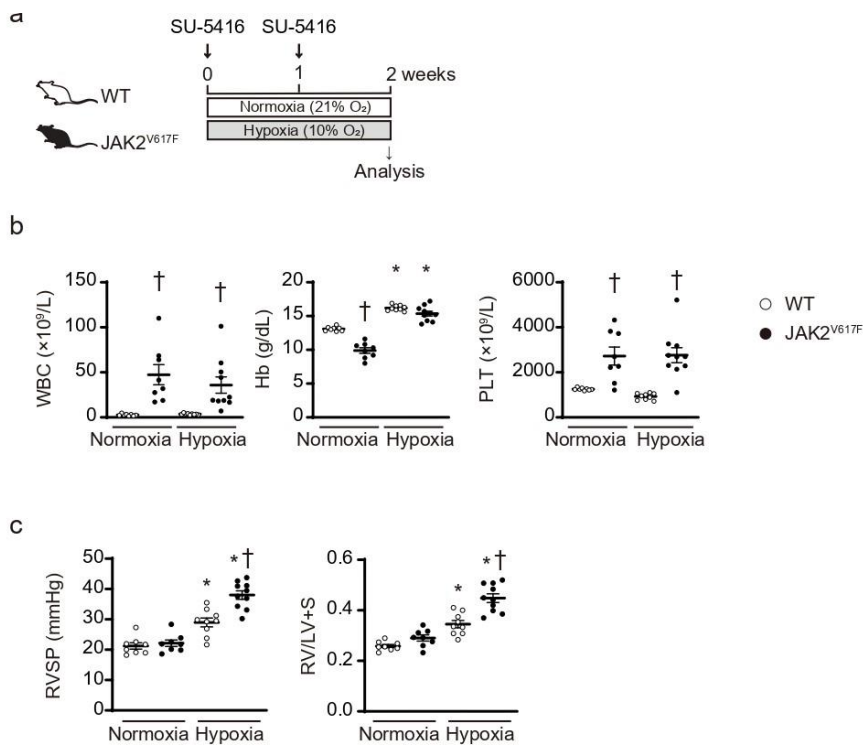


1622

1623 Left, triple-labeled immunofluorescent staining ( $\alpha$ SMA, green; Ly6G, red; DAPI, blue)  
 1624 of the lung sections in JAK2V617F mice. Perivascular regions were determined as the  
 1625 area within 100  $\mu$ m from distal pulmonary arteries with diameters of 50  $\mu$ m. Scale bars,  
 1626 50  $\mu$ m. Right, quantitative analyses of the numbers of Ly6G+ cells in perivascular regions  
 1627 as well as non-perivascular regions (n = 3). More than 10 fields were analyzed in each  
 1628 group. One field was defined as 200  $\mu$ m x 200  $\mu$ m. The percentages of the Ly6G+ cells  
 1629 in perivascular regions and non-perivascular regions in each group are shown. All data  
 1630 are presented as mean  $\pm$  SEM.

1631

1632 **Supplementary Figure 8.**



1633

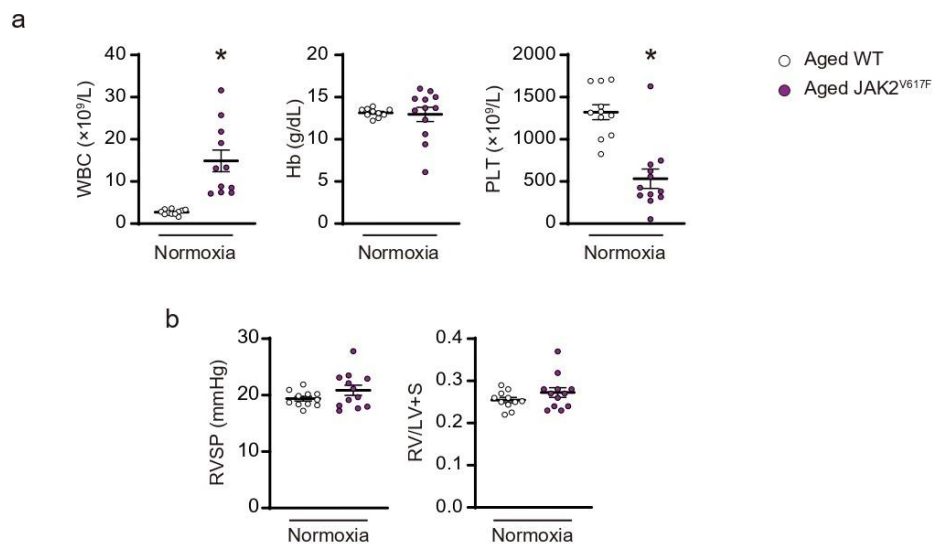
1634 (a) Experimental design. Single weekly injection of a VEGF inhibitor, SU-5416, at 20  
 1635 mg/kg followed by 2 weeks of normoxia (21% O<sub>2</sub>) or hypoxia (10% O<sub>2</sub>) in WT mice and  
 1636 JAK2V617F mice. (b) Peripheral blood cell counts (n = 8, 8, 9, 10, †P = 0.0014 [left],



1637 0.0142 [right] for WBC, n = 8, 8, 9, 10, \*P < 0.0001 [left], < 0.0001 [right], †P < 0.0001  
 1638 for Hb, n = 8, 8, 9, 10, †P = 0.0040 [left], < 0.0001 [right] for PLT). (c) Right ventricular  
 1639 systolic pressure (RVSP) and right ventricular hypertrophy determined by the ratio of  
 1640 right ventricle (RV) weight to left ventricle weight plus septum weight (RV/LV+S) (n =  
 1641 8, 8, 9, 10, \*P = 0.0012 [left], < 0.0001 [right], †P < 0.0001 for RVSP, n = 8, 8, 9, 10, \*P  
 1642 = 0.0007 [left], < 0.0001 [right], †P < 0.0001 for RV/LV+S). All data are presented as  
 1643 mean ± SEM. \*P < 0.05 versus the corresponding normoxia-exposed group and †P < 0.05  
 1644 versus the corresponding WT mice by the one-way ANOVA with Tukey post-hoc  
 1645 analysis. WBC, white blood cell count; Hb, hemoglobin concentration; PLT, platelet  
 1646 count. WT, wild-type mice; JAK2V617F, JAK2V617F-expressing transgenic mice.

1647

1648 **Supplementary Figure 9.**



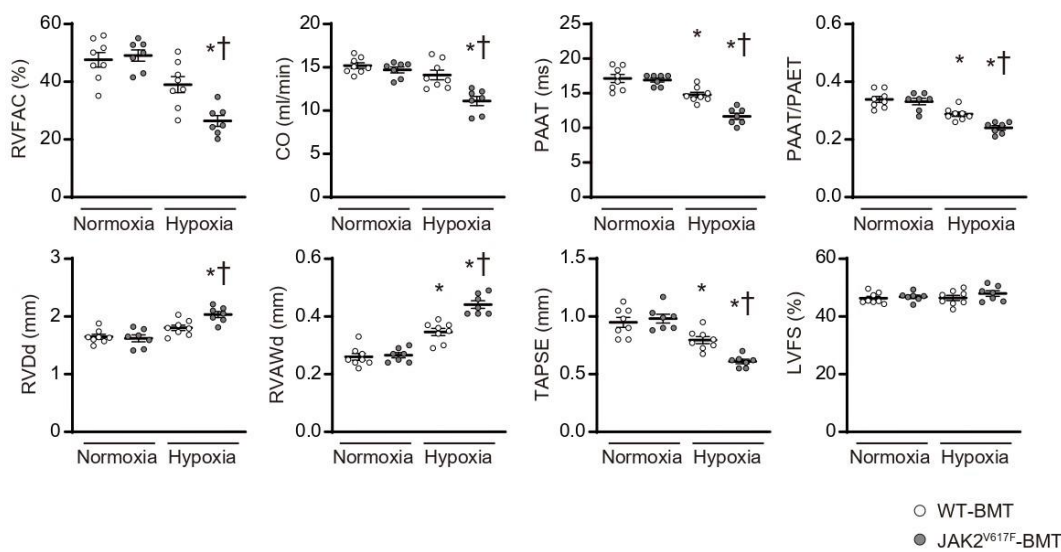
1649

1650 (a) Peripheral blood cell counts in WT and JAK2V617F female mice aged 8- to 9-month-  
 1651 old under normoxia (n = 12 in each group, \*P = 0.0001 for WBC, n = 10, 12 for Hb, n =  
 1652 11, 12, \*P < 0.0001 for PLT). (b) Right ventricular systolic pressure (RVSP) and right  
 1653 ventricular hypertrophy determined by the ratio of right ventricle (RV) weight to left

1654 ventricle weight plus septum weight (RV/LV+S) (n = 11, 12 in each). All data are  
 1655 presented as mean ± SEM. \*P < 0.05 versus WT mice by the unpaired Student's t-test  
 1656 (two-sided). WBC, white blood cell count; Hb, hemoglobin concentration; PLT, platelet  
 1657 count. WT, wild-type mice; JAK2V617F, JAK2V617F-expressing transgenic mice.

1658

1659 **Supplementary Figure 10.**



1660

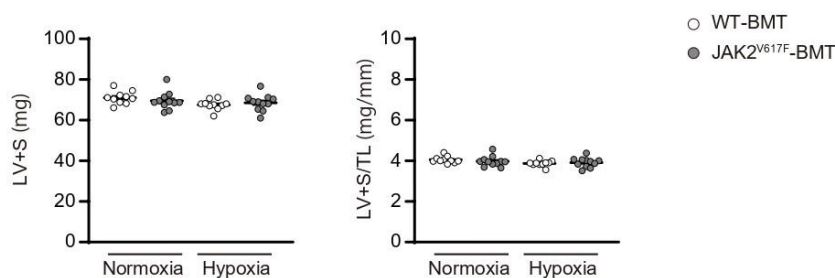
1661 Echocardiography was performed to evaluate pulmonary hemodynamics and cardiac  
 1662 function 3 weeks after normoxia or chronic hypoxia (n = 8, 7, 8, 7, \*P < 0.0001, †P =  
 1663 0.0047 for RVFAC, \*P < 0.0001, †P = 0.0004 for CO, \*P = 0.0036 [left], < 0.0001 [right],  
 1664 †P = 0.0002 for PAAT, \*P = 0.0027 [left], < 0.0001 [right], †P = 0.0075 for PAAT/PAET,  
 1665 \*P < 0.0001, †P = 0.0144 for RVDd, \*P < 0.0001 [left], < 0.0001 [right], †P < 0.0001 for  
 1666 RVAWd, \*P = 0.0168 [left], < 0.0001 [right], †P = 0.0041 for TAPSE). All data are  
 1667 presented as mean ± SEM. \*P < 0.05 versus the corresponding normoxia-exposed group  
 1668 and †P < 0.05 versus the corresponding WT mice by one-way ANOVA with Tukey post-  
 1669 hoc analysis. RVFAC, right ventricular fractional area change; CO, cardiac output;  
 1670 PAAT, pulmonary artery acceleration time; PAET, pulmonary artery ejection time;



1671 RVDd, right ventricular diastolic diameter, RVAWd, right ventricular anterior wall  
1672 diameter; TAPSE, tricuspid annular plane systolic excursion; LVFS, left ventricular  
1673 fractional shortening; WT-BMT, recipient WT mice transplanted with WT bone marrow  
1674 cells; JAK2V617F-BMT, recipient WT mice transplanted with JAK2V617F bone marrow  
1675 cells.

1676

1677 **Supplementary Figure 11.**



1678

1679 Left ventricular (LV) weight including septum (S) was measured after exposure to  
1680 normoxia (21% O<sub>2</sub>) or chronic hypoxia (10% O<sub>2</sub>) for 3 weeks (n = 10, 11, 10, 11 in each).

1681 LV+S was normalized by tibia length (TL). All data are presented as mean ± SEM. The  
1682 statistical comparison was performed by the one-way ANOVA. WT-BMT, recipient WT  
1683 mice transplanted with WT bone marrow cells; JAK2V617F-BMT, recipient WT mice  
1684 transplanted with JAK2V617F bone marrow cells.

1685

1686

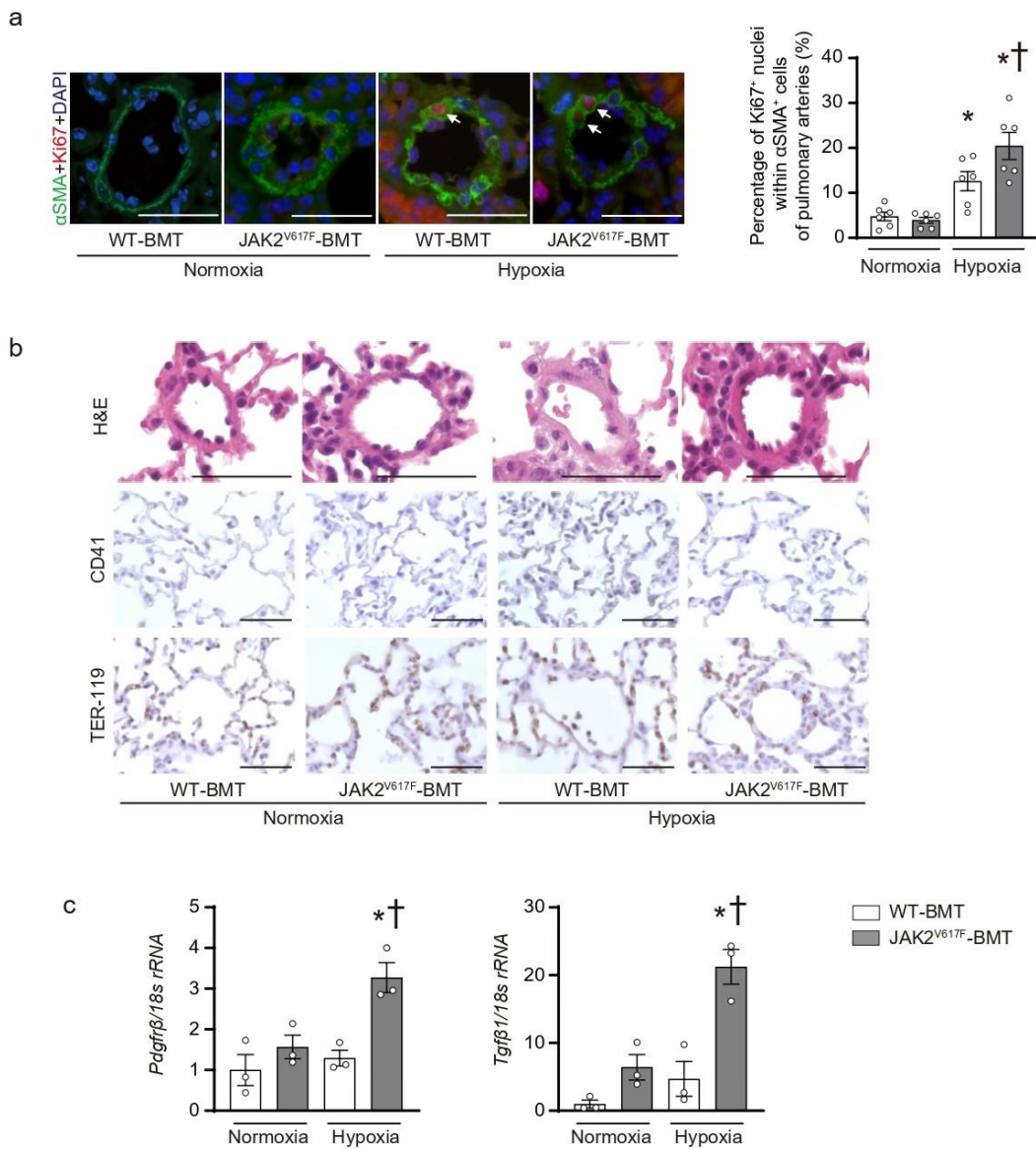
1687

1688

1689

1690

1691 **Supplementary Figure 12.**



1692

1693 (a) Left, triple-labeled immunofluorescent staining ( $\alpha$ SMA, green; Ki67, red; DAPI, blue)

1694 of the lung sections. Right, quantitative analyses of the percentage of Ki67-positive nuclei

1695 within  $\alpha$ SMA+ cells of distal pulmonary arteries with a diameter of 50-100  $\mu$ m (n = 6 in

1696 each group, \*P = 0.0430 [left], < 0.0001 [right], †P = 0.0425). More than 80  $\alpha$ SMA+ cells

1697 were counted in each section. White arrows indicate Ki67-positive nuclei within  $\alpha$ SMA+

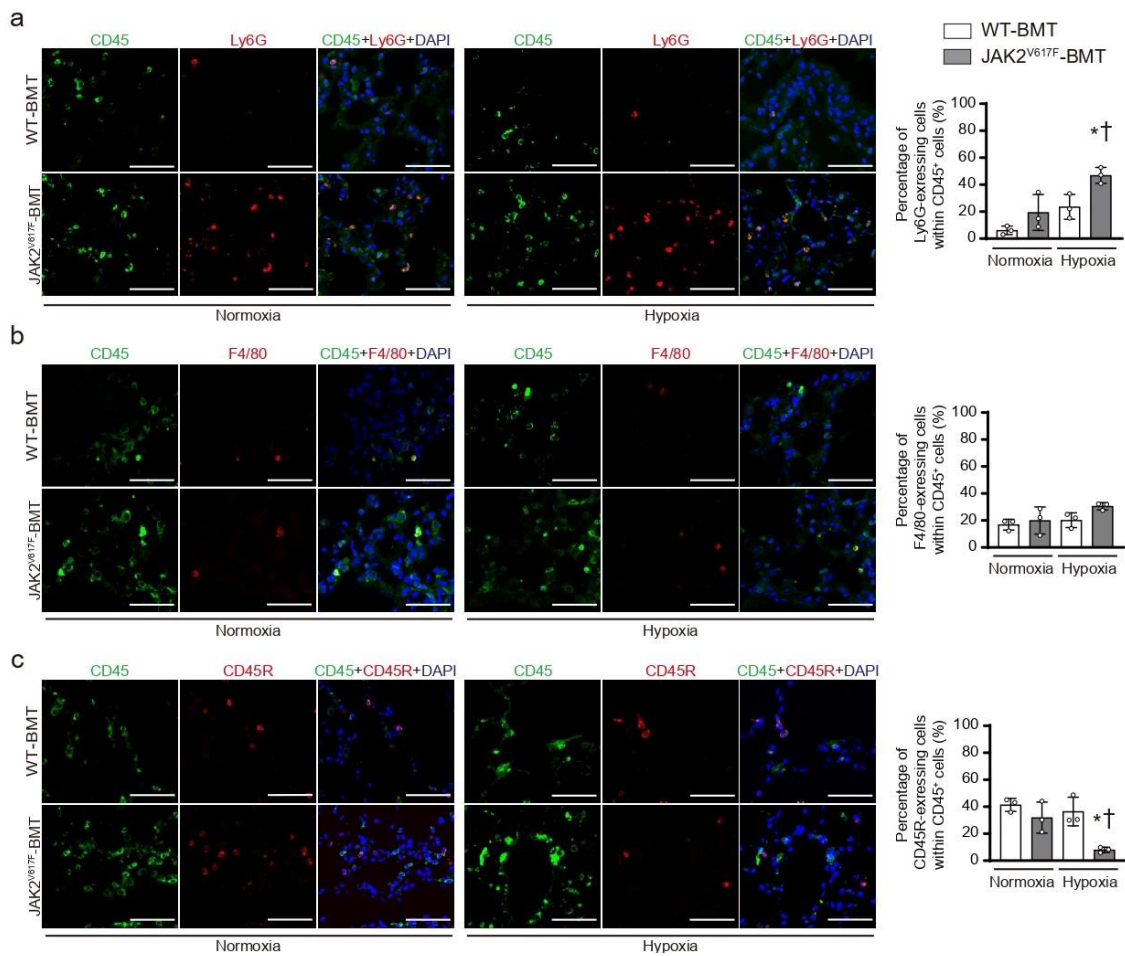
1698 cells. Scale bars, 50  $\mu$ m. (b) Representative images of the lung sections of H&E staining

1699 and immunostaining for CD41 and TER-119 from WT-BMT mice and JAK2V617F-BMT

1700 mice after normoxia and chronic hypoxia. Scale bars, 50  $\mu$ m. (c) mRNA levels of *Pdgfrb*  
 1701 and *Tgfb1* in the lungs. The 18s rRNA was used for the normalization. Data are presented  
 1702 as mean  $\pm$  SEM. The average value for the normoxia-WT-BMT mice was set to 1 ( $n = 3$   
 1703 in each group, \* $P = 0.0214$ , † $P = 0.0095$  for *Pdgfrb*, \* $P = 0.0041$ , † $P = 0.0021$  for *Tgfb1*).  
 1704 All data are presented as mean  $\pm$  SEM. \* $P < 0.05$  versus the corresponding normoxia-  
 1705 exposed group and † $P < 0.05$  versus the corresponding WT-BMT mice by one-way  
 1706 ANOVA with Tukey post-hoc analysis. WT-BMT, recipient WT mice transplanted with  
 1707 WT bone marrow cells; JAK2V617F-BMT, recipient WT mice transplanted with  
 1708 JAK2V617F bone marrow cells.

1709

1710 **Supplementary Figure 13.**

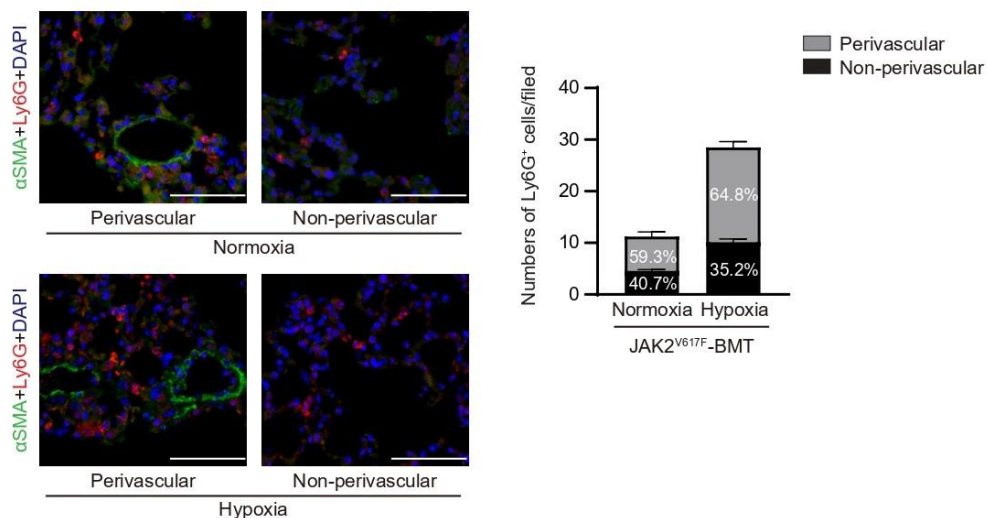


1711

1712 (a) Left, triple-labeled immunofluorescent staining (CD45, green; Ly6G, red; DAPI, blue)  
 1713 of the lung sections from WT mice and JAK2V617F mice after normoxia or chronic  
 1714 hypoxia. Right, quantitative analyses of the Ly6G-expressing cells within CD45<sup>+</sup> cells (n  
 1715 = 3 in each group, \*P = 0.0205, †P = 0.0459). (b) Left, triple-labeled immunofluorescent  
 1716 staining (CD45, green; F4/80, red; DAPI, blue). Right, quantitative analyses of the F4/80-  
 1717 expressing cells within CD45<sup>+</sup> cells (n = 3 in each group). (c) Left, triple-labeled  
 1718 immunofluorescent staining (CD45, green; CD45R, red; DAPI, blue). Right, quantitative  
 1719 analyses of the CD45R-expressing cells within CD45<sup>+</sup> cells (n = 3 in each group, \*P =  
 1720 0.0309, †P = 0.0125). At least 100 CD45<sup>+</sup> cells were counted in each. All data are  
 1721 presented as mean ± SEM. \*P < 0.05 versus the corresponding normoxia-exposed group  
 1722 and †P < 0.05 versus the corresponding WT-BMT mice by one-way ANOVA with Tukey  
 1723 post-hoc analysis. Scale bars, 50 μm. WT-BMT, recipient WT mice transplanted with WT  
 1724 bone marrow cells; JAK2V617F-BMT, recipient WT mice transplanted with JAK2V617F  
 1725 bone marrow cells.

1726

1727 **Supplementary Figure 14.**

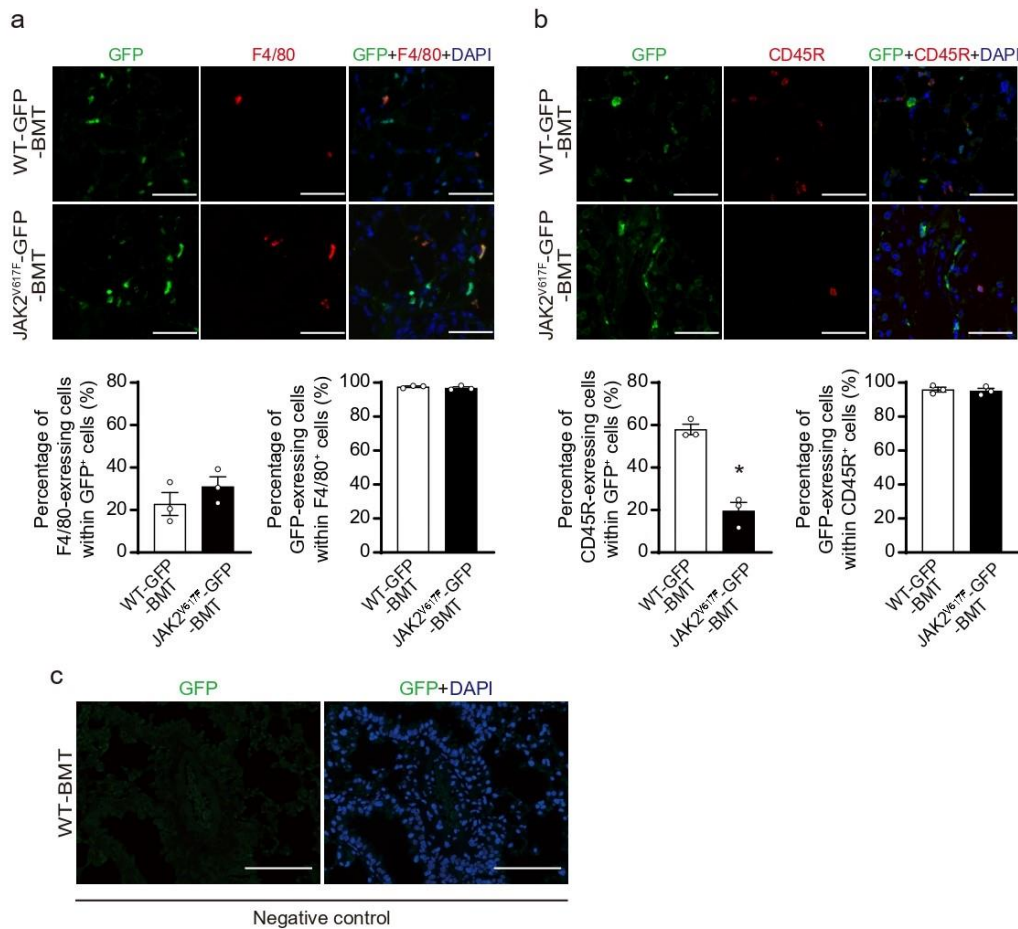


1728

1729 Left. triple-labeled immunofluorescent staining ( $\alpha$ SMA, green; Ly6G, red; DAPI, blue)  
 1730 of the lung sections in JAK2V617F-BMT mice. Perivascular regions were determined as  
 1731 the area within 100  $\mu$ m from distal pulmonary arteries with diameters of 50  $\mu$ m. Scale  
 1732 bars, 50  $\mu$ m. Right, quantitative analyses of the numbers of Ly6G<sup>+</sup> cells in perivascular  
 1733 regions as well as non-perivascular regions (n = 3). More than 10 fields were analyzed in  
 1734 each group. One field was defined as 200  $\mu$ m x 200  $\mu$ m. The percentages of the Ly6G<sup>+</sup>  
 1735 cells in perivascular regions and non-perivascular regions in each group are shown.  
 1736 JAK2V617F-BMT, recipient WT mice transplanted with JAK2V617F bone marrow cells.  
 1737 All data are presented as mean  $\pm$  SEM.

1738

1739 **Supplementary Figure 15.**

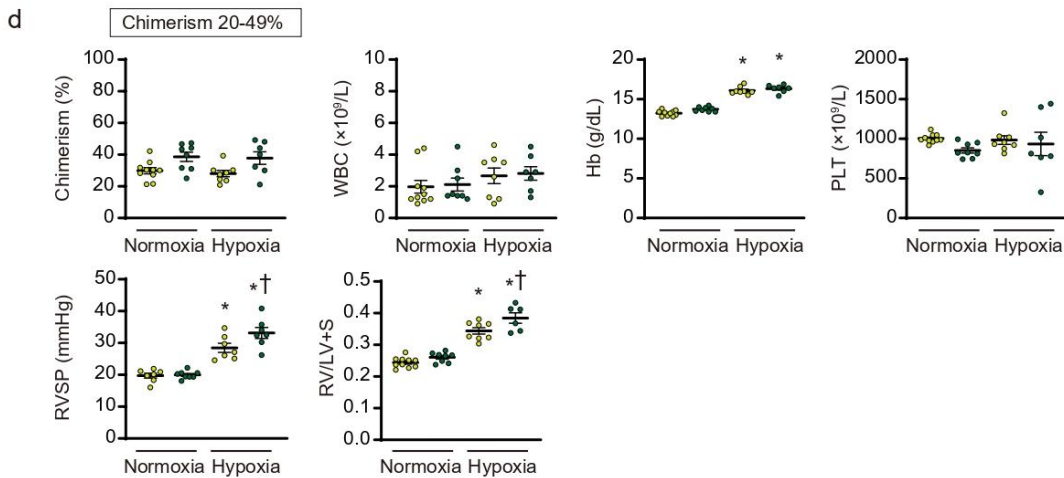
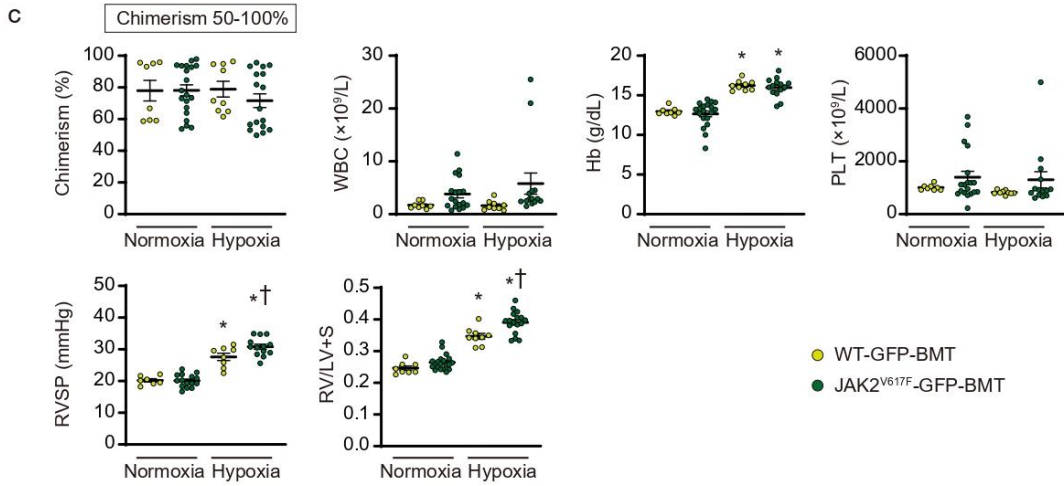
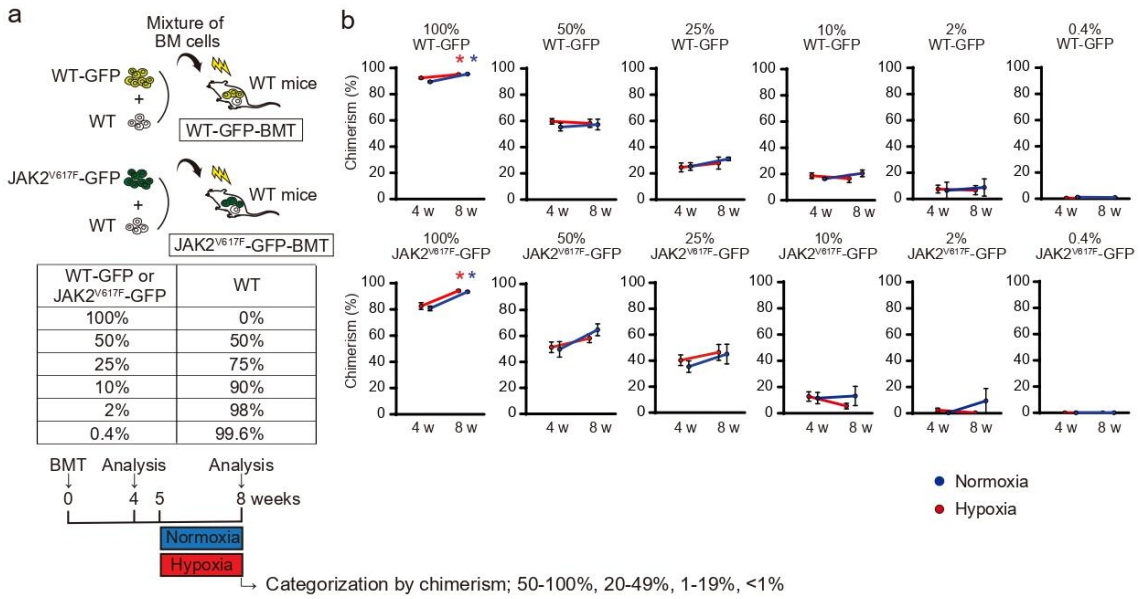


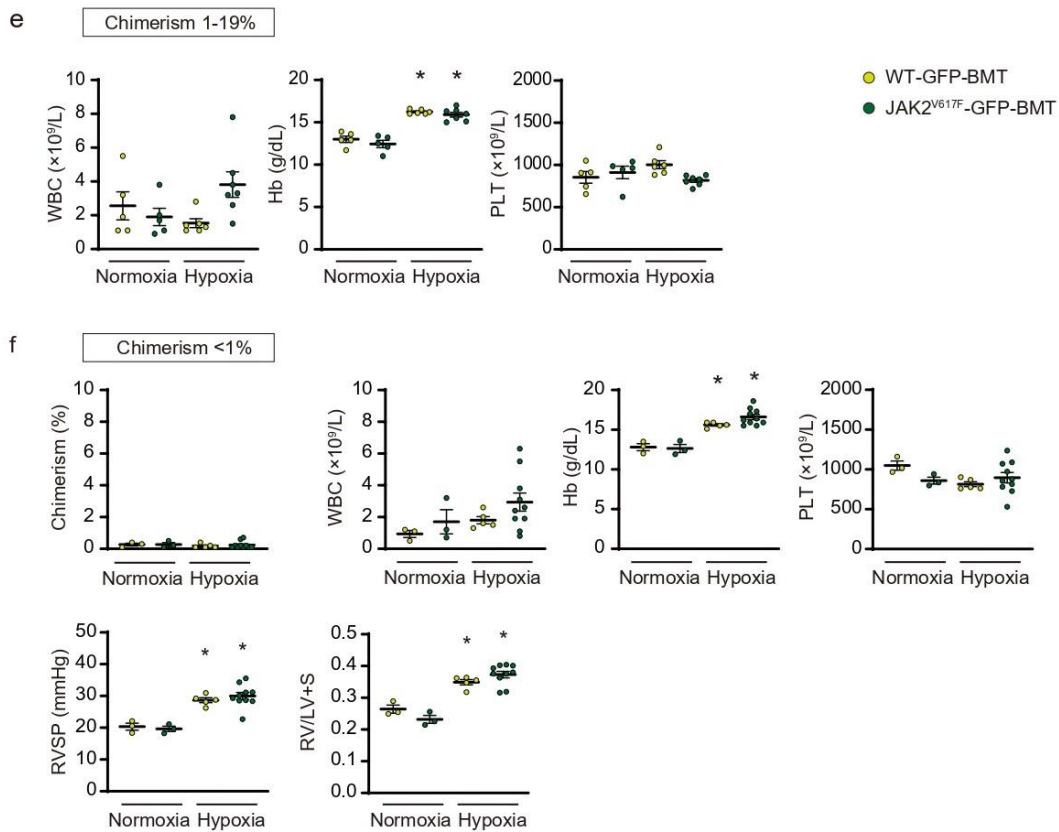
1740

1741 (a) Lethally irradiated WT mice were transplanted with bone marrow (BM) cells from  
1742 control WT/CAG-EGFP (WT-GFP) or JAK2V617F/CAG-EGFP (JAK2V617F-GFP)  
1743 double transgenic mice. Five weeks after BM transplantation (BMT), recipients were  
1744 subjected to chronic hypoxia for 3 weeks, and then the lungs were fixed and stained with  
1745 the indicated antibodies. Representative immunofluorescence images of lung sections  
1746 stained with anti-GFP (green) and anti-F4/80 (red) antibodies and DAPI (blue) in WT-  
1747 GFP-BMT or JAK2V617F-GFP-BMT mice are shown in top panels. Scale bars, 50  $\mu$ m.  
1748 Quantitative analyses of F4/80-expressing cells within GFP<sup>+</sup> cells and GFP-expressing  
1749 cells within F4/80<sup>+</sup> cells are shown in the graphs (n = 3 in each group). (b) Representative  
1750 immunofluorescence images of lung sections stained with anti-GFP (green) and anti-  
1751 CD45R (red) antibodies and DAPI (blue) in WT-GFP-BMT or JAK2V617F-GFP-BMT  
1752 mice. Scale bars, 50  $\mu$ m. Quantitative analyses of CD45R-expressing cells within GFP<sup>+</sup>  
1753 cells and GFP-expressing cells within CD45R<sup>+</sup> cells are shown in the graphs (n = 3 in  
1754 each group). More than 100 cells were counted in each. \*P = 0.0012 versus WT-GFP-  
1755 BMT mice by the unpaired t-test (two-sided). All data are presented as mean  $\pm$  SEM. (c)  
1756 The lung sections from WT recipient mice transplanted with WT BM cells without GFP  
1757 as a negative control. The sections were stained with an anti-GFP (green) antibody and  
1758 DAPI (blue). Representative images of three independent experiments are shown. Scale  
1759 bars, 100  $\mu$ m. WT-GFP-BMT, recipient WT mice transplanted with WT-GFP BM cells;  
1760 JAK2V617F-GFP-BMT, recipient WT mice transplanted with JAK2V617F-GFP BM  
1761 cells.  
1762  
1763  
1764



1765 **Supplementary Figure 16.**





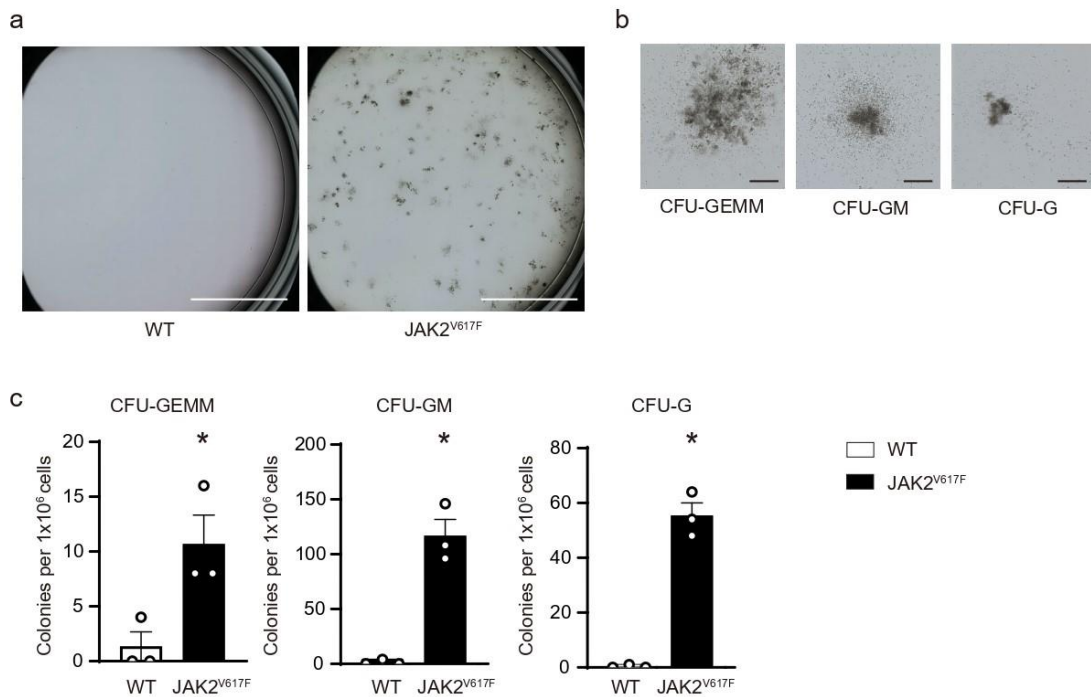
1767

1768 (a) Schematic depiction of the competitive bone marrow transplantation (BMT). The  
 1769 different ratio of WT-GFP or JAK2V617F-GFP and WT without GFP competitor was  
 1770 transplanted into the lethally irradiated recipient WT mice. The BMT mice at 8 weeks  
 1771 were categorized according to the chimerism; 50-100%, 20-49%, 1-19%, <1%. (b) The  
 1772 donor chimerism in the blood after BMT. The percentage of GFP<sup>+</sup> cells within CD45<sup>+</sup>  
 1773 cells was determined by flow cytometry at 4 and 8 weeks after BMT after normoxia or  
 1774 chronic hypoxia exposure (n = 9, 9, \*P = 0.0001 [normoxia], 0.0211 [hypoxia] for 100%  
 1775 WT-GFP, n = 5, 5 for 50% WT-GFP, n = 5, 5 for 25% WT-GFP, n = 5, 5 for 10% WT-  
 1776 GFP; n = 5, 6 for 2% WT-GFP, n = 5, 5 for 0.4% WT-GFP, n = 11, 9, \*P < 0.0001  
 1777 [normoxia], 0.0025 [hypoxia] for 100% JAK2V617F-GFP, n = 10, 6 for 50%  
 1778 JAK2V617F-GFP, n = 8, 14 for 25% JAK2V617F-GFP, n = 5, 4 for 10% JAK2V617F-  
 1779 GFP, n = 5, 8 for 2% JAK2V617F-GFP, n = 5, 7 for 0.4% JAK2V617F-GFP). \*P < 0.05



1780 versus the corresponding 4-week group by the two-sided paired Student's t-test (blue,  
1781 normoxia group; red, hypoxia group). (c, d) The recipients with donor chimerism of 50-  
1782 100% (c, n = 8, 20, 9, 17) and 20-49% (d, n = 10, 8, 8, 7) at 8 weeks after BMT were  
1783 enrolled for statistical comparison. Peripheral blood cell counts, RVSP, and RV/LV+S are  
1784 shown (c, n = 8, 18, 9, 14 for WBC, n = 8, 19, 9, 14, \*P < 0.0001 [left], < 0.0001 [right]  
1785 for Hb, n = 8, 19, 9, 14 for PLT, n = 7, 15, 8, 13, \*P < 0.0001 [left], < 0.0001 [right], †P  
1786 = 0.0339 for RVSP, n = 8, 20, 9, 17, \*P < 0.0001 [left], < 0.0001 [right], †P < 0.0021 for  
1787 RV/LV+S; d, n = 10, 8, 8, 7 for WBC, n = 10, 8, 8, 7, \*P < 0.0001 [left], < 0.0001 [right]  
1788 for Hb, n = 10, 8, 8, 7 for PLT, n = 7, 8, 7, 7, \*P = 0.0001 [left], < 0.0001 [right], †P =  
1789 0.0445 for RVSP, n = 10, 8, 8, 6, \*P < 0.0001 [left], < 0.0001 [right], †P = 0.0291 for  
1790 RV/LV+S). (e) Peripheral blood cell counts in the BMT mice with donor chimerism of 1-  
1791 19% at 8 weeks after BMT (n = 5, 5, 6, 7 for WBC, n = 5, 5, 6, 7, \*P < 0.0001 [left], <  
1792 0.0001 [right] for Hb, n = 5, 5, 6, 7 for PLT). The data of chimerism, RVSP, and RV/LV+S  
1793 are shown in main Fig. 4. (f) The donor chimerism, peripheral blood cell counts, RVSP  
1794 and RV/LV+S in the BMT mice with donor chimerism with <1% (n = 3, 3, 5, 10 for  
1795 chimerism, n = 3, 3, 5, 10 for WBC, n = 3, 3, 5, 10, \*P = 0.0014 [left], < 0.0001 [right]  
1796 for Hb, n = 3, 3, 5, 10 for PLT, n = 3, 3, 5, 10, \*P = 0.0043 [left], 0.0002 [right] for RVSP,  
1797 n = 3, 3, 5, 10, \*P = 0.0027 [left], < 0.0001 [right] for RV/LV+S). All data are presented  
1798 as mean ± SEM. \*P < 0.05 versus the corresponding normoxia-exposed group and †P <  
1799 0.05 versus the corresponding WT-GFP-BMT mice by the one-way ANOVA with Tukey  
1800 post-hoc analysis. WBC, white blood cell count; Hb, hemoglobin concentration; PLT,  
1801 platelet count; WT-GFP-BMT, recipient WT mice transplanted with WT-GFP BM cells;  
1802 JAK2V617F-GFP-BMT, recipient WT mice transplanted with JAK2V617F-GFP BM  
1803 cells.

1804 **Supplementary Figure 17.**



1805

1806 CD117 (c-kit)<sup>+</sup> cells were sorted from the mouse lung tissue in WT and JAK2V617F

1807 mice using a magnetic bead method. On a 35-mm plate, 5x10<sup>5</sup> were grown in Methocult

1808 GF M3434. After 7 days, the colonies derived from colony-forming unit (CFU)-

1809 granulocyte, -erythroid, -macrophage, -megakaryocyte (CFU-GEMM), CFU-

1810 granulocyte, -monocyte (CFU-GM), CFU-granulocyte (CFU-G) were counted according

1811 to the morphology. (a, b) Representative images of the plates and colonies. Scale bars, 10

1812 mm (a) and 300 μm (b). (c) Quantification of numbers of the colonies (n = 3 in each

1813 group, \*P = 0.0352 for CFU-GEMM, \*P = 0.0016 for CFU-GM, \*P = 0.0003 for CFU-

1814 G). All data are presented as mean ± SEM. \*P < 0.05 versus WT by the unpaired t-test

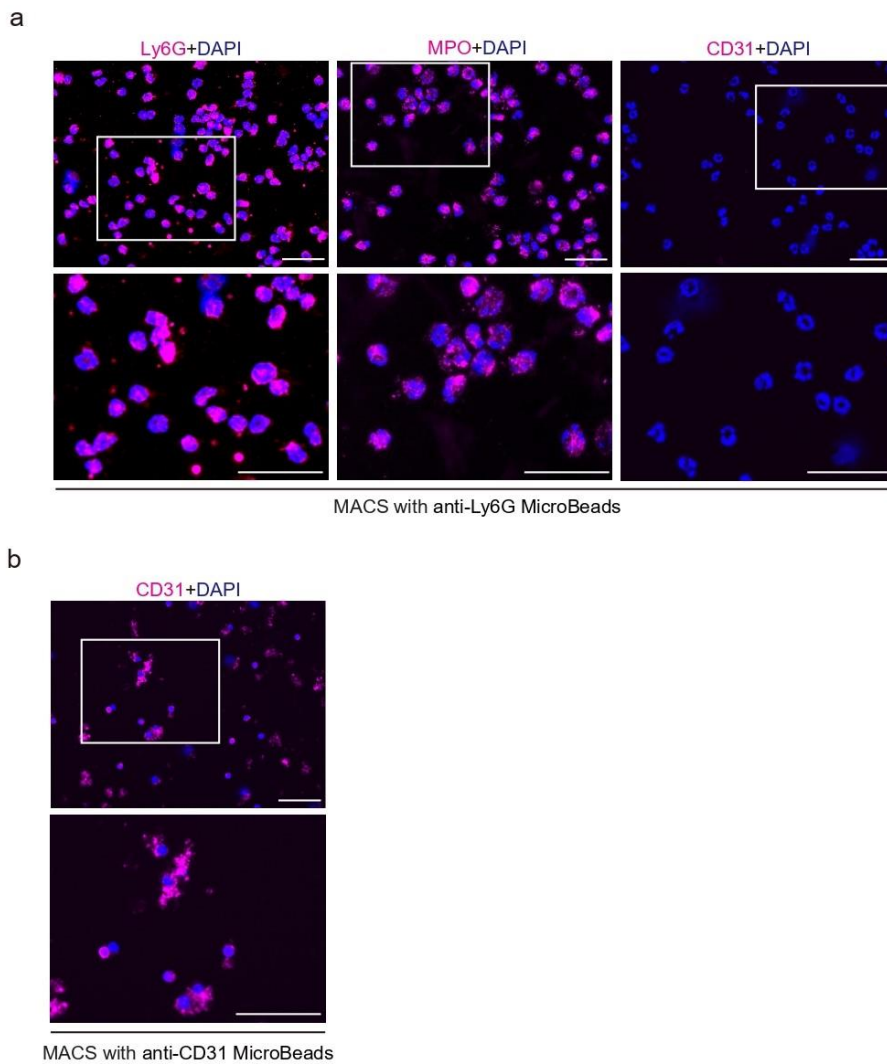
1815 (two-sided). WT, wild-type mice; JAK2V617F, JAK2V617F-expressing transgenic mice.

1816

1817

1818

1819 **Supplementary Figure 18.**



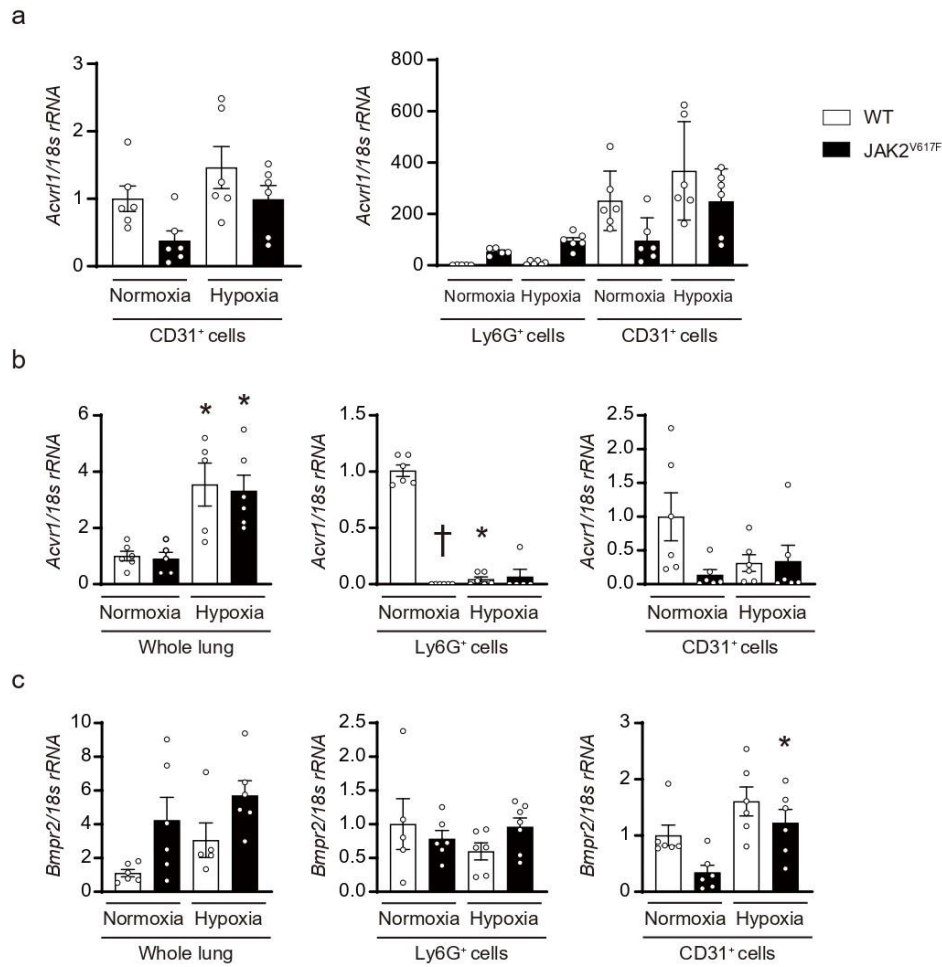
1820

1821 The cell suspensions from the lungs in wild-type mice were subjected to MACS with anti-  
1822 Ly6G MicroBeads (a) or anti-CD31 MicroBeads (b). The sorted cells were fixed and  
1823 stained with indicated antibodies (magenta) with DAPI (blue). Images in boxed areas at  
1824 higher magnification are shown in bottom panels. Scale bars, 50 um. Nearly 100% of the  
1825 MACS-isolated Ly6G<sup>+</sup> cells were stained with anti-Ly6G and anti-myeloperoxidase  
1826 (MPO) antibodies, a specific marker for neutrophils, while these cells were not stained  
1827 with an anti-CD31 antibody, a specific marker for endothelial cells. Representative

1828 images of three independent experiments are shown. MACS, Magnetic-activated cell  
 1829 sorting.

1830

1831 **Supplementary Figure 19.**



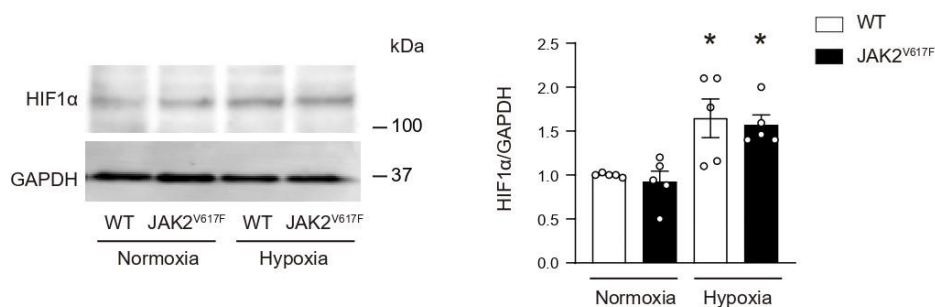
1832

1833 (a) Left, mRNA expression of Acvr11 in the sorted cells by MACS with anti-CD31  
 1834 MicroBeads from the lungs of WT mice and JAK2V617F mice after normoxia or hypoxia  
 1835 (n = 6 in each group). Right, The comparison of Acvr11 mRNA expression levels between  
 1836 Ly6G<sup>+</sup> and CD31<sup>+</sup> cells from the lungs (n = 5, 5, 6, 6, 6, 6, 6). The data of Ly6G<sup>+</sup> cells  
 1837 are from main Figure 6. (b) mRNA expression of Acvr1 in the whole lung extracts (left  
 1838 graph, n = 6, 5, 5, 6, \*P = 0.0079 [left], 0.0116 [right]), Ly6G<sup>+</sup> cells from the lungs

1839 (middle graph, n = 6, 6, 6, 5, †P < 0.0001), CD31+ cells from the lungs (right graph, n =  
 1840 6 in each group). (c) mRNA levels of Bmpr2 in the whole lung extracts (left graph, n =  
 1841 6, 6, 5, 6), Ly6G+ cells from the lungs (middle graph, n = 5, 5, 6, 7), CD31+ cells from  
 1842 the lungs (right graph, n = 6 in each group, \*P = 0.0338). The 18s rRNA was used for the  
 1843 normalization. Data are presented as mean ± SEM. The average value for the normoxia-  
 1844 WT mice was set to 1. \*P < 0.05 versus the corresponding normoxia-exposed group and  
 1845 †P < 0.05 versus the corresponding WT mice by the one-way ANOVA with Tukey post-  
 1846 hoc analysis. WT, wild-type mice; JAK2V617F, JAK2V617F-expressing transgenic  
 1847 mice.

1848

1849 **Supplementary Figure 20.**

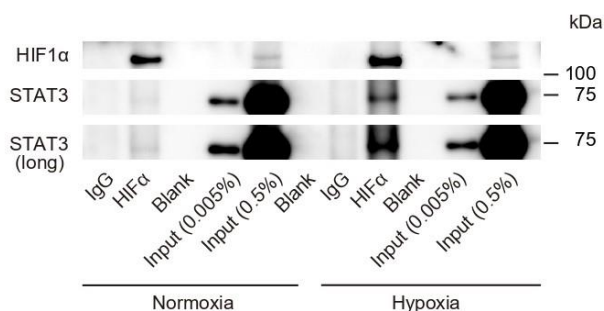


1850

1851 Immunoblotting of HIF1α in WT mice and JAK2V617F mice after normoxia and chronic  
 1852 hypoxia. Left panels show representative blots. Densitometric analysis is shown in the  
 1853 right graph (n = 5 in each group, \*P = 0.0200 [left], 0.0200 [right]). GAPDH was used as  
 1854 the loading control. The average value for the normoxia-WT mice was set to 1. Data are  
 1855 presented as mean ± SEM. \*P < 0.05 versus the corresponding normoxia-exposed group  
 1856 by the one-way ANOVA with Tukey post-hoc analysis. WT, wild-type mice; JAK2V617F,  
 1857 JAK2V617F-expressing transgenic mice.

1858

1859 **Supplementary Figure 21.**



1860

1861 Co-immunoprecipitation of STAT3 and HIF1 $\alpha$  in the lung tissue of JAK2V617F mice  
1862 after exposure to normoxia and chronic hypoxia for 2 weeks. The lung homogenates were  
1863 immunoprecipitated with Rabbit IgG or an anti-HIF1 $\alpha$  antibody and subjected to  
1864 immunoblotting with anti-HIF1 $\alpha$  and anti-STAT3 antibodies. The two blots from the  
1865 bottom were originated from the same membrane, and the longer exposure time was used  
1866 in the bottom blot for clarity (long). Representative images of two independent  
1867 experiments are shown.

1868

1869

1870

1871

1872

1873

1874

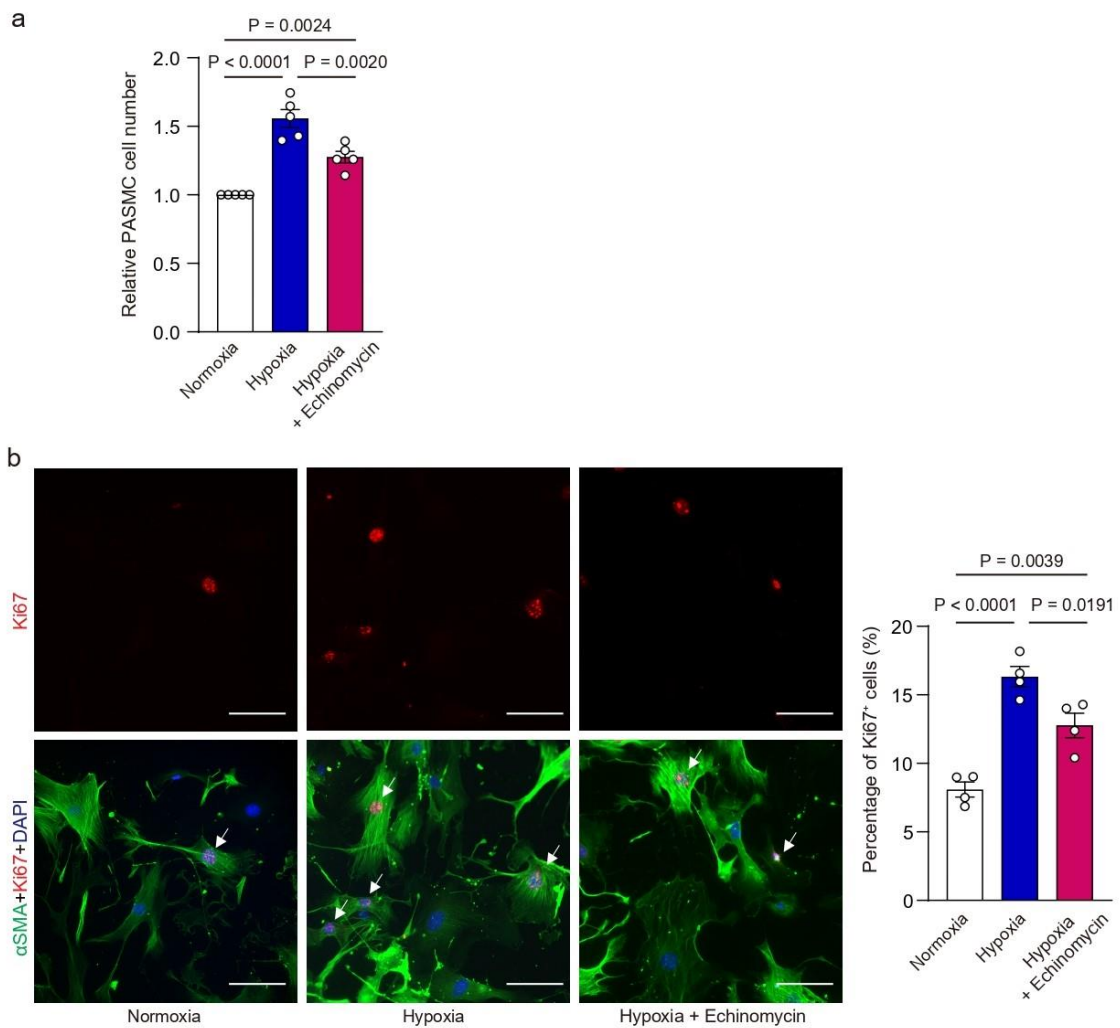
1875

1876

1877

1878

1879 **Supplementary Figure 22.**



1880

1881 (a) The neutrophils were collected from peripheral blood of JAK2V617F mice by MACS  
 1882 with Ly6G+ MicroBeads. Cells were starved and then incubated in a hypoxia incubator  
 1883 chamber (10% O<sub>2</sub>) for 3 h. The neutrophils were pretreated with Echinomycin (1 nM),  
 1884 an anti-HIF1 $\alpha$  inhibitor, prior to hypoxia for 1 h, and then the medium was freshly  
 1885 changed just before hypoxia stimulation. Control neutrophils were cultured in normoxic  
 1886 conditions for 3 h. The conditioned medium was collected and centrifuged to remove the  
 1887 cell debris. PASM were incubated with the neutrophil-derived conditioned medium for  
 1888 48 h. Cell numbers were determined by cell proliferation assay and expressed as a relative

1889 ratio over the group of PASMC incubated with conditioned medium from normoxic  
1890 conditions from 5 independent experiments. (b) Left, representative immunofluorescent  
1891 images of Ki67 staining and triple staining ( $\alpha$ SMA, green; Ki67, red; DAPI, blue) of  
1892 PASMC 48 h after neutrophil-derived conditioned medium stimulation. White arrows  
1893 indicate Ki67-positive nuclei. Right, quantitative analyses of the Ki67-positive cells.  
1894 More than 100 cells were counted (n = 4 independent experiments). Scale bars, 100  $\mu$ m.  
1895 Data are presented as mean  $\pm$  SEM. Statistical significance was determined by the one-  
1896 way ANOVA with Tukey post-hoc analysis.

1897

1898

1899

1900

1901

1902

1903

1904

1905

1906

1907

1908

1909

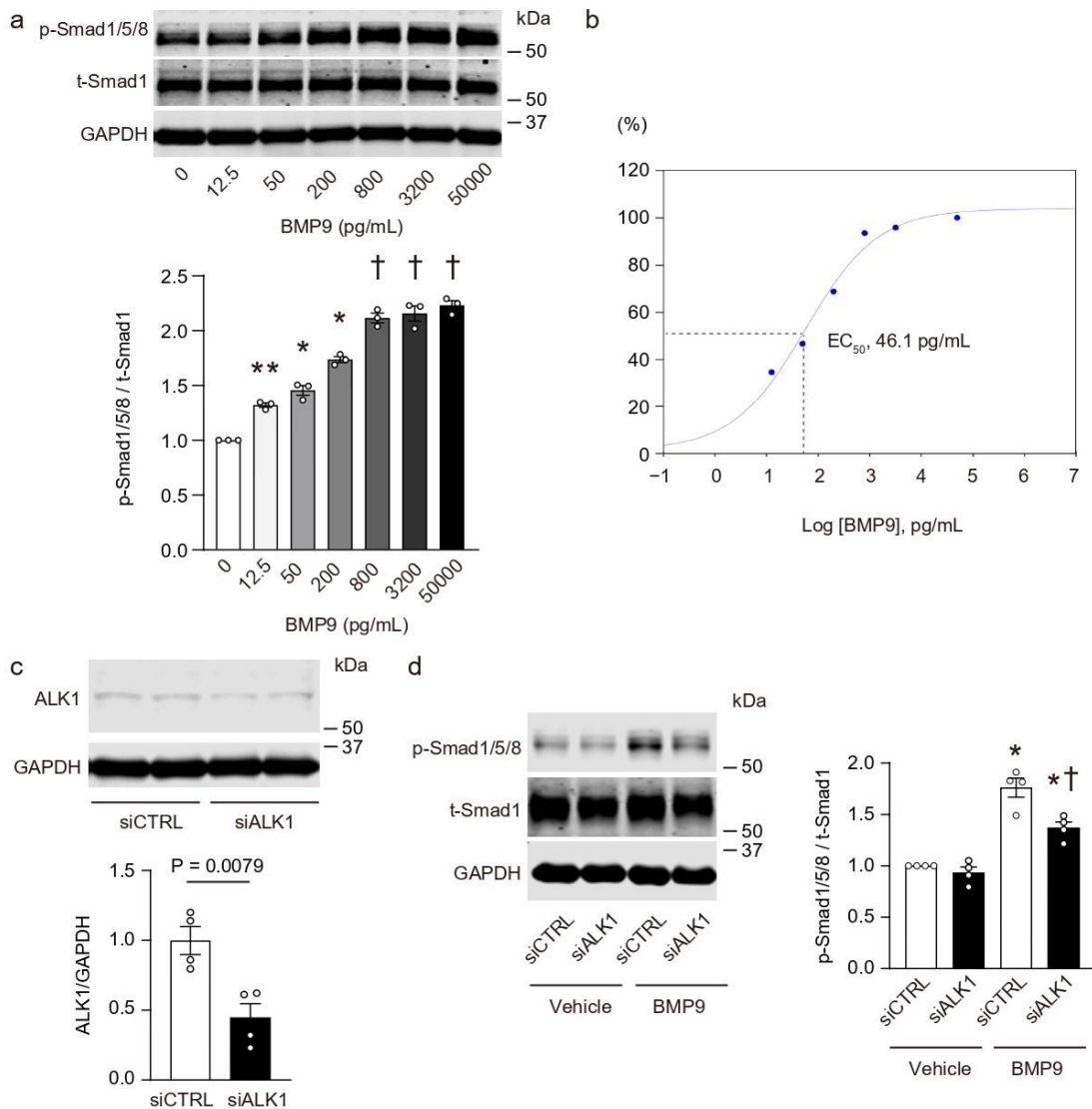
1910

1911

1912



1913 **Supplementary Figure 23.**



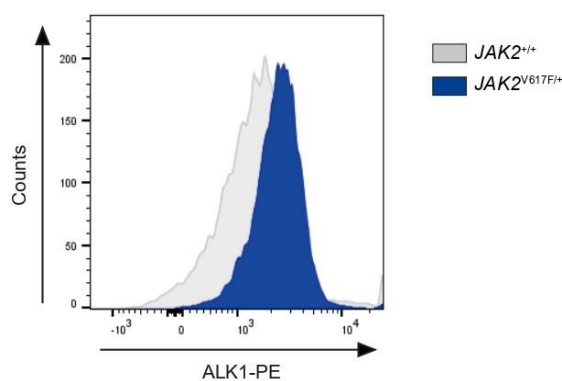
1914

1915 (a) Immunoblots of Smad1/5/8 phosphorylation in HCT116 cells. HCT116 cells were  
 1916 incubated with BMP9, a high-affinity ALK1 ligand, at the indicated concentration for 3  
 1917 h, and then the cell lysates were subjected to immunoblotting. p-Smad1/5/8 and t-Smad1  
 1918 indicate phosphorylated Smad1/5/8 and total Smad1, respectively. Data are presented as  
 1919 mean ± SEM (n = 3 independent experiments). \*P < 0.05 versus all other groups, \*\*P <  
 1920 0.05 versus all other groups except 50 pg/mL of BMP9 and †P < 0.05 versus all other  
 1921 groups except 800, 3200, 5000 pg/mL of BMP9 by the one-way ANOVA with Tukey

1922 post-hoc analysis.  $P = 0.0011$  (0 vs. 12.5),  $< 0.0001$  (0 vs. 50),  $< 0.0001$  (0 vs. 200),  $<$   
1923  $0.0001$  (0 vs. 800),  $< 0.0001$  (0 vs. 3200),  $< 0.0001$  (0 vs. 50000), 0.2984 (12.5 vs. 50),  $<$   
1924  $0.0001$  (12.5 vs. 200),  $< 0.0001$  (12.5 vs. 800),  $< 0.0001$  (12.5 vs. 3200),  $< 0.0001$  (12.5  
1925 vs. 50000), 0.0038 (50 vs. 200),  $< 0.0001$  (50 vs. 800),  $< 0.0001$  (50 vs. 3200),  $< 0.0001$   
1926 (50 vs. 50000), 0.0002 (200 vs. 800),  $< 0.0001$  (200 vs. 3200),  $< 0.0001$  (200 vs. 50000),  
1927 0.9902 (800 vs. 3200), 0.4820 (800 vs. 50000), 0.8638 (3200 vs. 50000). (b)  
1928 Concentration responses of BMP9 were calculated from (a). The BMP9 EC50 value was  
1929 estimated to be 46.1 pg/mL (AAT Bioquest, Inc. Quest Graph™ EC50 Calculator). (c)  
1930 HCT116 cells were transfected with ALK1-specific siRNA (siALK1) or non-targeting  
1931 control siRNA (siCTRL) with 40 nM for 48 h. Data are presented as the mean  $\pm$  SEM (n  
1932 = 4). Statistical comparisons were performed by the unpaired Student's t test (two-sided).  
1933 (d) Transfected cells were incubated with BMP9 of 200 pg/mL or vehicle for 3 h, and  
1934 then Smad1/5/8 phosphorylation was determined by immunoblotting. Data are presented  
1935 as mean  $\pm$  SEM (n = 4, \* $P < 0.0001$  [left], 0.0015 [right], † $P = 0.0033$ ). \* $P < 0.05$  versus  
1936 the corresponding vehicle groups and † $P < 0.05$  versus BMP9-stimulated siCTRL by the  
1937 one-way ANOVA with Tukey post-hoc analysis.

1938

1939 **Supplementary Figure 24.**

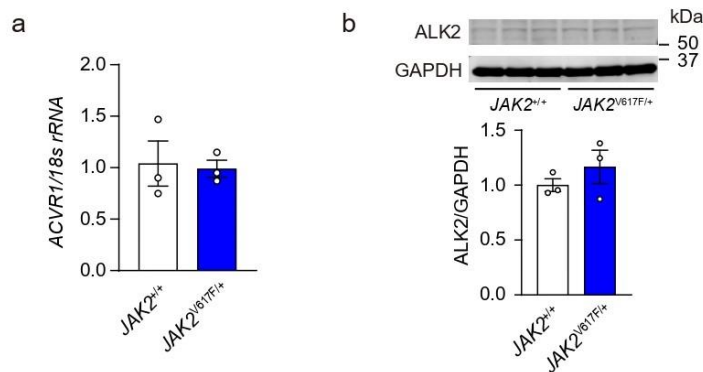


1940

1941 Flow cytometry analysis for ALK1 expression in JAK2<sup>+/+</sup> and JAK2V617F/+ HCT116  
 1942 cells. The cells were trypsinized and collected as a single cell suspension, and then stained  
 1943 with an anti-ALK1 antibody followed by a secondary anti-rabbit PE antibody and  
 1944 subjected to the flow cytometry. The representative histogram is shown.

1945

1946 **Supplementary Figure 25.**

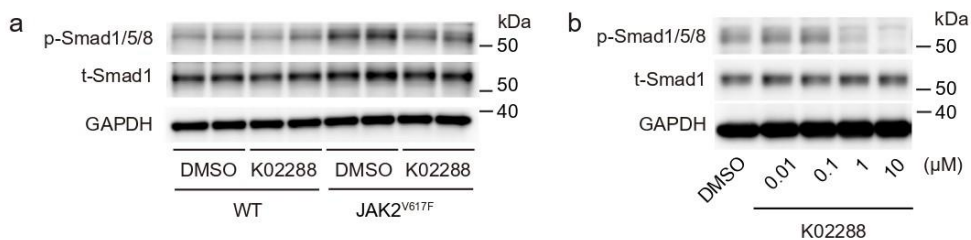


1947

1948 (a) mRNA expression of ACVR1 in JAK2V617F/+ knock-in HCT116 cells. The data  
 1949 were normalized to 18s rRNA and the average value of JAK2<sup>+/+</sup> cells was set to 1 (n =  
 1950 3). (b) ALK2 protein expression in JAK2V617F/+ HCT116 cells by Western blot  
 1951 analysis. GAPDH was used for the normalization and the average value of JAK2<sup>+/+</sup> cells  
 1952 was set to 1 (n = 3). The data are presented as mean  $\pm$  SEM (n = 3). Statistical comparisons  
 1953 were performed by the unpaired Student's t test (two-sided).

1954

1955 **Supplementary Figure 26.**

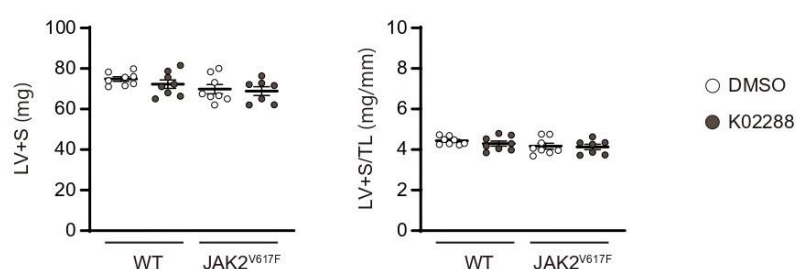


1956

1957 (a) Lung homogenates from the DMSO- or K02288-treated WT mice and JAK2V617F  
1958 mice 2 weeks after chronic hypoxia (10% O<sub>2</sub>) were analyzed by immunoblotting with p-  
1959 Smad1/5/8 and t-Smad1 antibodies. Representative images of two independent  
1960 experiments are shown. (b) JAK2V617/+ HCT116 cells were incubated with K02288 at  
1961 the indicated concentrations for 6 h. The cell lysates were subjected to immunoblotting  
1962 on p-Smad1/5/8 and t-Smad1. p-Smad1/5/8 and t-Smad1 indicate phosphorylated  
1963 Smad1/5/8 and total Smad1, respectively. Representative images of two independent  
1964 experiments are shown. GAPDH was used as the loading control. WT, wild-type mice;  
1965 JAK2V617F, JAK2V617F-expressing transgenic mice.

1966

1967 **Supplementary Figure 27.**



1968

1969 Left ventricular (LV) weight including septum (S) was measured after exposure to  
1970 normoxia (21% O<sub>2</sub>) or chronic hypoxia (10% O<sub>2</sub>) for 2 weeks (n = 8, 8, 8, 7 in each).

1971 LV+S was normalized by tibia length (TL). All data are presented as mean  $\pm$  SEM. The  
1972 statistical comparison was performed by the one-way ANOVA.

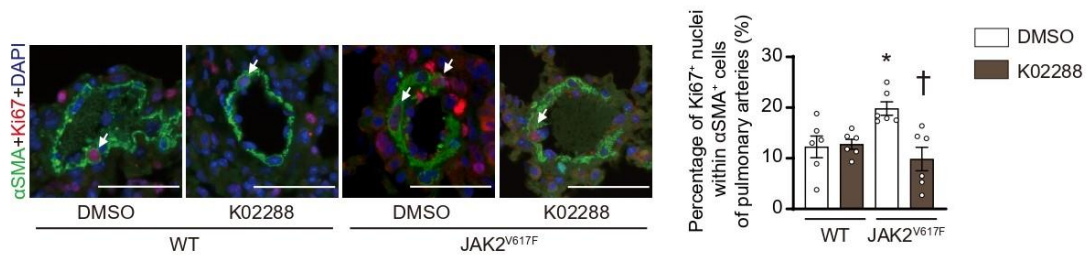
1973

1974

1975

1976

1977 **Supplementary Figure 28.**

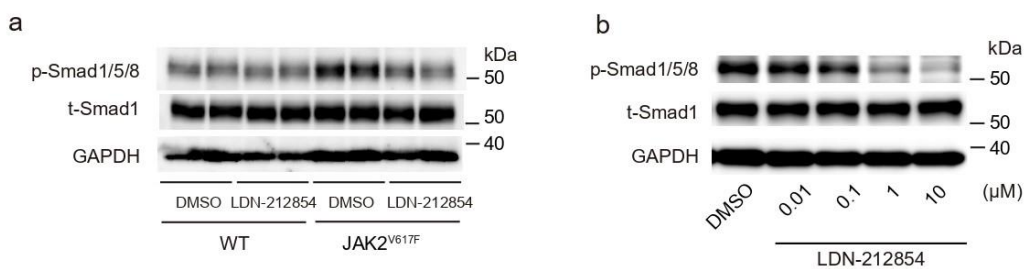


1978

1979 Left, triple-labeled immunofluorescent staining ( $\alpha$ SMA, green; Ki67, red; DAPI, blue) of  
 1980 the lung sections in DMSO- or K02288-treated WT mice and JAK2V617F mice 2 weeks  
 1981 after chronic hypoxia. White arrows indicate Ki67-positive nuclei within  $\alpha$ SMA+ cells.  
 1982 Scale bars, 50  $\mu$ m. Right, quantitative analyses of the percentage of Ki67-positive nuclei  
 1983 within  $\alpha$ SMA+ cells of distal pulmonary arteries with a diameter of 50-100  $\mu$ m (n = 6).  
 1984 More than 80  $\alpha$ SMA+ cells were counted in each section. Data are presented as mean  $\pm$   
 1985 SEM. \*P = 0.0330 versus the corresponding WT mice and †P = 0.0040 versus DMSO-  
 1986 treated JAK2V617F mice by the one-way ANOVA with Tukey post-hoc analysis.

1987

1988 **Supplementary Figure 29.**



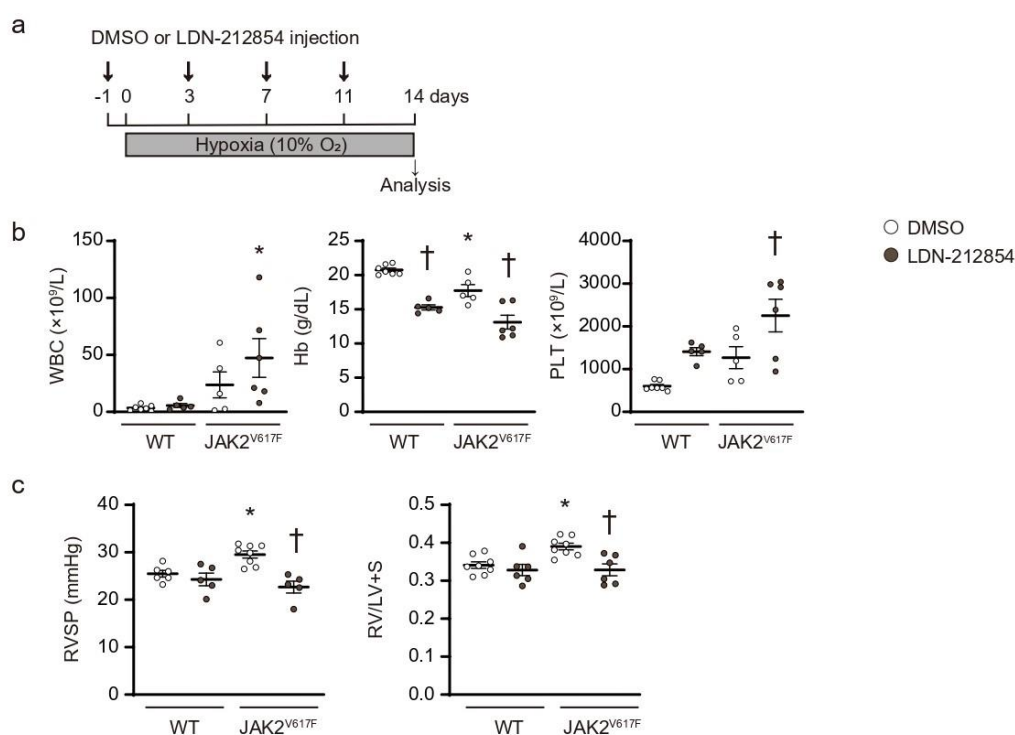
1989

1990 (a) Lung homogenates from the DMSO- or LDN-212854-treated WT mice and  
 1991 JAK2V617F mice after chronic hypoxia (10% O<sub>2</sub>) for 2 weeks were analyzed by  
 1992 immunoblotting with p-Smad1/5/8 and t-Smad1 antibodies. Representative images of two  
 1993 independent experiments are shown. (b) JAK2V617/+ HCT116 cells were incubated with  
 1994 LDN-212854 at the indicated concentrations for 6 h. The cell lysates were subjected to

1995 immunoblotting on p-Smad1/5/8 and t-Smad1. p-Smad1/5/8 and t-Smad1 indicate  
 1996 phosphorylated Smad1/5/8 and total Smad1, respectively. Representative images of two  
 1997 independent experiments are shown. GAPDH was used as the loading control. WT, wild-  
 1998 type mice; JAK2V617F, JAK2V617F-expressing transgenic mice.

1999

2000 **Supplementary Figure 30.**



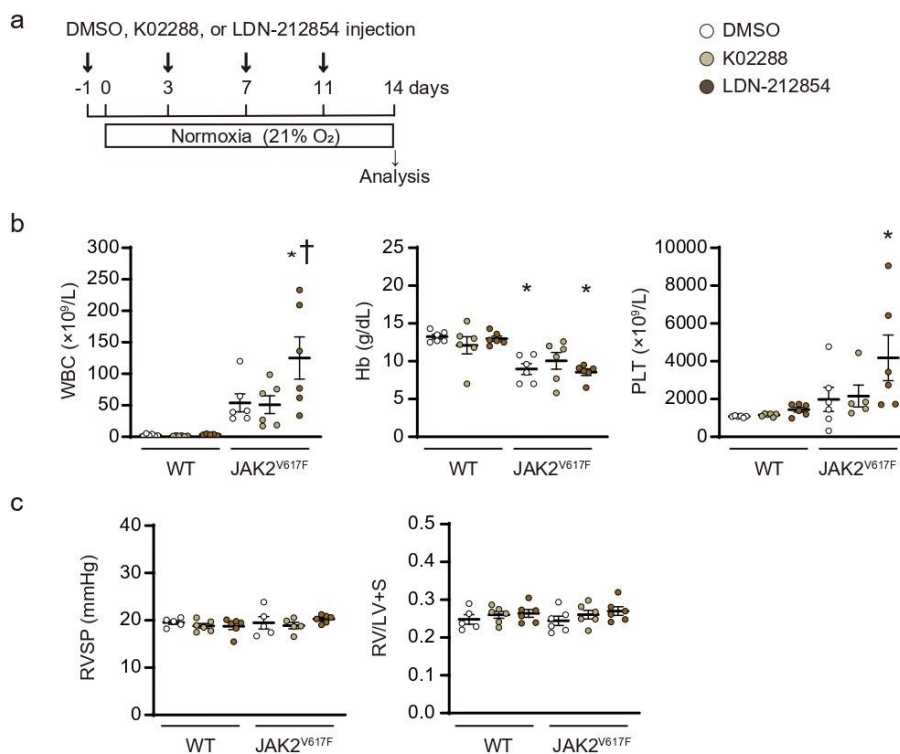
2001

2002 (a) Schematic protocol. Vehicle (DMSO) or LDN-212854 was administered via an  
 2003 intraperitoneal injection of 9 mg/kg body weight during 2-week chronic hypoxia-  
 2004 exposure as indicated. (b) Peripheral blood cell counts in DMSO- or LDN-212854-treated  
 2005 WT mice and JAK2V617F mice after exposure to chronic hypoxia for 2 weeks (n = 7, 5,  
 2006 5, 6, \*P = 0.0496 for WBC, n = 7, 5, 5, 6, \*P < 0.0001, †P = 0.0261 [left], 0.0010 [right]  
 2007 for Hb, n = 7, 5, 5, 6, †P = 0.0403 for PLT). (c) RVSP and RV hypertrophy determined by  
 2008 RV/LV+S in DMSO- or LDN-212854-treated WT mice and JAK2V617F mice (n = 6, 5,

2009 8, 5, \*P = 0.0249, †P = 0.0003 for RVSP, n =8, 6, 8, 6, \*P = 0.0197, †P = 0.0054 for  
 2010 RV/LV+S). Data are presented as mean ± SEM. \*P < 0.05 versus the corresponding WT  
 2011 mice and †P < 0.05 versus DMSO-treated JAK2V617F mice by the one-way ANOVA  
 2012 with Tukey post-hoc analysis.

2013

2014 **Supplementary Figure 31.**



2015

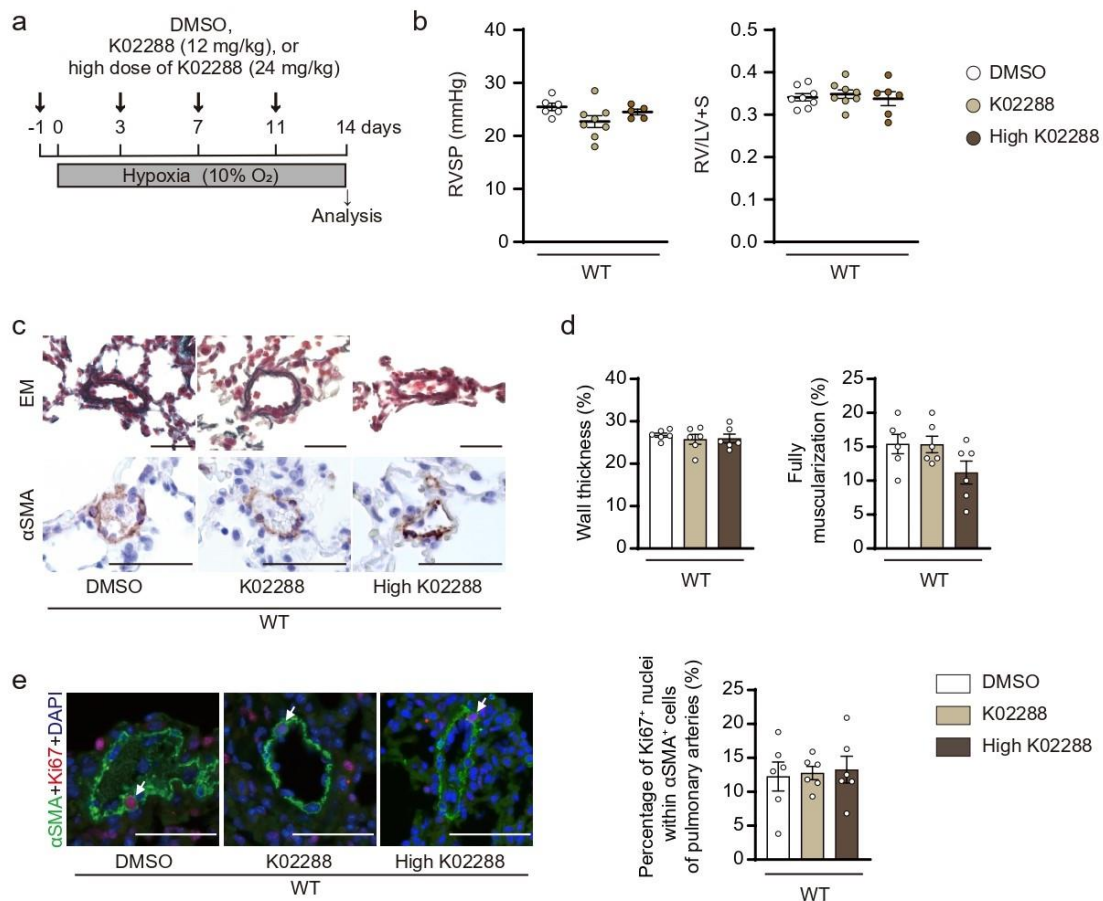
2016 (a) Schematic protocol. Vehicle (DMSO, 12 mg/kg), K02288 (12 mg/kg), or LDN-  
 2017 212854 (9 mg/kg) was administered via an intraperitoneal injection during 2-week  
 2018 normoxia-exposure as indicated. (b) Peripheral blood cell counts in DMSO-, K02288-, or  
 2019 LDN-212854-treated WT mice and JAK2V617F mice after exposure to normoxia for 2  
 2020 weeks (n = 6, 6, 5, 6, 6, 6, \*P = 0.0003, †P = 0.0440 for WBC, n =6 in each group, \*P =  
 2021 0.0045 [left], 0.0031 [right] for Hb, n = 6, 6, 6, 6, 5, 6, \*P = 0.0340 for PLT). (c) RVSP  
 2022 and RV hypertrophy determined by RV/LV+S in DMSO-, K02288-, or LDN-212854-



2023 treated WT mice and JAK2V617F mice (n = 5, 6, 6, 5, 5, 6 for RVSP, n = 5, 6, 6, 6, 6, 6  
 2024 for RV/LV+S). Data are presented as mean ± SEM. \*P < 0.05 versus the corresponding  
 2025 WT mice and †P < 0.05 versus DMSO-treated JAK2V617F mice by the one-way ANOVA  
 2026 with Tukey post-hoc analysis. WT, wild-type mice; JAK2V617F, JAK2V617F-  
 2027 expressing transgenic mice.

2028

2029 **Supplementary Figure 32.**



2030

2031 (a) Schematic representation. Vehicle (DMSO, 12 mg/kg), K02288 (12 mg/kg), or high  
 2032 dose of K02288 (24 mg/kg) was administered via an intraperitoneal injection during 2-  
 2033 week chronic hypoxia-exposure as indicated. The data of DMSO- and K02288 (12  
 2034 mg/kg)-treated WT mice are from the main Fig. 8 for comparison. (b) RVSP (n = 6, 8, 5)



2035 and RV hypertrophy determined by RV/LV+S (n = 8, 8, 6). (c) Representative images of  
2036 EM-stained sections and sections immunostained with an anti- $\alpha$ SMA antibody. Scale bar,  
2037 25  $\mu$ m. (d) Quantitative analysis of medial wall thickness in EM-stained sections (left, n  
2038 = 6 in each group) and the percentage of muscularized distal pulmonary arteries in  $\alpha$ SMA-  
2039 immunostained sections (right, n = 6 in each group). (e) Left, representative images of  
2040 triple-labeled immunofluorescent staining ( $\alpha$ SMA, green; Ki67, red; DAPI, blue). White  
2041 arrows indicate Ki67-positive nuclei within  $\alpha$ SMA+ cells. Scale bars, 50  $\mu$ m. Right,  
2042 quantitative analyses of the percentage of Ki67-positive nuclei within  $\alpha$ SMA+ cells of  
2043 distal pulmonary arteries with a diameter of 50-100  $\mu$ m (n = 6 in each group). More than  
2044 80  $\alpha$ SMA+ cells were counted in each section. All data are presented as mean  $\pm$  SEM.  
2045 The statistical comparison was performed by the one-way ANOVA.

2046

2047

2048

2049

2050

2051

2052

2053

2054

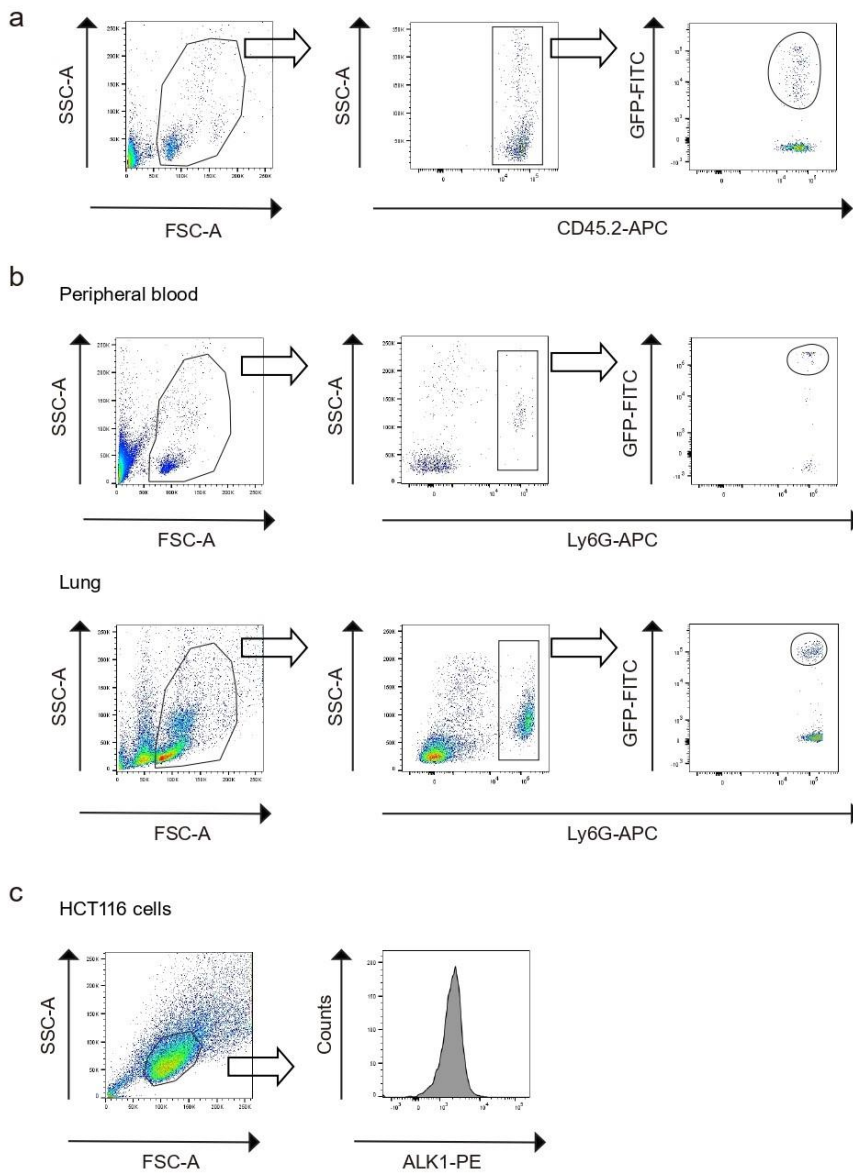
2055

2056

2057

2058

2059 **Supplementary Figure 33.**



2060

2061 (a) Gating strategy used to analyze the chimerism in the peripheral blood. The percentages  
 2062 of GFP+ cells in the circulating CD45.2+ cells are shown in Figure 4b and Supplementary  
 2063 Figure 16. (b) Gating strategy used to analyze the percentages of GFP+ cells in Ly6G+  
 2064 cells in comparison to the peripheral blood and lungs. Data are shown in Figure 4c and  
 2065 4d. (c) Gating strategy used to analyze ALK1 expressions in HCT116 cells. Data are  
 2066 shown in Supplementary Figure 24.

2067 **Supplementary Table 1. Comparisons of the presence of *JAK2V617F* between**  
 2068 **control subjects and patients with PH.**

2069

	Control subjects (n = 83)	Patients with PH (n = 70)	P value
Age, years	59 ± 17	59 ± 15	0.904
Female, n (%)	45 (54)	47 (67)	0.104
Presence of <i>JAK2V617F</i> , n (%)	0	5 (7.1)	0.019

2070

2071 Values are mean ± SD or number (%). PH, pulmonary hypertension. Comparisons of  
 2072 means between the two groups were performed by the unpaired Student's t-test (two-  
 2073 sided). Categorical variables were compared using Chi-square test (two-sided) or Fisher's  
 2074 exact test (two-sided).

2075

2076 **Supplementary Table 2. The cases of PH patients with *JAK2V617F*-positive clonal**  
 2077 **hematopoiesis.**

2078

Case	Age (years)	Gender (M/F)	Group of PH	<i>JAK2V617F</i> allele frequency (%)	WBC ( $\times 10^9/L$ )	Hb (g/dL)	PLT ( $\times 10^9/L$ )	Mean PAP (mmHg)	PVR (wood , unit)
1	60s	F	IV	14.90	8.1	12.7	360	25	3.6
2	50s	F	I	0.54	5.6	12.9	212	58	8.1
3	30s	F	I	0.06	7.8	12.8	236	64	21.1
4	60s	F	IV	16.08	7.2	13.6	339	57	14.9
5	70s	M	IV	70.96	8.7	11.4	206	41	4.2

2079 Group category is defined by the WHO classification of PH; Group I, pulmonary arterial  
 2080 hypertension; Group IV, chronic thromboembolic pulmonary hypertension. WBC, white  
 2081 blood cell count; Hb, hemoglobin concentration; PLT, platelet count; PAP, pulmonary  
 2082 arterial pressure; PVR, pulmonary vascular resistance.

2083

2084

2085

2086

2087 **Supplementary Table 3. Comparison of the PH patients with and without**  
 2088 ***JAK2V617F*.**  
 2089

	<i>JAK2V617F</i> positive (n = 5)	<i>JAK2V617F</i> negative (n = 65)	P value
Age, years	58 ± 15	59 ± 15	0.902
Female, n (%)	4 (80)	43 (66)	1.000
Group of PH, I/II/III/VI/V, n (%)	2 (40) / 0 (0) / 0 (0) / 3 (60) / 0 (0)	30 (46) / 0 (0) / 9 (14) / 24 (37) / 2 (3)	NA
NYHA functional class, I/II/III/VI, n (%)	0 (0) / 3 (60) / 2 (40) / 0 (0)	9 (14) / 29 (45) / 23 (35) / 4 (6)	NA
Laboratory data			
WBC, ×10 <sup>9</sup> /L	7.4 ± 1.1	6.4 ± 2.2	0.287
Hb, g/dL	12.6 ± 0.7	13.6 ± 2.2	0.331
Hematocrit, %	38.7 ± 7.9	41.4 ± 6.4	0.384
PLT, ×10 <sup>9</sup> /L	270 ± 73	221 ± 78	0.118
Total bilirubin, mg/dL	0.88 ± 0.43	0.97 ± 0.62	0.767
Aspartate aminotransferase, IU/L	25.8 ± 11.7	27.6 ± 13.6	0.779
Lactate dehydrogenase, IU/L	262 ± 82	246 ± 91	0.697
Creatinine	0.83 ± 0.27	0.82 ± 0.29	0.917
Estimated GFR, mL/min/1.73 m <sup>2</sup>	67.0 ± 26.7	70.7 ± 26.6	0.763
Serum iron, µg/dL	57 ± 29	85 ± 57	0.276
Ferritin, ng/mL	64 ± 64	117 ± 180	0.518
Uric acid, mg/dL	6.3 ± 2.5	6.1 ± 1.8	0.785
C-reactive protein, mg/dL	1.2 ± 1.8	0.7 ± 1.4	0.484
B-type natriuretic peptide, pg/mL	44.9 (33.1 – 542.7)	135 (40.8 – 291.6)	0.511
Echocardiography			
Left ventricular ejection fraction, %	68.2 ± 5.4	63.1 ± 12.0	0.348
RV end-diastolic area, cm <sup>2</sup>	25.6 ± 10.3	25.1 ± 12.0	0.931
RV fractional area change, %	27.2 ± 9.1	32.4 ± 14.2	0.429
TR-PG, mmHg	66.4 ± 16.0	64.3 ± 25.6	0.864
Hemodynamics			
Mean PAP, mmHg	49 ± 15	44 ± 13	0.422
Mean PAWP, mmHg	16 ± 8	11 ± 5	0.261
Cardiac index, L/min/m <sup>2</sup>	2.7 ± 0.4	2.6 ± 0.8	0.839
PVR, wood unit	10.3 ± 7.4	9.4 ± 5.3	0.688

2090  
 2091 Data are presented as mean ± SD, number (%) or median (inter-quartile range). The

2092 patients were classified into 5 groups according to the WHO clinical classification of PH;  
2093 Group I, pulmonary arterial hypertension; Group II, pulmonary hypertension due to left  
2094 heart disease; Group III, pulmonary hypertension due to lung diseases and/or hypoxia;  
2095 Group IV, chronic thromboembolic pulmonary hypertension; Group V, pulmonary  
2096 hypertension with unclear multifactorial mechanisms. NA, not applicable; NYHA, New  
2097 York Heart Association; WBC, white blood cell count; Hb, hemoglobin concentration;  
2098 PLT, platelet count; GFR, glomerular filtration rate; RV, right ventricular; TR-PG,  
2099 tricuspid regurgitation pressure gradient; PAP, pulmonary arterial pressure; PAWP,  
2100 pulmonary arterial wedge pressure; PVR, pulmonary vascular resistance. Comparisons of  
2101 values between the two groups were performed by the unpaired Student's t-test (two-  
2102 sided) or Mann-Whitney U-test (two-sided). Categorical variables were compared using  
2103 Fisher's exact test (two-sided).  
2104

2105 **Supplementary Table 4. Primers used for RT-qPCR.**

2106

Gene		Sequences			
Mouse	<i>Ccl2</i>	Forward	5'-	GGCTCAGCCAGATGCAGTTAAC	-3'
		Reverse	5'-	GCCTACTCATTGGGATCATCTTG	-3'
	<i>Cxcl1</i>	Forward	5'-	ACTCAAGAATGGTCGCGAGG	-3'
		Reverse	5'-	ACTTGGGGACACCTTTTAGCA	-3'
	<i>Ccr1</i>	Forward	5'-	TTAGCTTCCATGCCTGCCTTATA	-3'
		Reverse	5'-	TCCACTGCTTCAGGCTCTTGT	-3'
	<i>Cxcr2</i>	Forward	5'-	TCGTAGAACTACTGCAGGATTAAG	-3'
		Reverse	5'-	GGGACAGCATCTGGCAGAATA	-3'
	<i>Pdgfrb</i>	Forward	5'-	ACTACATCTCCAAAGGCAGCACCT	-3'
		Reverse	5'-	TGTAGAACTGGTCGTTTCATGGGCA	-3'
	<i>Tgfb1</i>	Forward	5'-	AGCTGCGCTTGCAGAGATTA	-3'
		Reverse	5'-	AGCCCTGTATTCCGTCTCCT	-3'
	<i>Acvr11</i>	Forward	5'-	GGCCTTTGGCCTAGTGCTAT	-3'
		Reverse	5'-	GGAGAGGACCGGATCTGC	-3'
	<i>Acvr1</i>	Forward	5'-	CGCTTCAGACATGACCTCCA	-3'
		Reverse	5'-	CCGAAGGCAGCTAACCGTAT	-3'
	<i>Bmpr2</i>	Forward	5'-	GGATGGCAGCAGTATACAGATAGG	-3'
		Reverse	5'-	CGCCACCGCTTAAGAGAGTAT	-3'
	<i>18s rRNA</i>	Forward	5'-	GTCTGTGATGCCCTTAGATG	-3'
		Reverse	5'-	AGCTTATGACCCGCACTTAC	-3'
Human	<i>ACVRL1</i>	Forward	5'-	CCATCGTGAATGGCATCGTG	-3'
		Reverse	5'-	GAGGGGTTTGGGTACCAGCA	-3'
	<i>ACVRI</i>	Forward	5'-	GAAGGGCTCATCACCACCAA	-3'
		Reverse	5'-	CCATACCTGCCTTTCCCGAC	-3'
	<i>18s rRNA</i>	Forward	5'-	GTAACCCGTTGAACCCATT	-3'
		Reverse	5'-	CCATCCAATCGGTAGTAGCG	-3'

2107

2108

2109

2110 **Supplementary Table 5. Primers used for ChIP-qPCR.**

2111

Gene		Sequences			
<i>ACVRL1</i> TSS-875bp	Forward	5'-	CCTGCCGGTATGAAGCCATT	-3'	
	Reverse	5'-	ACAGTCAGGATGGAGGGACA	-3'	
<i>ACVRL1</i> TSS-1660bp	Forward	5'-	TTGGGTGTGTCAGGGTTCTG	-3'	
	Reverse	5'-	AGGAATAGAGGCTGGGGGAG	-3'	

2112

2113

2114

2115

2116 **Supplementary Table 6. Primers and probes used for allele-specific qPCR.**

2117

2118

Primers and probes		Sequences			
<i>JAK2</i>	Forward	5'-	CTTCTTTGAAGCAGCAAGTATGA	-3'	
<i>JAK2</i> wild- type	Reverse	5'-	GTAGTTTACTTACTCTCGTCTCCACATA	-3'	
<i>JAK2</i> V617F	Reverse	5'-	GTAGTTTACTTACTCTCGTCTCCACATA	-3'	
<i>JAK2</i>	Probe	5'-	FAM- TGAGCAAGCTTTCTCACAAGCATTTGGT TT-TAMRA	-3'	